Title
Mitochondrial degradation and chronic hyperactivity in Parkinson’s disease

Author
Doric, Zak

Publication Date
2022

Peer reviewed|Thesis/dissertation

Mitochondrial degradation and chronic hyperactivity in Parkinson's disease

by
Zak Doric

DISSERTATION
Submitted in partial satisfaction of the requirements for degree of
DOCTOR OF PHILOSOPHY

in

Neuroscience

in the

GRADUATE DIVISION
of the
UNIVERSITY OF CALIFORNIA, SAN FRANCISCO

Approved:

DocuSigned by:
Robert Edwards
91579E192F544AF...

Robert Edwards
Chair

DocuSigned by:
Aimee Kao
D6C8E...494...

Aimee Kao

DocuSigned by:
Steve Finkbeiner

Steve Finkbeiner

DocuSigned by:
Ken Nakamura
83D6801FCC3C4A4...

Ken Nakamura

Committee Members

Dedication and acknowledgements

My PhD at UCSF has been an edifying and transformative adventure that has taught me the value of resilience, hard work, and dedication. However, this experience would not have been as successful without the unwavering support of incredible colleagues, mentors, and loved ones.

I am grateful for the opportunity to work with Dr. Ken Nakamura—the best advisor a graduate student could ask for. Initially, it was Ken's scientific approach that drew me in for a first-year lab rotation, but it is his human qualities that convinced me to join his lab for my thesis work.

Ken is incredibly honest and generous in his interactions with trainees and has not once broken a promise he made to me. Perhaps most importantly—Ken taught me how to stay calm and collected in the face of adversity throughout graduate school, and to find anchors when the winds are at their worst. I would be remiss if I did not mention the fantastic lab members that Ken attracted over the years and with whom I shared wonderful moments in our best and most trying times. All lab members, past and present, contributed to my success in their own way. I am also indebted to the fantastic collaborators I worked with at the Gladstone Institutes, UCSF, and UC Berkeley.

I am thankful for my thesis committee members—Robert Edwards, Aimee Kao and Steve Finkbeiner—for their guidance and sincerity during my scientific training and for always seeking the best out of me.

Last but not least, I would like to thank my friends, my partner Allison, and my family for their unconditional love and support in this challenging endeavor. I am incredibly fortunate to

have been raised in a marvelous family by loving parents and grandparents and alongside my wonderful brother, Mak. My grandparents—Šemsa, Nada, and Nedeljko—are the most tenacious people I know and have stayed true to their values and principles despite seeing atrocities of a magnitude that would be hard to describe. My parents, Branka and Sead, have shown me what it takes to live a moral and courageous life through their own perseverance and tenacity.

The struggles that I endured in graduate school pale in comparison to the adversity faced by those that came before me. Consider this work an homage to these brave individuals who have led me to fruitful and opportune times—a debt I will never be able to repay in full.

Contributions

Chapter 2 of this thesis is reproduced in its entirety from the following publication:

Li, H.*, Doric, Z.*, Berthet, A.*, Jorgens, D. M., Nguyen, M. K., Hsieh, I., Margulis, J., Fang, R., Debnath, J., Sesaki, H., Finkbeiner, S., Huang, E. & Nakamura, K. (2021). Longitudinal tracking of neuronal mitochondria delineates PINK1/Parkin-dependent mechanisms of mitochondrial recycling and degradation. *Science advances*, 7(32), eabf6580.

H.L., Z.D., A.B., M.K.N., J.M., E.H., and K.N. designed the research. H.L., Z.D., A.B., D.M.J., M.K.N., I.H., J.M., and R.F. performed research. D.M.J., J.D., H.S., S.F., and E.H. provided guidance and reagents for critical techniques. H.L., Z.D., A.B., M.K.N., J.M., R.F., E.H., and K.N. analyzed data. K.N. and Z.D. wrote the paper with assistance from co-authors.

Chapter 3 of this thesis contains unpublished experimental results with contributions from Zak Doric, Dominik Haddad, Aphroditi A. Mamaligas, Joseph Garcia, Yutao Liu, Anatol Kreitzer and Ken Nakamura.

Chapter 4 of this thesis is adapted from the following publication:

Doric, Z., Li, H., & Nakamura, K. (2022). The PINK1 advantage: recycling mitochondria in times of trouble? *Autophagy*, 18:1, 231-232.

Mitochondrial degradation and chronic hyperactivity in Parkinson's disease

By Zak Doric

Abstract

Parkinson's disease (PD), like other neurodegenerative diseases, lacks a disease-modifying therapy. While we have solutions to counteract the dopaminergic depletion that ensues at the level of the striatum following the progressive loss of substantia nigra neurons in the midbrain, and therefore, are capable of reversing the motor symptoms experienced by patients, our understanding of the molecular mechanisms that trigger degeneration is minimal. Even following the discovery of single mutations in several genes that can cause familial forms of PD, like PINK1 and PRKN, we are still deprived of a deep appreciation of the basic biological mechanisms that drive disease initiation and progression.

In Chapter 1 of this thesis, I describe the remarkable research progress that was made in the last two centuries following the original description of the disease. I detail how the mitochondrial hypothesis of PD emerged from brilliant discoveries, the advent of new biochemical and genomic tools, and even a few accidents, and how it may underlie the selective vulnerability of midbrain dopamine neurons that die in PD. Finally, I introduce some key unanswered questions in the field of PD research that I begin to address in this thesis.

In Chapter 2, I describe the novel approach we developed to study a pathway of mitochondrial turnover that is critical in PD, which allowed us to track individual mitochondria at every step of the degradation process in neurons. We gained unprecedented insight into the fate of these mitochondria once they reach the lysosomal compartment which led to us to

identify new steps of PINK1/PRKN-mediated mitochondrial degradation. These findings may have important implications for both basic biology and disease pathophysiology.

In Chapter 3, I describe a mouse model we developed to assess the impact that chronic changes in neural activity have on the function and survival of midbrain dopamine neurons. We find that the substantia nigra dopamine neurons are preferentially vulnerable to chronic increases in neural activity, while other dopamine neurons are more resilient, suggesting a potential role for chronic hyperactivity as a driver of disease.

Lastly, in Chapter 4, I elaborate and speculate on disease implications of the findings described in Chapter 2. I contextualize our contribution within the broader effort to understand why PINK1 and PRKN are so crucial to neurons under certain high-stress conditions, but are dispensable at baseline.

Table of Contents

List of Figures

Chapter 1 Introduction

1.1 Parkinson's disease: from observation to early molecular understanding

Our desire to understand and treat ailments of the brain long precedes the field's appreciation for the underlying biology. The first known descriptions of neurological conditions and their symptoms date back to ancient history (1), when physicians developed clever ways to ever-so-slightly deepen our understanding of these strange and debilitating conditions. It is this same spirit of curiosity that led the neurologist James Parkinson to rediscover and describe the motor condition that bears his name two centuries ago (2), a time when neuroscience was still largely observational. And while modern neuroscience has since, through experimentation, allowed us to develop treatments to help manage the most crippling symptoms of Parkinson's disease (PD), we remain deprived of a cure or a therapy that slows disease progression.

Prior to the advent of modern biochemical and genetic tools, our understanding of PD was limited to anatomical findings from postmortem brains, which pointed to the substantia nigra pars compacta (SNc) and the striatum as the primary targets of a pathology characterized by neuronal death (3) and accumulation of intracellular protein aggregates termed Lewy bodies (4). This chapter will detail how technical advances, seminal experiments, and even a few serendipitous accidents have led to the emergence of mitochondrial dysfunction as a known but still poorly understood driver of PD, and how neuronal energy homeostasis may be critical in influencing neuronal vulnerability to disease.

The first biological research revolution happened in the early- to mid-20th century with the application of chemical principles to biology, which led to the development of biochemical techniques and large-scale isolation and synthesis of bioactive compounds. For the first time, PD

researchers had at their disposal tools that would allow them to gain mechanistic insight into the disease. They had a particular interest in characterizing and understanding the function of the basal ganglia, a collection of interconnected subcortical nuclei of which the SNc and the striatum are integral components. Anatomical studies had revealed disease-associated changes in those two regions, but their contribution to disease remained highly controversial, and it was still unclear how they were functionally related.

But surprisingly, perhaps the most illuminating finding was serendipitous. It came not from scientists who had a primary interest for studying PD, but rather from the study of neuropsychopharmacology. Advances in chemical techniques had allowed the isolation and synthesis of several psychoactive molecules, including LSD (5), and the widespread interest in these molecules led to a concerted effort to understanding their impact on human behavior and underlying brain chemistry. One of those drugs was the antipsychotic drug reserpine, which had as a striking side-effect the capacity to act as a sedative and even to induce Parkinsonism in humans (6-8). It was famously hypothesized by Arvid Carlsson and colleagues that reserpine was mediating its effect on neural function via action on the catecholamine noradrenaline (9), which was known to be decreased in the periphery in response to reserpine (10). To test their hypothesis, the group reasoned that if neural noradrenaline was indeed lowered by reserpine, it would follow that the administration of L-DOPA, a brain-penetrating noradrenaline precursor, would at least partially restore normal function in reserpine-treated animals. Indeed, injection of L-DOPA completely reversed the depression and akinesia caused by reserpine (9), but a careful examination of brain contents revealed an astonishing detail. L-DOPA supplementation did not alter noradrenaline levels in the brain, but rather replenished the levels of another catecholamine—dopamine—in the striatum (11). It was reserpine's blockade of striatal

dopamine that was causing depression and hypoactivity in animals, which meant that dopamine was acting as a critical molecule in mediating those complex behaviors.

The importance of that finding and the impact it had on neuroscience cannot be overstated. First of all, in the middle of the 20th century, communication between neurons in the central nervous system was believed to happen mainly through electrical signal transmission. The effect of reserpine and its reversal by L-DOPA was clear evidence for chemical transmission playing a major role in regulating fundamental neural functions, and it marked a clear paradigm shift in our understanding of neurobiology. Second, it provided the missing link between the anatomical areas impacted in postmortem PD brains, the neural function mediated by those brain regions, and the symptoms experienced by PD patients: depletion of striatal dopamine was likely causing the motor symptoms in PD. Finally, Carlsson and colleagues had inadvertently discovered a method to reestablish normal levels of dopamine following depletion, an obvious candidate for PD therapy. In the years that followed this seminal discovery, L-DOPA was shown to relieve motor symptoms in patients (12), and was adopted as the primary treatment for PD, which it remains to this day. It was later confirmed through lesion studies and immunostaining that SNc neurons do indeed produce dopamine, which they release into the striatum via a direct anatomical projection known as the nigrostriatal pathway (13). But despite this immense progress, what was triggering the degeneration of this pathway and causing subsequent dopamine depletion in PD remained a mystery.

1.2 Mitochondrial hypothesis of Parkinson's disease

The first insights into the potential causes of PD were the result of a tragic accident. In the 1970s, a chemistry graduate student synthesized the opioid desmethylprodine for recreational use, without an appreciation for the byproducts generated in his synthesis. A mere three days

following self-administration, he developed several PD-like symptoms, and immediately became the subject of a case study among neurologists. They eventually deduced that one of the byproducts he and subsequently others (14) had injected themselves with was MPTP, a drug that gets metabolized to MPP+ by glial cells and which is in turn exclusively taken up by dopamine neurons, where it mediates cytotoxicity. This mechanism was brilliantly demonstrated in a series of follow-up studies (15-17).

However, the crux of the matter was understanding how MPP+ causes neurotoxicity, because it would reveal at least one point of vulnerability of SNc dopamine neurons, which could prove to be relevant to PD initiation. MPP+ was found to accumulate in the mitochondrial matrix and inhibit complex I of the electron transport chain (18-20), marking the birth of the mitochondrial hypothesis of PD. However, this finding was far from definitive, since that type of stress could presumably kill any other neuron if MPP+ uptake was not limited to dopamine neurons. A decade later, evidence for decreased complex I function in the SNc of PD patients emerged (21-24), reinforcing the concept that mitochondrial dysfunction was a causative factor in PD. Around the same time, a mouse model was developed to achieve systemic inhibition of complex I using the naturally-occurring mitochondrial poison rotenone (25). Exceptionally, despite systemic administration of rotenone, SNc dopamine neurons are selectively vulnerable in this model, which leads to the recapitulation of PD symptoms.

While the case for mitochondrial dysfunction in PD was getting increasingly strong, it was the advent of genomics and the discoveries that followed that put it on firm footing. PD was once believed to be the archetypal non-genetic disorder, but the advent of next-generation sequencing enabled the identification of several familial forms of the disease caused by mutations in single genes, which account for around 10% of PD cases. The promise of these PD-causing genes was

that an understanding of their disease-relevant cellular functions would not only open the door to new therapeutic approaches for the corresponding disease subtype, but also that those molecular pathways would be relevant to the much more frequent cases of sporadic PD (those cases for which there is no known single genetic cause). The first PD-causing gene to be identified was SNCA, which codes for α-synuclein, a protein later found to be the most abundant component of Lewy bodies (26), the protein aggregates that accumulate in disease. Understandably, α-synuclein became and remains to this day the main area of focus for PD research. Its normal function is still being elucidated, but great strides have been made in understanding its role in neuronal vesicle trafficking and neurotransmitter release (27-32). Several groups have also shown its ability to aggregate in pathological conditions, and it is hypothesized that cell-to-cell aggregate spread may constitute a driver of disease. Whether these aggregates have a toxic gain-of-function or whether they reduce normal function through sequestration of monomeric α-synuclein remains the subject of immense controversy in the field. Interestingly, α-synuclein also interferes with normal mitochondrial function in several ways, including through direct association with mitochondrial membranes (33), inhibition of complex I activity (34-37) and disruption of mitochondrial dynamics (38). However, it remains to be elucidated whether α-synuclein's impact on mitochondrial function drives neurodegeneration.

In the series of PD genes identified following α-synuclein, PRKN and PINK1, coding for Parkin and PINK1 respectively, are of particular interest. Early evidence from Drosophila research indicated that normal Parkin function was necessary to maintain healthy mitochondria (39), which led to seminal work from Richard Youle and his group, which demonstrated that Parkin, a cytosolic ubiquitin ligase, is recruited to the surface of damaged mitochondria to signal for their degradation via autophagy (i.e. mitophagy) (40). While it was not clear whether this

particular function of Parkin accounted for its neuroprotective effect in PD, the discovery that the mitochondrial kinase PINK1 served as a sensor of mitochondrial damage and directly recruited Parkin to dysfunctional mitochondria (41-43), made it a much more compelling proposition. This finding led to a large effort to characterize the PINK1/Parkin pathway, and remarkable progress has been made over the past 15 years to define the steps of PINK1/Parkin-mediated mitochondrial turnover (40-47). However, most of this work was done in non-neuronal cell lines, which can survive without mitochondria (40), and using non-physiological mitochondrial uncouplers to induce pathway activation. Therefore, the relevance of this pathway to PD remains unclear.

There are several open questions that need to be addressed in order to potentially leverage this pathway for disease-modifying therapies. Why do rodent dopamine neurons resist the deletion of PINK1 and Parkin (48, 49)? Under what conditions of cellular stress and/or mitochondrial damage is PINK1/Parkin mitophagy activated in human neurons in vivo? How do neurons with high metabolic demand maintain energy homeostasis while actively turning over mitochondria? How and to what extent are complex organelles like mitochondria degraded during autophagy? Why can't the PINK1/Parkin pathway be compensated for by alternative pathways of mitochondrial turnover under certain conditions of neuronal stress? In Chapter 2 of this thesis, I begin to answer these questions by studying PINK1/Parkin-mediated turnover in primary mouse neurons, and in animals that lack the mitochondrial fission protein Drp1 specifically in dopamine neurons. The latter approach was previously established by our group as a type of mitochondrial damage that is relevant to PD and neurodegeneration (50, 51), and that leads to the selective loss of SNc dopamine neurons. In the present study, we demonstrate that this type of damage leads to PINK1 and Parkin recruitment, and that loss of PINK1 worsens

neuronal survival *in vivo*. In addition, we take advantage of the altered morphology of Drp1KO mitochondria to track them at a single-organelle level for several hours, and we uncover their fate after PINK1/Parkin-mediated lysosomal targeting. These findings begin to answer some of the open questions postulated above, and paint a clearer picture of how PINK1/Parkin-mediated quality control operates in neurons.

1.3 Selective vulnerability of SNc dopamine neurons

Another important question that remains to be addressed in relation to the mitochondrial hypothesis is why SNc dopamine neurons are preferentially vulnerable to a wide array of mitochondrial insults as well as sporadic PD, while other neurons, including neighboring dopamine neurons of the ventral tegmental area (VTA), are much more resilient. It has been posited that SNc neurons have unusually high intrinsic metabolic demands, and that slight chronic increases in bioenergetic stress due to environment, aging or genetic factors, could be sufficient to lead to their demise. Indeed, SNc dopamine neurons need to maintain autonomous pacemaking activity for normal function, and unlike for other more resilient neuron types which rely on sodium channels for pacemaking, in SNc dopamine neurons the activity is supported by L-type calcium channels (52). Due to a steeper electrochemical gradient, pumping out calcium following its influx during pacemaking is markedly more expensive from a bioenergetic perspective. This is made even worse by the low intrinsic calcium buffering capacity observed in SNc dopamine neurons, which express lower levels of the calcium-binding protein calbindin than their VTA counterparts. SNc dopamine neurons also have highly arborized axons, which may contribute to their high intrinsic energy demand. In rats, for example, an estimated 75,000 striatal neurons are innervated by a single dopamine neuron, accounting for around 245,000 synapses (53, 54). In humans, the number of synapses is 10-fold larger (54). Given that close to

half of mitochondria-derived energy is used to support neural activity-related functions like neuronal firing and synaptic release (55), it follows that even small chronic increases in neural activity could have dramatic impacts on the survival of SNc dopamine neurons over the course of several years. However, the impact of such changes has never been investigated empirically. In Chapter 3 of this thesis, I describe a mouse model that we designed to understand the impact of chronic changes in neural activity on the function and survival of dopamine neurons. We find that SNc dopamine neurons are preferentially vulnerable to this type of stress, and that chronic activation over the course of weeks is sufficient to initiate axonal degeneration. Understanding why SNc neurons are more vulnerable than VTA neurons when exposed to the same stressor may be critical for understanding their preferential vulnerability in PD.

1.4 References

1. B. V. Manyam, Paralysis agitans and levodopa in “Ayurveda”: ancient Indian medical treatise. Movement disorders: official journal of the Movement Disorder Society 5, 47-48 (1990).

2. J. Parkinson, An essay on the shaking palsy. The Journal of neuropsychiatry and clinical neurosciences 14, 223-236 (2002).

3. C. Trétiakoff, Contribution à l'étude de l'Anatomie pathologique du Locus Niger de Soemmering avec quelques déduction relatives à la pathogénie des troubles du tonus musculaire et de la maladie de Parkinson. Theses de Paris, (1919).

4. F. Lewy, Zur pathologischen Anatomie der Paralysis agitans. Dtsch Z Nervenheilk 50, 50-55 (1913).

5. A. Hofmann, J. Ott, LSD, my problem child. (McGraw-Hill New York, 1980), vol. 5.

6. J. A. Schneider, A. E. Earl, Effects of serpasil on behavior and autonomic regulating mechanisms. Neurology, (1954).

7. J. Tripod, H. Bein, R. Meier, Characterization of central effects of serpasil (reserpin, a new alkaloid of Rauwolfia serpentina B.) and of their antagonistic reactions. Archives internationales de pharmacodynamie et de therapie 96, 406-425 (1954).

8. F. Freyhan, Psychomotility and parkinsonism in treatment with neuroleptic drugs. AMA Archives of Neurology & Psychiatry 78, 465-472 (1957).

9. A. Carlsson, M. Lindqvist, T. Magnusson, 3, 4-Dihydroxyphenylalanine and 5-hydroxytryptophan as reserpine antagonists. Nature 180, 1200-1200 (1957).

10. A. Carlsson, Effect of reserpine on the metabolism of catecholamines. Psychotropic drugs 6, 363-372 (1957).

11. A. Carlsson, The occurrence, distribution and physiological role of catecholamines in the nervous system. Pharmacological reviews 11, 490-493 (1959).

12. G. C. Cotzias, M. H. Van Woert, L. M. Schiffer, Aromatic amino acids and modification of parkinsonism. New England Journal of Medicine 276, 374-379 (1967).

13. T. Hökfelt, U. Ungerstedt, Specificity of 6-hydroxydopamine induced degeneration of central monoamine neurones: an electron and fluorescence microscopic study with special reference to intracerebral injection on the nigro-striatal dopamine system. Brain research 60, 269-297 (1973).

14. J. W. Langston, P. Ballard, J. W. Tetrud, I. Irwin, Chronic Parkinsonism in humans due to a product of meperidine-analog synthesis. Science 219, 979-980 (1983).

15. B. R. Ransom, D. M. Kunis, I. Irwin, J. W. Langston, Astrocytes convert the parkinsonism inducing neurotoxin, MPTP, to its active metabolite, MPP+. Neuroscience letters 75, 323-328 (1987).

16. R.-S. Shen, C. Abell, W. Gessner, A. Brossi, Serotonergic conversion of MPTP and dopaminergic accumulation of MPP+. FEBS letters 189, 225-230 (1985).

17. J. W. Langston, The MPTP story. Journal of Parkinson's disease 7, S11-S19 (2017).

18. R. R. Ramsay, J. Dadgar, A. Trevor, T. P. Singer, Energy-driven uptake of N-methyl-4-phenylpyridine by brain mitochondria mediates the neurotoxicity of MPTP. Life sciences 39, 581-588 (1986).

19. R. R. Ramsay, A. T. Kowal, M. K. Johnson, J. I. Salach, T. P. Singer, The inhibition site of MPP+, the neurotoxic bioactivation product of 1-methyl-4-phenyl-1, 2, 3, 6-tetrahydropyridine is near the Q-binding site of NADH dehydrogenase. Archives of biochemistry and biophysics 259, 645-649 (1987).

20. R. R. Ramsay, J. I. Salach, T. P. Singer, Uptake of the neurotoxin 1-methyl-4-phenylpyridine (MPP+) by mitochondria and its relation to the inhibition of the mitochondrial oxidation of NAD+-linked substrates by MPP+. Biochemical and biophysical research communications 134, 743-748 (1986).

21. A. Schapira et al., Mitochondrial complex I deficiency in Parkinson's disease. The Lancet 333, 1269 (1989).

22. A. Schapira et al., Mitochondrial complex I deficiency in Parkinson's disease. Journal of neurochemistry 54, 823-827 (1990).

23. A. Schapira et al., Anatomic and disease specificity of NADH CoQ1 reductase (complex I) deficiency in Parkinson's disease. Journal of neurochemistry 55, 2142-2145 (1990).

24. N. Hattori, M. Tanaka, T. Ozawa, Y. Mizuno, Immunohistochemical studies on complexes I, II, III, and IV of mitochondria in Parkinson's disease. Annals of Neurology: Official Journal of the American Neurological Association and the Child Neurology Society 30, 563-571 (1991).

25. R. Betarbet et al., Chronic systemic pesticide exposure reproduces features of Parkinson's disease. Nature neuroscience 3, 1301-1306 (2000).

26. M. G. Spillantini, R. A. Crowther, R. Jakes, M. Hasegawa, M. Goedert, α-Synuclein in filamentous inclusions of Lewy bodies from Parkinson's disease and dementia with Lewy bodies. Proceedings of the National Academy of Sciences 95, 6469-6473 (1998).

27. J. T. Bendor, T. P. Logan, R. H. Edwards, The function of α-synuclein. Neuron 79, 1044-1066 (2013).

28. D. E. Cabin et al., Synaptic vesicle depletion correlates with attenuated synaptic responses to prolonged repetitive stimulation in mice lacking α-synuclein. Journal of Neuroscience 22, 8797-8807 (2002).

29. D. L. Fortin et al., Lipid rafts mediate the synaptic localization of α-synuclein. Journal of Neuroscience 24, 6715-6723 (2004).

30. D. D. Murphy, S. M. Rueter, J. Q. Trojanowski, V. M.-Y. Lee, Synucleins are developmentally expressed, and α-synuclein regulates the size of the presynaptic vesicular pool in primary hippocampal neurons. Journal of Neuroscience 20, 3214-3220 (2000).

31. V. M. Nemani et al., Increased expression of α-synuclein reduces neurotransmitter release by inhibiting synaptic vesicle reclustering after endocytosis. Neuron 65, 66-79 (2010).

32. L. Yavich, H. Tanila, S. Vepsäläinen, P. Jäkälä, Role of α-synuclein in presynaptic dopamine recruitment. Journal of Neuroscience 24, 11165-11170 (2004).

33. K. Nakamura et al., Direct Membrane Association Drives Mitochondrial Fission by the Parkinson Disease-associated Protein α-Synuclein*♦. Journal of Biological Chemistry 286, 20710-20726 (2011).

34. L. Devi, V. Raghavendran, B. M. Prabhu, N. G. Avadhani, H. K. Anandatheerthavarada, Mitochondrial import and accumulation of α-synuclein impair complex I in human dopaminergic neuronal cultures and Parkinson disease brain. Journal of Biological Chemistry 283, 9089-9100 (2008).

35. G. Liu et al., α-Synuclein is differentially expressed in mitochondria from different rat brain regions and dose-dependently down-regulates complex I activity. Neuroscience letters 454, 187-192 (2009).

36. S. J. Chinta, J. K. Mallajosyula, A. Rane, J. K. Andersen, Mitochondrial alpha-synuclein accumulation impairs complex I function in dopaminergic neurons and results in increased mitophagy in vivo. Neuroscience letters 486, 235-239 (2010).

37. V. Loeb, E. Yakunin, A. Saada, R. Sharon, The transgenic overexpression of α-synuclein and not its related pathology associates with complex I inhibition. Journal of Biological Chemistry 285, 7334-7343 (2010).

38. K. Nakamura, α-Synuclein and mitochondria: partners in crime? Neurotherapeutics 10, 391-399 (2013).

39. J. C. Greene et al., Mitochondrial pathology and apoptotic muscle degeneration in Drosophila parkin mutants. Proceedings of the National Academy of Sciences 100, 4078-4083 (2003).

40. D. Narendra, A. Tanaka, D.-F. Suen, R. J. Youle, Parkin is recruited selectively to impaired mitochondria and promotes their autophagy. The Journal of cell biology 183, 795-803 (2008).

41. S. M. Jin et al., Mitochondrial membrane potential regulates PINK1 import and proteolytic destabilization by PARL. Journal of Cell Biology 191, 933-942 (2010).

42. D. P. Narendra et al., PINK1 is selectively stabilized on impaired mitochondria to activate Parkin. PLoS biology 8, e1000298 (2010).

43. C. Vives-Bauza et al., PINK1-dependent recruitment of Parkin to mitochondria in mitophagy. Proceedings of the National Academy of Sciences 107, 378-383 (2010).

44. S. Geisler et al., PINK1/Parkin-mediated mitophagy is dependent on VDAC1 and p62/SQSTM1. Nature cell biology 12, 119-131 (2010).

45. A. C. Poole, R. E. Thomas, S. Yu, E. S. Vincow, L. Pallanck, The mitochondrial fusion-promoting factor mitofusin is a substrate of the PINK1/parkin pathway. PloS one 5, e10054 (2010).

46. S. A. Sarraf et al., Landscape of the PARKIN-dependent ubiquitylome in response to mitochondrial depolarization. Nature 496, 372-376 (2013).

47. F. Koyano et al., Ubiquitin is phosphorylated by PINK1 to activate parkin. Nature 510, 162-166 (2014).

48. S. Gispert et al., Parkinson phenotype in aged PINK1-deficient mice is accompanied by progressive mitochondrial dysfunction in absence of neurodegeneration. PloS one 4, e5777 (2009).

49. M. S. Goldberg et al., Parkin-deficient mice exhibit nigrostriatal deficits but not loss of dopaminergic neurons. Journal of Biological Chemistry 278, 43628-43635 (2003).

50. A. Berthet et al., Loss of mitochondrial fission depletes axonal mitochondria in midbrain dopamine neurons. Journal of Neuroscience 34, 14304-14317 (2014).

51. K. Itoh, K. Nakamura, M. Iijima, H. Sesaki, Mitochondrial dynamics in neurodegeneration. Trends in cell biology 23, 64-71 (2013).

52. D. J. Surmeier, Calcium, ageing, and neuronal vulnerability in Parkinson's disease. The Lancet Neurology 6, 933-938 (2007).

53. W. Matsuda et al., Single nigrostriatal dopaminergic neurons form widely spread and highly dense axonal arborizations in the neostriatum. Journal of Neuroscience 29, 444-453 (2009).

54. J. P. Bolam, E. K. Pissadaki, Living on the edge with too many mouths to feed: why dopamine neurons die. Movement Disorders 27, 1478-1483 (2012).

55. C. Pacelli et al., Elevated mitochondrial bioenergetics and axonal arborization size are key contributors to the vulnerability of dopamine neurons. Current Biology 25, 2349-2360 (2015).

Chapter 2 PINK1/Parkin-dependent mechanisms of mitochondrial degradation

2.1 Introduction

Changes in mitochondrial quality control and dynamics, the balance of mitochondrial fission and fusion, are implicated in the pathogenesis of several neurodegenerative diseases, especially Parkinson's disease (PD) (1). The dopamine (DA) neurons in the substantia nigra (SN) that degenerate in PD are sensitive to changes in mitochondrial fission (2) and fusion (3), and altered expression or mutation of proteins implicated in familial forms of PD (e.g., synuclein, DJ-1, Parkin, PINK1, LRRK2, and VPS35) influences mitochondrial morphology and quality control (1, 4–6).

These findings raise the possibility that familial PD genes produce toxicity by altering mitochondrial fission and quality control and call into question how the level of fission and quality control may converge to affect cytotoxicity. In Drosophila, PINK1 compensates for the loss of the central mitochondrial fission protein dynamin-related protein 1 (Drp1) to maintain mitochondrial morphology and survival (7), and loss of PINK1 leads to neurodegeneration and death (8). Moreover, when mitochondria are depolarized, the mitochondrial fusion proteins Mfn1 and Mfn2 are targeted for degradation by Parkin in a PINK1-dependent manner (9, 10), suggesting that PINK1 increases the fission-fusion balance. However, it is unclear whether the effects of losing PINK1 on mitochondrial morphology are important to the toxicity of Drp1 loss. Instead, mitochondrial fission and PINK1 may converge at mitochondrial turnover, and the extent of fission may influence the toxicity of PINK1 loss by affecting the number of mitochondria needing degradation.

Drp1-dependent fission may be critical to mitochondrial turnover. In INS1 and COS cells, fission isolates mitochondria with lower mitochondrial membrane potential, and the depolarized mitochondria are degraded by autophagy (11). Fission may be required to produce mitochondria small enough to be engulfed by autophagosomes. Supporting this possibility, cardiomyocytes and mouse embryonic fibroblasts (MEFs) lacking Drp1 have decreased Parkin-dependent mitophagy after depolarization by the protonophore carbonyl cyanide m-chlorophenyl hydrazone (CCCP) (9). They may also have fewer mitochondria targeted to lysosomes (12, 13). However, if fission is truly required for mitochondrial turnover, then the mitochondrial content of neurons would be expected to increase (rather than decrease) when fission is compromised (2), and several studies have failed to find a critical role for Drp1 in mitochondrial turnover (14–16). Moreover, the physiology of mitochondrial turnover is different in neurons from that in other cell types. In many cell lines, depolarization with CCCP causes rapid Parkin accumulation on the outer mitochondrial membrane (OM) and the complete removal of all mitochondria, while in neurons, the induction of Parkin-based mitophagy is far less robust, and there is no clear effect on mitochondrial content (17–19), suggesting that neuronal mitochondria may be more resistant to degradation.

To better understand how mitochondrial fission and PINK1/Parkin promote mitochondrial quality control in neurons, we developed neuronal culture and mouse models with deletion of Drp1 in DA neurons, with and without PINK1. We took advantage of the individual, large, and swollen Drp1KO mitochondria to track the fates and functions of individual mitochondria and delineate new mechanisms of mitochondrial quality control.

2.2 Results

Midbrain DA neurons require PINK1 to survive when fission is compromised

Midbrain DA neurons lacking Drp1 have reduced mitochondrial mass, although the size of individual mitochondria is increased (2). We hypothesized that this reflects the ongoing degradation of Drp1KO mitochondria that is critical to DA neuron health. To determine whether disrupting turnover would enhance the toxicity of losing Drp1, we assessed the impact of deleting PINK1 (6, 20, 21). If Drp1KO mitochondria are turned over through a PINK1-dependent mechanism, loss of PINK1 would increase the toxicity of Drp1 loss, although PINK1 loss alone does not produce degeneration (22). Conversely, if Drp1KO mitochondria can no longer be turned over by conventional mitophagy, loss of PINK1 might have no effect.

We generated mice with targeted deletion of Drp1 in DA neurons on a PINK1 KO (knockout) background (DATcre-Drp1KO;PINK1 KO). In our prior report, loss of Drp1 alone in DA neurons led to the death of ~25% of mice by day 50 [(2); data reproduced in Fig. 1A, left]. As expected, loss of PINK1 alone had no effect on survival. However, loss of PINK1 in mice with Drp1KO DA neurons markedly impaired survival; ~85% of DATcre-Drp1KO;PINK1KO mice died by 50 days of age, while ~40% of mice with heterozygous loss of PINK1 died over the same period (Fig. 1A).

We used stereology to examine survival of midbrain DA neurons from postnatal day 18 (P18) mice. We found that concurrent loss of PINK1 decreased the survival of Drp1KO DA neurons in the SN and ventral tegmental area (VTA) of Drp1KO mice, although PINK1 KO alone had no detectable impact (Fig. 1, B and C).

The terminals of Drp1KO DA neurons degenerate before the cell bodies (2). To determine whether PINK1 KO exacerbates this effect, we measured the optical density of TH (tyrosine hydroxylase) immunostaining. Drp1KO alone caused almost complete loss of DA terminals in the caudate and putamen by P18 but spared most terminals in the nucleus accumbens and olfactory tubercule (Fig. 1, D, top row, and E). On the PINK1 KO background, many of these otherwise resistant Drp1KO terminals were lost.

To determine whether PINK1 KO also causes degeneration when Drp1 is lost in adult animals, we injected AAVcre into 6- to 8-month-old Drp1lox/lox;PINK1KO and Drp1lox/lox mice. Mice were sacrificed after 2 months, and we assessed their striatal denervation. Deletion of Drp1 alone in adult mice produced severe loss of terminals in the caudate putamen, with only ~25% spared. However, many of those resistant terminals were lost when Drp1 was deleted on the PINK1 KO background (Fig. 1, D, bottom row, and F).

The increased toxicity of Drp1KO when PINK1 is absent could indicate that PINK1-dependent turnover of Drp1KO mitochondria enables neurons to survive or that PINK1 protects cells from loss of Drp1 (7) by increasing the fission/fusion balance, perhaps by degrading the fusion proteins Mfn1 and Mfn2 (9, 10). However, we failed to find evidence for the latter model, as PINK1 KO alone did not affect the morphology of mitochondria in DA neurons, and concurrent loss of PINK1 did not increase the proportion of Drp1KO DA neurons with swollen mitochondria at the cell body (fig. S1, A to D). Loss of either PINK1 or Drp1 can also increase oxidative stress (23, 24). However, neither Drp1KO, PINK1 KO, or the combination increased oxidative stress, as assessed by mitochondria-targeted redox-sensitive green fluorescent protein (roGFP) (mito-roGFP) (fig. S1, E and F). Thus, changes in mitochondrial morphology or oxidative stress are unlikely to underlie the toxicity of PINK1 KO to Drp1KO DA neurons.

Drp1KO increases mitochondrial targeting to lysosomes

To investigate the fate of Drp1KO mitochondria, we evaluated their fusion with lysosomes. In the absence of Drp1, an increased percentage of mitochondria colocalized with the lysosomal marker lysosomal associated membrane protein 1 (LAMP1), both in cultured hippocampal neurons where LAMP1 fluorescence ringed mitochondria and in DA neurons in vivo where LAMP1 fluorescence overlapped with mitochondria (fig. S2, A and B). These differential patterns of colocalization might reflect different stages of mitochondrial degradation or result from technical differences.

To quantify the impact of Drp1KO on mitochondrial pH, we used mitochondria-targeted mKeima (mitoKeima), a pH-sensitive reporter that changes fluorescence as mitochondria are delivered to lysosomes [peak excitation, 586 nm (acidic pH) and 440 nm (neutral pH)] (25). Drp1KO increased the ratio of red (acidic) to green (neutral) fluorescence, indicating that Drp1KO mitochondria are at a lower pH (Fig. 2, A to C). The increased red/green ratio in the Drp1KO group was driven by an upward shift in the mitoKeima signal in >50% of cells, while other Drp1KO cells remained at control levels (fig. S2, C and D). The increase was quenched by both ammonium chloride (NH_4Cl), to alkalinize cells, and bafilomycin, which blocks the acidification of lysosomes and fusion of autophagosomes with lysosomes (26). To confirm that Drp1KO mitochondria fuse with lysosomes, we performed a Magic Red assay and observed fluorescence in some Drp1KO mitochondria (Fig. 2D and fig. S2E), indicating cleavage of the substrate by the lysosomal enzyme cathepsin B.

To test whether the increased mitochondrial acidification and lysosomal fusion indicated a faster turnover rate, we examined the dissipation of a photoconvertible mitochondria-targeted

fluorophore as a surrogate for mitochondrial turnover. Neurons were cotransfected with mitochondrial matrix–targeted EOS2 (mito-EOS2) and Drp1 short hairpin RNA (shRNA) or scrambled shRNA. EOS2 was irreversibly photoconverted from green to red with a single pulse of 405-nm light and longitudinally imaged by robotic microscopy at 12-hour intervals for 30 to 40 hours to measure clearance of the red fluorescence. Single-cell red fluorescence intensities were normalized to the baseline, and the half-life of mito-EOS2 was calculated for each cell (Fig. 2, E and F, and fig. S2F). Unexpectedly, we found no difference in mean mito-EOS2 half-life or the distribution of mito-EOS2 half-lives in neurons with Drp1 knockdown. Combined with the mitoKeima data, this suggests either that most Drp1KO mitochondria are not degraded despite being acidified or that the acidified mitochondria are degraded, but at least a subset of mitochondrial proteins (including the photoconverted red mito-EOS2 reporter) remain intact in the resulting acidified structures for long periods.

Parkin is targeted across the OM of polarized mitochondria

The synthetic lethality of PINK1 and Drp1KO suggests that PINK1 may be required for quality control of dysfunctional Drp1KO mitochondria. Consistent with this, the increase in acidified mitoKeima signal in Drp1KO neurons was largely blocked when PINK1 was also absent (Fig. 2G). Parkin KO also markedly decreased the acidified mitoKeima signal (Fig. 2H) in the setting of Drp1 loss. We next tested the requirement for the core autophagy protein ATG5. Hippocampal neurons from ATG5lox/lox mice (27) were cotransfected with mitoKeima, Cre (to delete ATG5), or vector control and with Drp1 or scrambled shRNA. Similar to PINK1 KO and Parkin KO, deletion of ATG5 decreased the acidification of Drp1-deficient mitochondria (Fig. 2I and fig. S2, G and H).

To further assess how PINK1 and Parkin contribute to mitochondrial quality control in neurons, we next asked whether Parkin is recruited to Drp1KO mitochondria by examining the colocalization of Parkin [visualized with green fluorescent protein (GFP)–Parkin] with mitochondria (mito-BFP). In many Drp1KO neurons, Parkin was dispersed evenly throughout the cytosol (Fig. 3, A and B). However, in ~5% of Drp1KO neurons, GFP-Parkin encircled a single mitochondrion. In others, punctae of GFP-Parkin were adjacent to mitochondria, perhaps representing an earlier stage before Parkin fully encircles mitochondria. Of interest, ~30% of neurons contained one or more mitochondria where the GFP-Parkin signal overlapped with the mitochondria, suggesting that Parkin had transited through the OM and either localized to the inner mitochondrial membrane or entered the mitochondrial matrix. Confocal imaging of 0.4-μm z-stacks of live and fixed neurons revealed an overlapping pattern consistent with GFP-Parkin in the matrix or inner mitochondrial membrane and confirmed that the circling pattern is GFP-Parkin at the OM (hereafter referred to as OM-Parkin; Fig. 3C and fig. S3, A and B). Live imaging of GFP targeted to the OM versus the matrix and immunostaining against Tom20 (an OM protein) versus pyruvate dehydrogenase (PDH; a matrix protein) confirmed our ability to distinguish these compartments. Although the OM pattern of GFP-Parkin fluorescence could be explained by increased acidity in the matrix of mitochondria, quenching the GFP fluorescence in the matrix, adding NH_4Cl to alkalinize the mitochondrial contents (28) failed to restore GFP fluorescence within the matrix of mitochondria with OM-Parkin (fig. S3C), further suggesting that these are distinct patterns of GFP-Parkin recruitment. In the absence of both PINK1 and Drp1, all three forms of Parkin configuration around the mitochondria were absent (Fig. 3B). Moreover, although most Drp1KO mitochondria are polarized (Fig. 3D) (2), the mean

mitochondrial membrane potential was markedly decreased in Drp1KO;PINK1KO neurons, consistent with PINK1's role in protecting against Drp1KO toxicity.

Notably, this overlapping pattern of Parkin accumulation was not unique to neurons. In immortalized Drp1KO MEFs (4), a subset of cells contained one or more mitochondria with either OM, overlapping, or adjacent Parkin patterns (fig. S3, D to F). In contrast, treatment of wild-type (wt) MEFs with carbonyl cyanide 4-(trifluoromethoxy)phenylhydrazone (FCCP) for 2 hours led to Parkin recruitment on the OM but not to the overlapping pattern (fig. S3G).

We next aimed to characterize the mitochondria with overlapping Parkin. Only one-third of mitochondria with overlapping Parkin had normal Tom20 signal, while the remaining had either decreased or no detectable Tom20 immunofluorescence (fig. S4, A and B). This raises the possibility of partial or complete degradation of the OM in a subset of mitochondria with overlapping Parkin. In contrast, the inner mitochondrial membrane markers MTCO1 and COX7B were fully intact in mitochondria with the overlapping-Parkin pattern (fig. S4, C to E), suggesting that the subset of mitochondria with overlapping Parkin that lack Tom20 staining have features of mitoplasts, where the inner mitochondrial membrane is preserved despite degradation of the OM (29). Parkin has been shown to mediate OM rupture, independent of mitophagy, leaving mitoplast-like structures behind (30). Alternatively, the subset of mitochondria with disrupted Tom20 immunofluorescence may actually be degrading mitochondria that retain normal immunoreactivity to mitochondrial matrix markers.

To confirm that Parkin did indeed enter mitochondria, we also performed immunostaining against Parkin. Using two separate Parkin antibodies, we first confirmed that Parkin immunofluorescence directly overlapped with GFP fluorescence ringing OM-Parkin

mitochondria (fig. S5, A to C). Moreover, we confirmed that Parkin immunofluorescence also localized to the matrix of many overlapping-Parkin mitochondria. Notably, the Parkin immunofluorescence failed to localize to a subset of overlapping-Parkin mitochondria, although the frequency of this differed depending on the antibody used, suggesting that Parkin either has a different conformation or has been partially degraded in a subset of the overlapping-Parkin mitochondria. In addition, the cytosolic GFP-Parkin fluorescence intensity was independent of the observed Parkin pattern (fig. S5D), indicating that the different patterns of GFP-Parkin distribution are not artifacts of expression level. Some cells contained mitochondria with all three patterns of Parkin distribution (OM, overlapping, and diffuse; fig. S5E).

We hypothesized that Parkin localizes to the OM of depolarized mitochondria, which might precede targeting to the matrix or the inner mitochondrial membrane, and hence that both OM and overlapping-Parkin mitochondria would be depolarized. To assess this, we examined mitochondrial membrane potential by tetramethyl-rhodamine methyl ester (TMRM) fluorescence before and after treatment with FCCP (2). Although most mitochondria with OM-localized Parkin were depolarized, ~25% were polarized (Fig. 3, E and F), consistent with Parkin being recruited to these mitochondria secondary to mitochondrial stress that occurs independent of depolarization (16, 31). In contrast, although some mitochondria with overlapping-Parkin were depolarized, many others were polarized and functional, as they maintained their membrane potential even after treatment with oligomycin, indicating that membrane potential was not being supported by reverse pumping of adenosine triphosphate (ATP) synthase with ATP hydrolysis (Fig. 3G).

These findings on mitochondrial membrane integrity, Parkin localization, and mitochondrial membrane potential all indicate that there are two subsets of mitochondria with overlapping-

Parkin patterns. Consistent with this, analysis of mitoKeima signals revealed a bimodal distribution; some overlapping-Parkin mitochondria had very high mitoKeima signals, while others had relatively low (but still elevated) mitoKeima signals consistent with mild acidification. In contrast, most mitochondria with OM-Parkin had low (neutral) mitoKeima signals (fig. S5, E and F). Despite these differences, in all populations of mitochondria with overlapping Parkin or OM-Parkin, the mitoKeima signal was present throughout the matrix, consistent with homogeneous pH throughout the matrix.

To define the ultrastructure of polarized and depolarized mitochondria with overlapping Parkin, we performed correlative light and electron microscopy (CLEM). Using this approach, we confirmed that polarized mitochondria containing overlapping Parkin are intact mitochondria with cristae with enhanced electron density and honeycomb or concentric onion patterns (Fig. 3H and fig. S5G), as can be observed in mitochondria from patients with mitochondrial disorders (32). In contrast, depolarized overlapping-Parkin mitochondria are actually degrading mitochondrial remnants that we hypothesized had been degraded by autophagy to form a mitolysosome, presumably explaining why some mitochondria with overlapping Parkin failed to exhibit immunoreactivity to the Parkin antibody.

Although GFP-Parkin is commonly used to study Parkin localization, its expression could potentially artificially amplify Parkin-dependent mitophagy. To verify that GFP-Parkin patterns are independent of overexpression, we also performed CLEM in neurons with only endogenous Parkin expression, using Parkin antibodies to detect recruitment patterns. With this approach, we were able to observe mitochondria with overlapping endogenous Parkin and intact cristae (fig. S5H). No mitochondria with overlapping endogenous Parkin were found to be degrading mitochondria structures, consistent with a disruption of Parkin conformation or degradation of

Parkin in these structures. Therefore, although the depolarized overlapping-Parkin mitochondria are indistinguishable from other mitochondria by typical mitochondrial markers (e.g., mito-BFP), they are actually in the process of degradation.

Parkin dynamically accumulates in functional and degrading mitochondria through distinct pathways

We next used time-lapse imaging to define the steps of Parkin recruitment to neuronal mitochondria. First, to delineate when lysosomal fusion occurs in relation to Parkin recruitment to the OM and matrix, we simultaneously tracked Parkin distribution with GFP-Parkin and mitochondrial acidity using mitoKeima. We found that Parkin accumulates on the OM of Drp1KO mitochondria with normal pH (Fig. 4, A and B). This pattern of OM-Parkin accumulation was maintained for 3.6 ± 0.4 hours (n = 11 mitochondria, means ± SEM; fig. S5I), before Parkin began to dissipate from the OM. Parkin dissipation occurred simultaneously with a marked increase in the acidity of the mitochondrial contents (Fig. 4, C and D). Following mitochondrial acidification, there was a rapid decrease in mitochondrial size, followed by the redistribution of Parkin to an overlapping pattern within ~80 min of OM-Parkin dissipation (Fig. 4D). Loss of OM-Parkin was invariably followed by the accumulation of overlapping Parkin in the acidic, shrunken mitochondrial structures (hereafter referred to as "indirect" overlapping-Parkin recruitment), previously identified by CLEM as degrading mitochondrial structures (Fig. 3H). These data suggest that conversion to the overlapping-Parkin pattern via the indirect pathway marks the fusion with lysosomes and the associated transition to a mitolysosome.

Notably, Parkin also accumulated in the matrix of mitochondria directly, without passing through a stage of OM-Parkin (Fig. 4, E and F). In these instances, Parkin began accumulating in

the matrix of mitochondria with normal pH. However, direct Parkin recruitment to the matrix occurred more slowly than indirect recruitment to the overlapping pattern via the OM, taking 14.5 ± 0.6 hours (n = 23 mitochondria, means ± SEM) to reach maximal recruitment, during which time the mitochondria also gradually became mildly acidic. This suggests that the mildly acidified overlapping-Parkin mitochondria are the larger intact mitochondria with preserved mitochondrial membrane potential (Fig. 3E) that we visualized by CLEM (Fig. 3H and fig. S5G). To further confirm this, we performed CLEM on mitochondria expressing mitoKeima and showed that small highly acidic mitochondria with overlapping Parkin are mitolysosomes, while larger mitochondria with lower acidity are intact mitochondria (Fig. 4G). Preserved mitochondrial membrane potential in the context of mild acidification may suggest partial lysosomal fusion or ion channel–driven changes (33). In contrast, when Parkin recruitment to the OM precedes mitochondrial acidification, Parkin triggers mitochondrial acidification by initiating lysosomal fusion, ultimately leading to mitochondrial degradation.

During direct recruitment of matrix-Parkin, we also observed large, repetitive fluctuations in GFP-Parkin fluorescence (hereafter called “Parkin spikes”), suggesting rapid and repetitive bursts of Parkin entry and exit from the mitochondrial matrix (Fig. 4, H and I). These fluctuations were observed in ~26% (6 of 23) of cases of direct matrix-Parkin recruitment, with the individual spikes occurring on average every 3.2 ± 0.3 hours (n = 6 mitochondria, means ± SEM) and lasting less than 40 min each (Fig. 4, H and I, and fig. S6). The spikes of Parkin entry were strongly correlated with small but sharp decreases in mitochondrial acidity ($r = -0.77$, $P < 0.001$; Fig. 4J), indicating that Parkin accumulation is intimately associated with mitochondrial pH, although it remains unclear whether matrix-Parkin triggers or resolves the acidification. Notably, loss of GFP-Parkin fluorescence was not due to quenching of GFP fluorescence at low

pH, as we observed far higher mitoKeima signals indicative of low mitochondrial pH without any loss of GFP fluorescence in other mitochondria. The rapid fluctuations in acidity may be mediated by direct fusion with lysosomes at points of transient contact between lysosomes and mitochondria (34), although we cannot exclude the possibility of fusion with already acidified mitochondria (see below) or other ion channel–driven changes (33). Regardless of the mechanism, the existence of Parkin spikes establishes that both Parkin recruitment to mitochondria and mitochondrial acidification are not always irreversible processes.

Mitochondria with indirect Parkin recruitment are degraded by autophagy

We next assessed whether mitochondria with indirect overlapping-Parkin accumulation undergo canonical macroautophagy in which they are engulfed by autophagosomes to produce mitophagosomes, before fusing with lysosomes to form mitolysosomes. To visualize and define the kinetics of autophagosome formation and fusion with lysosomes, we examined GFP-LC3 localization at different stages following indirect overlapping-Parkin recruitment. No GFP-LC3 accumulation on Drp1KO mitochondria was visible at baseline, indicating either that Drp1KO mitochondria are degraded independent of microtubule-associated protein 1A/1B-light chain 3 (LC3) or that degradation occurs too rapidly for detection. In support of the latter, after a 4-hour treatment with the autophagy inhibitor bafilomycin, GFP-LC3 accumulated on a subset of LAMP1-circled Drp1KO mitochondria (Fig. 5A). In addition, of all GFP-LC3–positive mitochondria, most (~90%) were also encircled by LAMP1 (Fig. 5B), suggesting that lysosomal fusion occurs rapidly once autophagosomes are formed. Conversely, only ~30% of mitochondria encircled by LAMP1 were also encircled by GFP-LC3 (Fig. 5C), suggesting that LC3 on the inner autophagosome membrane is rapidly degraded following lysosomal fusion (35, 36). Subsequent time-lapse imaging showed that LC3 accumulates in a discrete spot on the OM of

OM-Parkin mitochondria, presumably representing the autophagosome formation site (37), before forming a ring around the organelle to seal the mitophagosome (Fig. 5D). After Parkin transitions to the overlapping pattern (i.e., after lysosomal fusion to form the mitolysosome), GFP-LC3 again rapidly clustered into a discrete punctum on the outer membrane of the mitophagosome before dissipating.

Notably, an additional ~20% of swollen Drp1KO mitochondria had a distinct overlapping pattern of LC3, suggestive of LC3 accumulation within mitochondria, while ~50% of LAMP1-circled mitochondria did not have any GFP-LC3 accumulation (Fig. 5C). These different patterns of GFP-LC3 distribution occurred independently of the level of GFP-LC3 in the cytosol (fig. S7A), indicating that the overlapping pattern is not an artifact of LC3 overexpression. To gain insight into the differences between mitochondria with distinct patterns of LC3 and Parkin accumulation, we again used CLEM. This confirmed that the mitochondria with ringing patterns of LC3 accumulation are indeed mitochondria encircled by autophagosomes (i.e., mitophagosomes; Fig. 5E, top). Therefore, degrading Drp1KO mitochondria up to at least 2 to 3 μm are engulfed by autophagosomes, but the structures are very short-lived. Time-lapse imaging confirmed that LAMP1 recruitment occurs rapidly and coincides with the transition from OM to overlapping Parkin after autophagosome formation (Fig. 5, D and F), while CLEM showed LAMP1 circling a degrading mitochondrion with overlapping Parkin (Fig. 5G). Thus, the acidic degrading mitochondrial structures that emerge from the indirect pathway are LAMP1 positive and depolarized, further confirming that they are indeed mitolysosomes. Conversely, and of particular interest, overlapping-Parkin mitochondria with the overlapping LC3 and LAMP1-circled patterns appear to be intact mitochondria packed with electron-dense cristae (Fig. 5E, bottom), perhaps suggestive of either stalled degradation or an alternate degradation pathway. To

assess the requirement for PINK1 in this LC3 accumulation, we examined GFP-LC3 in Drp1KO;PINK1KO neurons (Fig. 5, H and I). Without PINK1, most LAMP1-circled mitochondria had the overlapping pattern of GFP-LC3, and few had the LC3-circling or no-LC3 pattern, indicating that simultaneous accumulation of LAMP1 and the circling pattern of LC3 on the OM requires PINK1. It remains unclear how LC3 is recruited to the overlapping pattern, but this LC3 recruitment in the absence of PINK1 suggests that the overlapping pattern of GFP-LC3 may represent an as-yet undefined secondary quality control pathway. Notably, follow-up CLEM experiments to visualize the ultrastructure of mitochondria circled by endogenous LC3 revealed short stretches of membranes adjacent to the mitochondria rather than the intact autophagosome membranes visualized using GFP-LC3 (fig. S7B). This may be due to autophagosome membrane damage incurred during membrane permeabilization for antibody staining. However, we cannot exclude the possibility that GFP-LC3 promotes the formation of autophagosome membranes that are distinct from those formed by endogenous LC3. We similarly failed to visualize either Drp1KO or Drp1KO-PINK1KO mitochondria with the overlapping pattern of endogenous LC3. Hence, further characterization of LC3 action using endogenous markers is required.

Parkin is targeted into mitochondria in wt neurons

We also tested whether Parkin dynamics and mitochondrial acidification occur similarly in wt neurons. At baseline, most mitochondria in wt neurons had diffuse Parkin, while only occasional mitochondria had either OM or overlapping-Parkin patterns. However, treatment with either the oxidative stressor paraquat or deferoxamine (DFO), an iron chelator that can trigger mitophagy (38), caused robust Parkin recruitment in both the OM and the overlapping patterns (fig. S8, A and B). Moreover, consistent with the Drp1KO mitochondria, ≈2/3 of wt mitochondria with overlapping Parkin had either decreased or absent Tom20

immunofluorescence (fig. S8C), while the intensity of the inner mitochondrial marker MTCO1 was similar in mitochondria with and without Parkin accumulation (fig. S8D). Similar to Drp1KO mitochondria, time-lapse imaging showed that, following treatment with DFO, Parkin moved from the OM to an overlapping pattern in a subset of wt mitochondria, with a concomitant increase in acidity (fig. S8E). Notably, although much harder to detect, we also observed direct Parkin recruitment in wt neurons in response to DFO (fig. S8F), and the overlapping pattern of Parkin recruitment was also visualized with endogenous Parkin (fig. S8G).

A subset of mitolysosomes is engulfed by polarized mitochondria

The fate of mitolysosomes is poorly understood, especially in neurons. To delineate their fates, we tracked individual mitolysosomes over time. Mitochondria with indirect Parkin recruitment were identified on the basis of direct visualization of the OM-Parkin to overlapping-Parkin pattern transition and followed for an additional 2.3 to 19.7 hours following conversion into mitolysosomes. Unexpectedly, during this period, the mitolysosomes not only made repeated contacts with nonacidified mitochondria (visualized in 55 ± 7.2% of images, n = 12 mitochondria, means ± SEM) but also fused with and were periodically engulfed by seemingly healthy mitochondria with neutral pH (5 of 12 mitochondria engulfed; Fig. 6A). In some cases, these interactions were temporary, as mitolysosomes were observed to emerge from mitochondria after being engulfed (fig. S9A). Although the function of these interactions remains unclear, they may represent a mechanism to recycle mitochondrial components. If so, recipient mitochondria would presumably be functional. To test this, we used TMRM to track mitochondrial membrane potential during engulfment of overlapping-Parkin mitochondria. We observed engulfment of a depolarized overlapping-Parkin mitochondrion by a polarized,

mitoBFP-positive mitochondrion (Fig. 6B). This indicates that mitochondria with overlapping Parkin can be engulfed by functional mitochondria, although the short half-life of TMRM dye limited our ability to quantify this phenomenon.

We next used CLEM to visualize the ultrastructure of internalized mitochondria. Analysis of a mitochondrion containing a region of increased acidity (based on mitoKeima signal) revealed an internal double-membrane structure enclosing mitochondrial remnants (Fig. 6C). Using EM, we observed healthy-appearing mitochondria (based on intact cristae morphology) containing membrane-bound structures with degraded contents resembling mitolysosomes (Fig. 6D), which we hypothesize may have been engulfed. We also observed a depolarized mitochondrion with GFP-Parkin–positive, membrane-bound structures (fig. S9B). The presence of the GFP reporter suggests that these membrane-bound structures underwent Parkin-mediated degradation before being engulfed by the recipient mitochondria. Notably, we also observed mitochondrial engulfment in wt neurons, where mitochondria with acidified overlapping-Parkin patterns contacted and were engulfed by other nonacidified mitochondria (fig. S9, C and D). However, only a limited number of mitochondria could be definitively tracked in wt neurons because of their small size and greater number and mobility.

Mitolysosomes persist and dynamically interact with other mitochondria

We hypothesized that mitochondrial engulfment of mitolysosomes enables the recycling of mitochondrial materials. Moreover, some materials may no longer be useful to mitochondria but still useful to other cellular functions, while other materials may need complete degradation. However, we found that mitolysosomes are stable structures, making it difficult to determine their fates. None of the definitively identified indirect overlapping-Parkin mitolysosomes tracked

for at least 5 hours (and up to 19.7) underwent notable change in morphology or acidity or loss of expression of the targeted fluorescent probes, following the OM- to overlapping-Parkin transition over the duration of the imaging period (0 of 11), indicating that mitochondrial degradation in neurons is often a slow process.

To better assess their fates, we tracked mitolysosomes at a later stage by selecting mitochondria that already had overlapping-Parkin localization at the start of the live imaging session, instead of trying to capture both the recruitment and fate in a single session. Although we did not directly visualize whether Parkin onset was direct or indirect in these mitochondria, most were both acidified (high mitoKeima signal) and small in size, suggesting that they were predominantly mitolysosomes in the indirect pathway (Fig. 7A). In ~41% of the cases, GFP-Parkin remained localized in the mitolysosomes for the entire imaging session (12 to 21 hours), and the mitochondrial pH was stable, showing only a small decrease in acidity (Fig. 7, B and C), suggesting that mitolysosomes can maintain a stable status for many hours. In another ~43% of cases, the mitolysosomes underwent a sudden, large decrease in signal of both mitoKeima channels and of GFP-Parkin intensity, which coincided with a decrease in size (Fig. 7, B, D, and E), presumably reflecting lysosomal membrane permeabilization or rupture and diffusion of degrading materials into the cytosol. This phenomenon was not unique to Drp1KO mitochondria, as we also observed it in wt neurons (fig. S10A). If this resulted from bursting of mitolysosomes, we reasoned that it should be accompanied by an increase of emitted fluorescent signal in the cytosol. To test this, we measured cytosolic Keima signals, given that they are low at baseline and would therefore allow for the detection of even a small change in signal. We observed a sharp increase in cytosolic Keima fluorescence in both channels (Fig. 7, F and G) that occurred

simultaneously with the decrease in mitolysosome size and signal, strongly supporting that mitolysosomes do indeed release partially degraded materials into the cytosol.

In ~50% of these bursting cases, the mitolysosomes vanished following bursting (fig. S10B), suggesting complete degradation, while in the others, a remnant structure persisted for the duration of the imaging session (up to 15.3 hours) (Fig. 7E). In most cases, the mitolysosome pH partially normalized in the few hours preceding bursting (Fig. 7D), indicative of lysosomal deacidification that may prevent the release of potentially harmful acidic contents into the cytosol. Thus, some mitochondrial proteins can withstand the acidity of the lysosome for several hours before getting released to the cytosol.

In the remaining ~15% of mitolysosomes, mitoKeima fluorescence persisted, but the Parkin signal gradually dissipated (Fig. 7, B, H, and I). Unexpectedly, a subset of these structures partially or fully normalized their pH following Parkin dissipation. The mechanism of this pH normalization remains to be defined and could involve increased proton leakage and inhibition of lysosomal acidification (39). However, live imaging showed that the mitolysosomes normalized their pH as they made repeated contacts with both adjacent mitolysosomes and neutral mitochondria (Fig. 7J and fig. S10C). This raises the possibility that these contacts may also contribute to the deacidification by enabling the transfer of partially degraded mitochondrial contents (fig. S10, D and E).

2.3 Discussion

Disruption in mitochondrial quality control is implicated in the pathophysiology of PD and other neurodegenerative diseases, but little is known about the fate of degrading mitochondrial

contents in neurons. Here, we simultaneously tracked the acidity and fate of individual mitochondria for up to 21 hours, taking advantage of the enlarged, segregated, and relatively immobile nature of Drp1KO mitochondria in neurons. We identified distinct patterns of Parkin recruitment to mitochondria and delineated the specific sequence and timing by which mitochondria are degraded in Drp1KO and wt neurons. We found that following fusion of mitophagosomes with lysosomes, the resulting acidic mitolysosomes continue to actively interact with other healthy mitochondria for many hours and are sometimes engulfed by functional mitochondria. Moreover, a subset eventually normalize their pH, burst, and release their contents into the cytosol (Fig. 8).

Loss of mitochondrial fission promotes PINK1-dependent mitochondrial quality control in DA neurons

Fission is thought to be required for mitochondrial turnover. However, we found that Drp1KO increases the Parkin- and PINK1-dependent engulfment of even very large mitochondria by autophagosomes to produce mitophagosomes, as well as their subsequent fusion and acidification by lysosomes to form mitolysosomes. Therefore, in contrast to previous reports in other cell types (13, 40), Drp1KO increases mitophagy in neurons. Our finding that Drp1KO mitochondria continue to be degraded is in line with the finding that Drp1KO DA neurons and MEFs have decreased (rather than increased) mitochondrial content (2, 14) and that Drp1KO increases the number of acidified mitochondria in HeLa cells (16). Moreover, ongoing turnover indicates that primary mitochondrial dysfunction is the cause of increased toxicity in Drp1KO neurons and suggests that the toxicity of Drp1KO is not due to a primary deficit in mitochondrial degradation.

The findings that PINK1 protects against Drp1KO toxicity and that loss of PINK1 decreases Drp1KO-induced mitochondrial acidification and membrane potential suggest that PINK1-mediated mitochondrial quality control is critical in protecting against toxic Drp1KO mitochondria. However, the mechanism by which Drp1KO triggers mitochondrial dysfunction and increased turnover is unknown. Previous work suggested that Drp1 may protect against unchecked PINK1-Parkin activity (16); however, this is seemingly inconsistent with our finding that concurrent loss of Drp1 and PINK1 is more toxic than loss of Drp1 alone.

Our data also clarify the epistatic relationship between Drp1KO and PINK1 KO. The synergistic toxicity of PINK1 and Drp1 loss in Drosophila (7, 41) is preserved in mice, but the effect is independent of mitochondrial morphology. This likely explains the variable effects of PINK1 KO on mitochondrial morphology in mammalian cell culture (9, 10, 41–43). Our in vivo system is among the most robust examples of PINK1 KO toxicity in a mouse model. Although PINK1 KO alone fails to produce neurodegeneration or affect survival in mice (22, 42), it increases toxicity of A53T synuclein in vivo (44) and the size of mitochondrial inclusions (45, 46). Notably, inhibiting Drp1 with the small molecule mdivi-1 or expression of a dominant negative Drp1 normalizes decreased striatal DA release in PINK1 KO mice (47). Several important differences in experimental design likely explain these contrasting results, including that Rappold et al. assessed partial inhibition of Drp1 function. Mdivi-1 also has potent antioxidant effects that may be more prominent than its effects on mitochondrial morphology, and the effects of mdivi-1 may differ from Drp1KO (48). In addition, we assayed neurodegeneration of DA neurons, whereas Rappold et al. assessed changes in DA homeostasis, which may represent compensatory changes rather than toxicity.

Parkin accumulates in mitochondria through distinct pathways

We found that Parkin is targeted into mitochondria through two distinct pathways (Fig. 8). In the indirect pathway, depolarized mitochondria first accumulate Parkin on their OM. This is followed by engulfment by an autophagosome, rapid fusion with lysosomes, and acidification to form a mitolysosome, with concurrent redistribution of Parkin across the OM into the degrading mitochondria. Although hypothesized based on work in cell lines, this temporal sequence of events has not previously been directly visualized and correlated with the cellular ultrastructure in individual mitochondria. We found that the indirect pathway occurs both in Drp1KO mitochondria and in wt mitochondria exposed to stressors. In the "direct" pathway, polarized mitochondria directly accumulate Parkin, without any apparent preceding accumulation on the OM. Notably, we also tried to track the fates of these intact, mildly acidic, and polarized mitochondria with direct overlapping-Parkin mitochondria. However, the long duration of direct Parkin recruitment precluded us from following the fates of mitochondria with proven direct Parkin recruitment. Understanding the fates and function of this subset of mitochondria will be an important subject for future studies. We also found that direct overlapping-Parkin accumulation occurs in wt neurons, supporting that the direct pathway is not only a unique response to loss of mitochondrial fission but also occurs normally and in response to other stressors in wt neurons.

Mitochondria with direct Parkin recruitment have an intact OM, supporting that Parkin internalization into mitochondria is not contingent on membrane rupture. Once inside mitochondria, Parkin may accumulate on the outer surface of the inner mitochondrial membrane. Alternatively, Parkin may be imported into the mitochondrial matrix, as demonstrated in proliferating cells using biochemical approaches and immunoEM (49). We found that many

mitochondria with the overlapping-Parkin pattern were polarized, indicating an intact membrane potential (50). Although Parkin is not predicted to have a mitochondrial targeting sequence, mitochondrial import might be mediated through interactions with other mitochondrial-targeted proteins, analogous to peroxisomal targeting receptors that import cytosolic proteins into the peroxisome matrix (51). Such a function is proposed for Klokin1, a splice variant of human chondroitin polymerizing factor (ChPF), that was found to transport Parkin to the mitochondrial matrix during the cell cycle (52). Other proteins may also contribute, for instance, F-box protein 7, which both binds and translocates Parkin to mitochondria and also enters and forms aggregates within mitochondria (53, 54). However, we speculate that some mitochondria may internalize Parkin as a by-product of engulfing or fusing with mitolysosomes, perhaps explaining why mitochondria in the direct pathway are far less acidic than the degrading mitolysosomes in the indirect pathway. If true, mitochondria in the "direct pathway" may be a downstream consequence of mitolysosomes formed by canonical mitophagy in the "indirect pathway." Notably, regardless of their origin, overlapping-Parkin mitochondria in the direct pathway retain polarization and at least partial function even after mild acidification, consistent with the finding that mitochondria can retain function in acidic environments (55, 56).

Mitolysosomes are dynamic structures with distinct fates

Although the machinery driving PINK1/Parkin-based mitophagy has been extensively studied, there is very little known regarding the kinetics of this process, especially in neurons, presumably because there has been no means to track individual mitochondria for prolonged periods of time. Hence, studies have primarily relied on snapshots of population-based changes following the administration of mitochondrial toxins or other stressors, as well as short imaging sessions visualizing individual steps such as Parkin recruitment, which have limited ability to

determine the timing and sequence of events in individual neurons. Here, we took advantage of the decreased mobility and large size of Drp1KO mitochondria, combined with the decreased total number of mitochondria in Drp1KO neurons, to track individual mitochondria for up to 21 hours, which allowed us to visualize key steps in the mitochondrial life cycle and define their kinetics. Moreover, we used a genetic model (Drp1KO) that produces a nonlethal stressor and drives mitophagy in only a fraction of mitochondria in a fraction of cells at any given time, presumably better recapitulating mitochondrial turnover in normal biology and in neurodegeneration in PD. These studies provided several important insights. First, we confirmed the proposed sequence of events in which depolarized mitochondria destined for degradation are first coated with OM-Parkin before being engulfed by an autophagosome and then acidified following lysosomal fusion. In addition, we defined the precise kinetics of this pathway, showing that autophagosome recruitment is followed rapidly (≈30 min) by lysosomal recruitment and fusion leading to acidification, Parkin redistribution, and formation of the mitolysosome. Notably, these findings differ from those of a recent study that used LysoTracker, superecliptic pHluorin (SEP)–LAMP1-RFP, and mitochondria-targeted EGFP-mCherry reporters to conclude that mitochondrial acidification is a very slow process that takes several hours following mitophagosome formation and LAMP1 accumulation (57). We hypothesize that these discrepant findings result from differences in the sensitivity of methodologies used to detect acidification, as we found that GFP and other mitochondrial-targeted fluorescent reporters continued to fluoresce even after acidification (as detected by mitoKeima and the circling of mitochondria by LAMP1) occurred due to formation of mitolysosomes. Tracking the time course of acidification in individual mitochondria, as opposed to snapshots at discrete time points, may also have

increased sensitivity, but further experiments will be required to determine whether these or other differences in the experimental paradigms underlie the discrepant results.

Our studies also used longitudinal tracking to provide some of the first insights into the fates of mitolysosomes. Fusion of mitochondria with lysosomes has been generally considered to inevitably lead to rapid and complete degradation. However, we found that ≈40% of mitolysosomes survived throughout the imaging period (≈12 to 21 hours), during which time they dynamically contacted other mitochondria. In some cases, these contacts may regulate mitochondrial motility (58), while in others, they may lead to transfer of contents, perhaps as a means of recycling mitochondrial components. A subset of mitolysosomes were fully engulfed by other mitochondria, an intriguing but perhaps not unexpected finding given the evolutionary origin of mitochondria as an endosymbiotic bacterium integrated into cells (59). We hypothesize that such events represent a mechanism to enable the recycling of mitochondrial contents, which may be a more efficient process than fully degrading mitochondria before rebuilding them.

Another subset of mitolysosomes suddenly burst and released their contents into the cytosol, which could enable some contents to be reused by other organelles and others to be degraded further by the proteosome. Notably, although lysosomes are known to release recycled amino acids and other nutrients (60), we show that at least some proteins (i.e., the mitochondrial-targeted fluorescent reporters) are not fully broken down but rather released in a functional state. Understanding which mitochondrial contents are degraded and to what extent, as well as what triggers the release of mitochondrial contents, will be of great interest. Notably, the pH of these mitolysosomes partially normalized before bursting, potentially representing a mechanism to avoid damaging cellular structures when the contents are released. Moreover, the cytosolic release of mitochondrial contents may also represent a key mechanism by which mitochondrial

contents enter the cytosol to trigger cell signaling pathways, including those involved in innate immunity and cell death (61–65). Recent evidence shows that chemically induced lysosomal rupture recruits the PD protein LRRK2 to lysosomes, further suggesting that a disruption in mitolysosome processing may be relevant to PD pathophysiology (66).

Last, a subset of mitolysosomes persisted for hours even after GFP-Parkin fluorescence dissipated and partially normalized their pH over time. The significance of this pH normalization is unclear, but we speculate that it reflects compensatory mechanisms to decrease lysosomal catabolism in the face of chronic mitochondrial dysfunction, to preserve residual mitochondria that are needed to sustain energy levels (67). It remains unclear whether these mitolysosomes eventually release their contents as well or if they have distinct fates from those mitolysosomes that burst.

In contrast, mitochondria in the direct pathway were larger and less acidic than those that first recruit Parkin to the OM, suggesting that these are distinct pathways. Mitochondria in the direct pathway may be healthy or mildly damaged mitochondria that have either engulfed or transiently fused with mitolysosomes. We speculate that these mitochondria have undergone targeted repair, consistent with prior work suggesting that the incorporation of lysosomal proteins within mitochondria may promote the elimination of oxidized mitochondrial proteins (68, 69). However, their slow accumulation of Parkin over many hours precluded us from determining their fates, which will require longer-term analysis.

Conclusions and questions

Critical questions raised by our findings include understanding how and why mitolysosomes fuse with and are engulfed by mitochondria, including the extent to which mitochondrial

contents are recycled through these processes. It will also be important to better define the process by which mitolysosomes burst and whether this facilitates recycling of degraded mitochondrial contents and degradation of nonrecyclable components. Particularly important will be understanding how and when these processes are required for neuronal health and survival. PINK1 and Parkin do not appear necessary for mitochondrial turnover in neurons, since loss of either Parkin or PINK1 does not affect mitochondrial content, and both PINK1 and Parkin KO mice are viable, indicating that alternative pathways compensate when they are lost. However, our data with PINK1 KO mice, and other findings with Parkin KO mice (70), suggest that these compensatory processes are insufficient when mitochondria are damaged and require increased turnover. The engulfment of mitolysosomes by mitochondria may represent a mechanism to recycle mitochondrial contents when mitochondria cannot be repaired and an opportunity to strengthen or repair the recipient mitochondria. Moreover, Parkin and PINK1 may also have specific functions in the matrix such as enhancing mitochondrial transcription to promote biogenesis (49, 52) or initiating quality control pathways by ubiquitinating specific matrix proteins. Such a mechanism might explain how Parkin KO differentially increases the half-life of mitochondrial proteins in Drosophila heads, including proteins in the matrix (71, 72).

In summary, our results not only define a distinct mitochondrial life cycle in neurons wherein mitolysosomes remain dynamically active for long periods but also reveal mechanisms that may enable cells to salvage and reuse components of damaged mitochondria. At the same time, our findings also show that at least a subset of proteins can remain functional in mitolysosomes despite being acidified, and the presence of these mitochondrial proteins and reporters may lead to the misidentification of mitolysosomes as intact mitochondria. Further research is required to determine whether the mechanisms of mitochondrial quality control we delineate here, including

the release of mitochondrial contents into the cytosol, may initiate immune and other signaling pathways and contribute to the selective vulnerability of neurons to PINK1 and Parkin mutations.

2.4 Methods

Molecular biology

AAV2/1.CMV.PI.Cre.RBG was purchased from Penn Vector Core (Philadelphia, PA). Drp1 shRNA-smCBA-mTagBFP2 was cloned into the pTR-CBA eGFP vector to replace eGFP [Drp1-targeting shRNA was a gift of S. Strack, University of Iowa (73)]. The following constructs were previously cloned into the pCAGGS vector downstream of the chicken actin promoter: ATP-YEMK (gift of H. Noji, Osaka University) (74), Cre recombinase (2), EGFP-LC3 (Addgene), mitoGFP (4), and mitoTagBFP (2). mitoFarRed was generated by fusing TagRFP657 [gift from V. Verkhusha (Albert Einstein)] to the mitochondria-targeting sequence, cytochrome C oxidase subunit VIII (75, 76), and mitoKeima was generated by cloning mito-mKeima from pIND-mito-mKeima (gift of A. Miyawaki) into pCAGGs. OM-GFP was made by fusing the OM-targeting sequence of rat Tom20 to GFP (77). GFP-Parkin was made by fusing GFP to Parkin (gift from A. Abeliovich, Columbia) and Matrix-roGFP from Addgene. pGW1-mitoEOS2 was cloned into the pGW1 from pEOS2-mito.

Mice

Following procedures previously described in (2), mice were group-housed in a colony maintained with a standard 12-hour light/dark cycle and given food and water ad libitum. All mice received food on the cage floor. Experiments were performed on age-matched mice of either sex, with the specific number of males and females matched between groups in each experiment (typically divided 50:50 between males and females). No differences between sexes

were noted in any of the experiments. Experiments were conducted in accordance with the Guide for the Care and Use of Laboratory Animals, as adopted by the National Institutes of Health (NIH), and with approval of the University of California, San Francisco Institutional Animal Care and Use Committee. Drp1lox/lox and ATG5lox/lox mice were maintained on the original mixed C57Bl/6 and 129/SvEv background. All other mouse lines were maintained on a pure C57Bl/6 background (the Jackson laboratory; RRID:IMSR_JAX:000664). Floxed Drp1KO mice (78) and PINK1 KO mice (46) have been described. DATcre mice (79) and Parkin KO mice (Stock No: 006582) were obtained from the Jackson laboratory.

Primary neuronal cultures

Primary hippocampal cultures were prepared from early postnatal (P0 to P1) mouse or rat pups of both sexes as described (2, 80). Neurons were transfected via electroporation (Amaxa) with the relevant constructs and cultured in minimum essential medium (MEM) Eagle's with Earle's balanced salt solution medium (UCSF Cell Culture Facility, CCFAC001) supplemented with 5% fetal bovine serum (HyClone, SH3007103), 21 mM glucose, 1% Glutamax (Gibco, 175007), 2% B27 supplement (Gibco, 17504-044), and 0.1% serum extender (Thermo Fisher Scientific, 355006). Neurons were plated at 600 to 900 cells/mm2, and uridine (10 μM, Sigma-Aldrich, U3750) was added on day 4 to minimize glial overgrowth. Neurons were cultured at 37°C and 5% CO2 for 9 to 11 days before live imaging or fixation.

Cell line

Immortalized Drp1KO MEFs were cultured in DMEM-H (UCSF Cell Culture Facility) containing 10% fetal bovine serum (JR Scientific) and penicillin-streptomycin at 37°C and 5% CO2 before live imaging or analysis.

Stereotaxic recombinant adeno-associated virus injection

For stereotaxic injection of AAV2/1.CMV.PI.Cre.RBG, 6- to 8-month-old Drp1wt/wt mice, Drp1lox/lox mice, and PINK1 KO and Drp1lox/lox PINK1 KO mice were used. Mice were anesthetized with ketamine/xylazine, and their skulls were immobilized with a stereotaxic frame (Kopf). A 0.5-μl volume of AAVcre (2.16 × 1013 genome copies/ml) was injected using a Hamilton syringe and a cannula (33 gauge) unilaterally into the SN/VTA (anteroposterior, −3.0 mm from bregma; mediolateral, 1.1 mm; dorsoventral, 4.3 mm) at a rate of 0.2 μl/min (2, 81). Animals were sacrificed 2 months after injection.

Histology

Mice were anesthetized and perfused with phosphate-buffered saline (PBS) and then 4% paraformaldehyde (PFA). Brains were removed, postfixed, cryoprotected in 30% sucrose, and frozen in isopentane. Coronal sections of 40-μm thickness were cut on a cryostat throughout the brain, including the SNc/VTA, and every sixth section was analyzed. Cells were fixed for 15 min in medium with 4% PFA.

For immunofluorescence, brain section and cells were rinsed with PBS and transferred in blocking solution containing either 0.2% Triton X-100 or 0.01% for CLEM, with either 3 to 5% bovine serum albumin or 5 to 10% goat serum for 1 hour. Samples were then incubated overnight at room temperature (RT) or for 24 to 48 hours at 4°C, with the appropriate primary antibody in blocking solution.

The following primary antibodies were used: rabbit anti-Tom20 (1:1000 to 1500; Santa Cruz Biotechnology, catalog no. SC-11415, RRID:AB_2207533), rabbit anti-COX7B (1:100; Abcam,

catalog no. ab137094), mouse anti-PDH (1:200 to 1500; Abcam, catalog no. ab110333, RRID:AB_10862029) (24), mouse anti-MTCO1 (1:1000; Abcam, catalog no. ab14705, RRID:AB_2084810), rat anti-Lamp1 (1:400; BD Pharmingen, catalog no. 553792, RRID:AB_2134499), or anti-TH (mouse; 1:20,000; EMD Millipore, catalog no. MAB318, RRID:AB_2201528; or rabbit, 1:1000; Millipore, catalog no. AB152, RRID:AB_390204). Sections were rinsed and incubated for 2 hours with the appropriate secondary antibodies as follows: Alexa Fluor 488, 594, 568, or 647 anti-mouse, anti-rat, or anti-rabbit immunoglobulin G (IgG) (1:400; Invitrogen). Samples were rinsed in PBS, and coverslips were mounted on glass slides immerged in ProLong Gold Antifade Mountant (Thermo Fisher Scientific, #P36934) and stored at 4°C.

Immunofluorescence samples were imaged and analyzed with the examiner blind to the genotype using either a laser scanning confocal microscope (Zeiss LSM 880 with Airyscan or LSM510-Meta, Carl Zeiss) equipped with 63× [1.4 numerical aperture (NA)] and 100× (1.3 NA) PlanApo objectives or with 10× (0.3 NA) and 100× oil immersion (1.4 NA) objectives, respectively, on a Nikon Ti-E inverted microscope with an Andor iXon EMCCD camera. Confocal z-stacks of individual mitochondria were acquired using the optimal step size (0.25 or 0.4 μm) along the mitochondrial thickness (2 to 5 μm). The exposure time to acquire images was calculated to make the z-stack duration to be less than 5 s, and the images were reconstructed with Zen Lite software (Zeiss).

For peroxidase experiments, sections were incubated with rabbit polyclonal anti-TH and visualized with biotinylated goat anti-rabbit IgG (1:300, Vector Laboratories, Burlingame, CA; BA-1000, RRID:AB_2313606), followed by streptavidin-conjugated horseradish peroxidase

(1:300; Vectastain ABC kit, Vector Laboratories). Positive immunostaining was visualized with 3,3′-diaminobenzidine (Sigma-Aldrich) after reaction with hydrogen peroxide.

Stereology

Total numbers of TH-positive neurons in the SNc and VTA were quantified with the examiner blind to the genotype using a computer-assisted image analysis system, consisting of an Olympus BX-51 microscope equipped with an XYZ computer-controlled motorized stage and a SIA-L9C digital camera (Scientific Instruments and Applications, Duluth, GA), and counted using the Optical Fractionator probe of Stereo Investigator software (MicroBrightfield, Williston, VT; RRID:nif-0000-00110).The numbers of TH-stained cells were counted at high power (100× oil; NA 1.4) using a 75 mm by 75 mm counting frame as described (2).

Correlative light and electron microscopy

Primary neurons cultured on gridded 35-mm MatTek glass-bottom dishes (MatTek Corp., Ashland, MA, USA) were imaged using a fluorescence microscope and then fixed in 2% glutaraldehyde and 2% PFA in phosphate buffer (pH 7.4) (EMS, Hatfield, PA, USA). Samples were washed (3×; 5 min, RT) in 0.1 M sodium cacodylate buffer (pH 7.2) and covered in 1% osmium tetroxide with 1.6% potassium ferricyanide in 0.1 M sodium cacodylate buffer for 30 min. Samples were washed (3×; 5 min, RT) in buffer and then in distilled water (1×; 5 min, RT). Samples were then put through an ascending ethanol gradient (7 min; 35, 50, 70, 80, and 90%) followed by pure ethanol (2×; 5 min, RT). Samples were incubated with Epon resin (EMS, Hatfield, PA, USA) and polymerized at 60°C for 24 hours. The glass coverslips were then removed using ultrathin Personna razor blades (EMS, Hatfield, PA, USA) and liquid nitrogen exposure as needed. The gridded alphanumerical labeling was used to identify regions of interest

that were dissected out and mounted for sectioning using cyanoacrylate glue. A Leica UC6 Ultramicrotome (Leica, Wetzlar, Germany) was used to cut thin sections (100 nm) from the surface of the block until reaching a depth of 4 to 5 μm to ensure full cell coverage. Formvar-coated 50-mesh copper grids were used to collect serial sections and were poststained with 2% uranyl acetate followed by Reynold's lead citrate, for 5 min each. Imaging was performed using a Tecnai 12 120-kV transmission electron microscope (FEI, Hillsboro, OR, USA), and data were recorded using UltraScan 1000 with Digital Micrograph 3 software (Gatan Inc., Pleasanton, CA, USA).

Live imaging

Magic Red

For cathepsin B activity assays, neurons were incubated with Magic Red (a cathepsin B substrate, ImmunoChemistry, #937) for 1 hour at 37°C before live imaging (572/35 excitation and 632/60 emission).

mito-roGFP

For mito-roGFP experiments, sequential images were acquired at 402/15 excitation and 535/50 emission and 490/20 excitation and 535/50 emission. Background was subtracted, and images were created on the basis of the ratio of the 402-nm/490-nm images on a pixel-per-pixel basis. To calibrate the assay, 2 mM dithiothreitol was used to fully reduce the mitochondria and determine the minimum fluorescence ratio and 100 μM Aldrithiol (DPS) to oxidize the mitochondria for the maximum value (82).

Mitochondrial membrane potential

Neurons were pretreated for 60 min with TMRM (20 nM) in neuron culture medium and then transferred to Tyrode's medium with 20 nM TMRM for live imaging. Images were captured before and 5 min after FCCP (1.25 μM) treatment. TMRM fluorescence of the mitochondria (an estimate of the extent of polarization of these mitochondria) was calculated as the average fluorescent intensity within the individual mitochondria subtracted by the average fluorescent intensity in the nucleus of the same cell.

mitoKeima

For mitoKeima experiments, images were acquired at 572/35 excitation and 632/60 emission and 430/24 excitation and 632/60 emission, or 561 excitation and 602 to 706 emission and 458 excitation and 602 to 706 emission on a laser scanning confocal microscope, for time-lapse imaging at 561 excitation and 607/36 emission and 440 excitation and 607/36 emission.

Time-lapse imaging of mitochondrial turnover

Live imaging of Drp1KO neurons coexpressing mitoKeima and GFP-Parkin was performed on a Nikon Ti-E microscope with Flash4.0 camera (Hamamatsu) controlled by NIS Elements 4.2 (Nikon Instruments). All components were encased in an environmental chamber (In Vivo Scientific) maintained at ~37°C and ~5% CO2. Z-stacks of single neurons were acquired every 20 min for up to 21 hours. Live imaging of Drp1KO and wt neurons incubated with TMRM or expressing GFP-LC3 or LAMP1-RFP was performed on a DeltaVision OMX SR imaging system with an environmental control module (~37°C and ~5% CO2) and controlled by AcquireSRsoftWoRx (GE Healthcare). Z-stacks were acquired every 10 to 20 min for up to 12

hours. For all time-lapse runs, the z section offering the best focus for the mitochondria of interest was selected at each time point. Images were then aligned using MultiStackReg in ImageJ (NIH). MitoKeima ratio was calculated after background subtraction using the ratio of red over green mitoKeima channels. Regions of interest were drawn around tracked mitochondria at every time point. Quantitative data were obtained from images using MetaMorph software (Universal Imaging), ImageJ (NIH), or ZEN 2.3 lite (Zeiss).

Automated fluorescence microscopy

Experiments involving neuronal survival analysis and optical pulse imaging used an automated microscopy platform as described (83). Briefly, images were obtained with an inverted microscope (Nikon TE2000) equipped with the PerfectFocus system, a 20× Plan Fluor S 0.45 NA ELWD objective, and a 16-bit Andor Clara digital camera with a cooled charge-coupled device. Illumination was provided by a Lambda XL Xenon lamp (Sutter). All of the components were encased in a custom-designed, climate-controlled environmental chamber (In Vivo Scientific), kept at ~37°C and ~5% CO2. The Semrock BrightLine full-multiband filter set [4′,6-diamidino-2-phenylindole (DAPI), fluorescein isothiocyanate (FITC), tetramethyl rhodamine isothiocyanate (TRITC), and cyanine 5 (Cy5)] was used for fluorophore photoactivation (DAPI) and excitation and detection (FITC and TRITC). The illumination, filter wheels, focusing, stage movements, and image acquisitions were fully automated and coordinated with publicly available (ImageJ and μManager) software.

Neurons expressing mitoEOS2 were photoconverted with a 4-s pulse of 405-nm light and longitudinally imaged using robotic microscopy, which can return to the same cell repeatedly over time (84). Single-cell red fluorescence intensities were normalized to the red fluorescence

immediately after photoconversion, and the half-life of the photoconverted red mito-EOS2 reporter was calculated for each cell using the standard half-life equation.

Relevant data were extracted from the raw, digital images in a sequential process using an original script developed in PipelinePilot (Accelrys, San Diego, CA). Briefly, the median background fluorescence from a portion of all images was calculated and subtracted from each individual image. The images were then assembled into montages representing each well at each time point. The montages were temporally sequenced and aligned automatically, and neuron cell bodies were segmented on the basis of intensity and morphology. Neurons with photoswitched mitoEOS2 values below 10 arbitrary units, neurons that survived <~30 hours after photoswitching, and those with a calculated half-life of >1000 hours were excluded from half-life analyses as this value was outside of the range of half-lives that the OPL technique is realistically able to detect. Statistical analyses and the generation of cumulative hazard plots and density plots were accomplished using custom-designed algorithms and the survival package within R, while scatterplots and bar graphs were created using Prism (GraphPad).

Statistical analysis

Data were compiled and processed using Microsoft Excel. GraphPad Prism (GraphPad Software) and SPSS (IBM) were used for statistical analyses, and GraphPad Prism was used to generate graphs. All statistical analyses, including the n, what n represents, description of error bars, statistical tests used, and level of significance, are found in the figure legends. Data were processed using two-tailed unpaired t tests with Welch's correction or by analysis of variance (ANOVA). Before ANOVA, the homogeneity of variance between experimental groups was assessed by Levene's test. If homogeneous ($P > 0.05$), data were subjected to one- or two-way

ANOVA followed by Bonferroni, Sidak, or Tukey post hoc test. If not homogeneous, data were processed by one-way ANOVA followed by Games-Howell post hoc test.

2.5 Figures

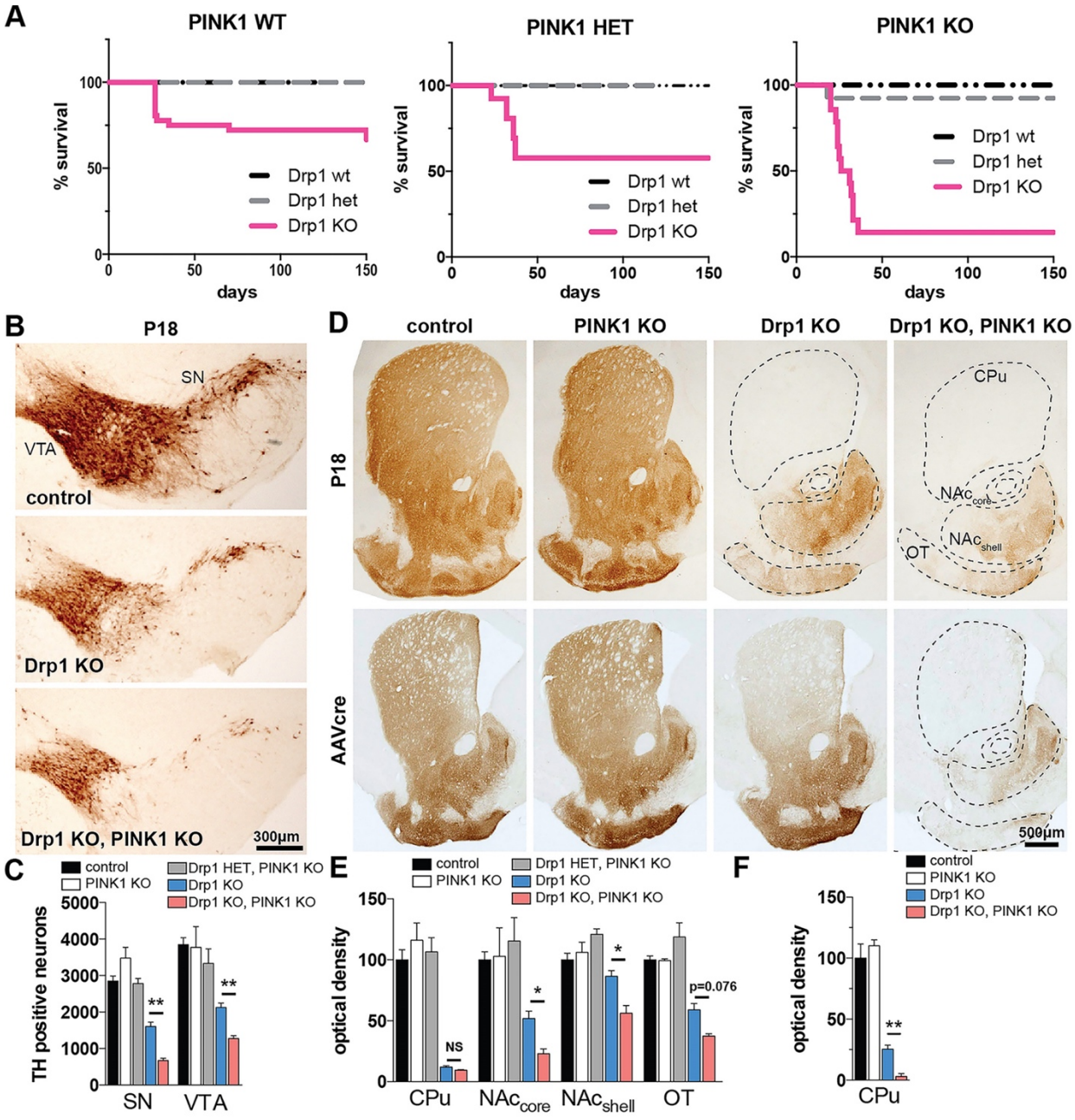

Figure 2.1

Midbrain dopamine neurons require PINK1 to survive when fission is compromised. (A) Kaplan–Meier survival curve of Drp1 wt, heterozygous (het), and Drp1KO mice on a PINK1 wt background (left), PINK1 het background (middle), and PINK1 KO background (right).

Drp1KO-PINK1KO mice were significantly more likely to die than either Drp1KO-PINK1 wt [HR 14.4, 95% CI: 4.67–44.6, $p<0.001$ by log-rank (Mantel–Cox) test] or Drp1KO-PINK1 het mice [HR 4.21, 95% CI: 1.50–11.8, $p<0.01$]. n=18-36 PINK1 wt mice/group, 5-13 PINK1 het mice/group and 13-15 PINK1 KO mice/group. Data in left panel (PINK1 WT) was published (1), reproduced here with permission from The Journal of Neuroscience. (B,C) Targeted deletion of Drp1 in DA neurons causes loss of DA cell bodies in the SN and VTA by P18 (assessed by tyrosine hydroxylase staining), which is exacerbated by concurrent PINK1 loss. Data show mean ±SEM, n=4 mice per group with 5-6 fields per mouse. (D(top),E) The loss of cell bodies is preceded by early loss of DA terminals projecting to the caudate putamen (CPu) by P18. Although DA projections to the nucleus accumbens (NAc) core and shell and to the olfactory tubercule (OT) are relatively spared in Drp1KO, concurrent loss of PINK1 markedly increases their susceptibility. n=4 mice/group, 14-20 fields per mouse. (D(bottom),F) AAVcre was delivered to the SNc of 6–7-month-old Drp1lox/lox and Drp1lox/lox;PINK1KO mice. Two months later, mice lacking PINK1 were more susceptible to Drp1 loss, indicating the synergistic effect also occurs in adult animals. n=3-5 mice per group with 4-5 fields per mouse, NS=not significant, *$p<0.05$, **$p<0.01$ by one-way ANOVA with Games-Howell post hoc test.

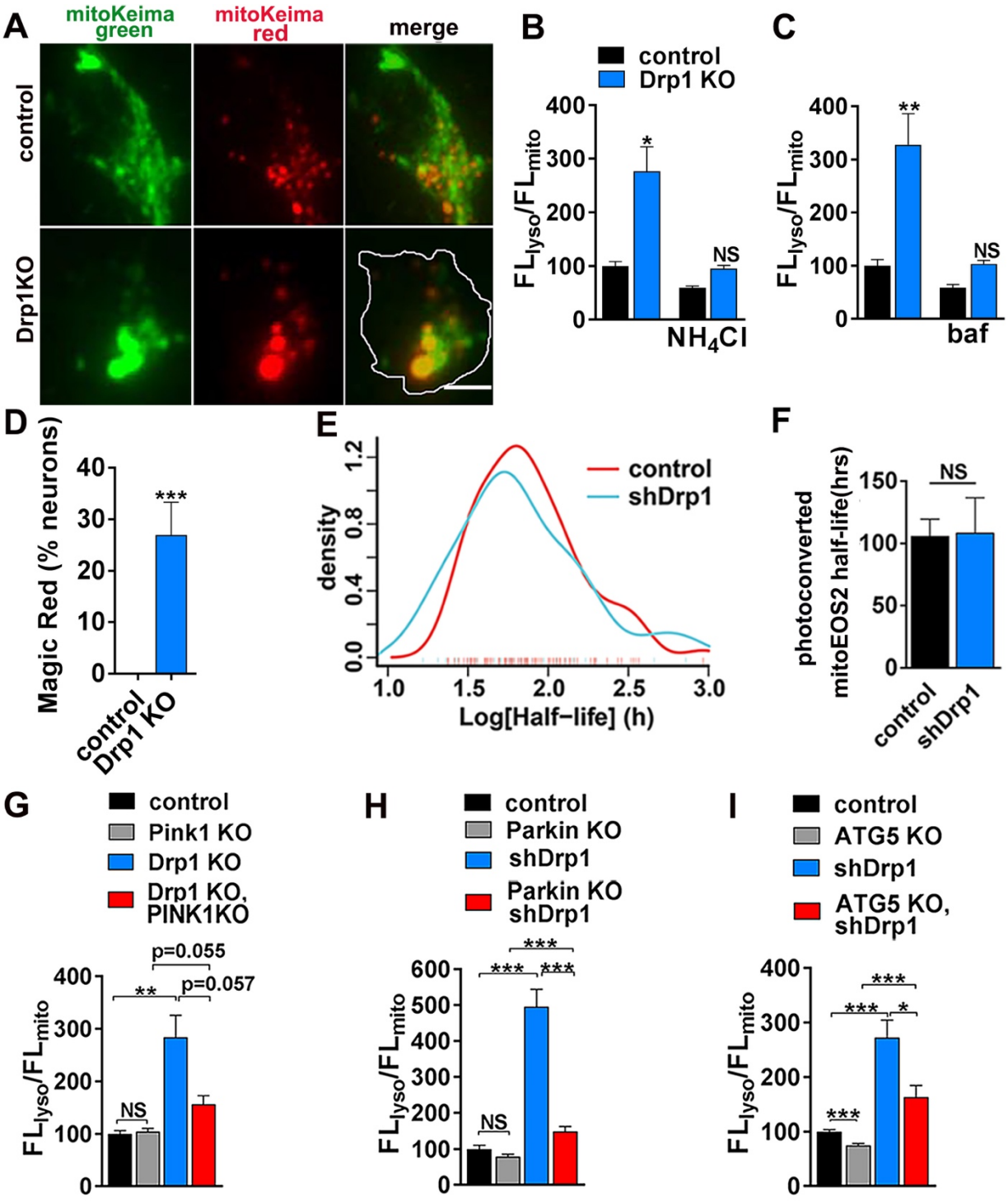

Figure 2.2

Drp1KO increases mitochondrial targeting to lysosomes in a process that is facilitated by PINK1 and Parkin. (A) Images show control and Drp1KO hippocampal neurons expressing

mitoKeima. The scale bar is 4 μm. (B) Quantification of Drp1KO hippocampal neurons expressing mitoKeima. Drp1KO mitochondria have proportionally increased fluorescence in the acidic, lysosomal (FLlyso) versus mitochondrial (FLmito) channel, and this signal is decreased by NH4Cl. Data show mean ± SEM, n=7-8 coverslips/group, 6-12 cells/coverslip, compilation of 2 experiments. (C) Bafilomycin (baf), which blocks lysosome acidification, also decreased the FLlyso/FLmito ratio. n=3 coverslips/group, 5-17 cells/coverslip. (D) Neurons were incubated with Magic Red for 1 hour. Magic Red signal accumulates in Drp1KO but not control neurons. n=9-10 coverslips/group, 4-12 cells/coverslip, compilation of 2 experiments. (E, F) Estimate of mitochondrial turnover in neurons expressing Drp1 shRNA or scramble shRNA assessed based on the rate of loss of photoconverted mitoEOS2 from the cell body. Individual neurons expressing mitoEOS2 were photoconverted and longitudinally imaged using robotic microscopy. Loss of Drp1 (shRNA) did not influence the rate of dissipation of red (photoconverted) fluorescence despite producing characteristic swollen mitochondria (fig. S2F). Data are means±SEM, NS=not significant versus scramble shRNA by two-sided Mann-Whitney test, n = 109 neurons total from two experiments. (G, H) Increased lysosomal targeting in Drp1KO neurons is inhibited by PINK1 KO or Parkin KO. (G) n=10-11 coverslips/group, n=3-15 cells/coverslip, compilation of 2 experiments; (H) n=16 coverslips/group, n=3-9 cells/coverslip from 3 experiments. (I) Increased lysosomal targeting in neurons treated with shDrp1 is also largely inhibited by ATG5 KO. n = 25-32 coverslips/group, n=3-5 cells/coverslip from 6 experiments; NS=not significant, *$p<0.05$, **$p<0.01$, ***$p<0.001$ by one-way ANOVA with Games-Howell post hoc test (B,G,H,I) or Tukey's multiple comparisons test (C), or t-test (D).

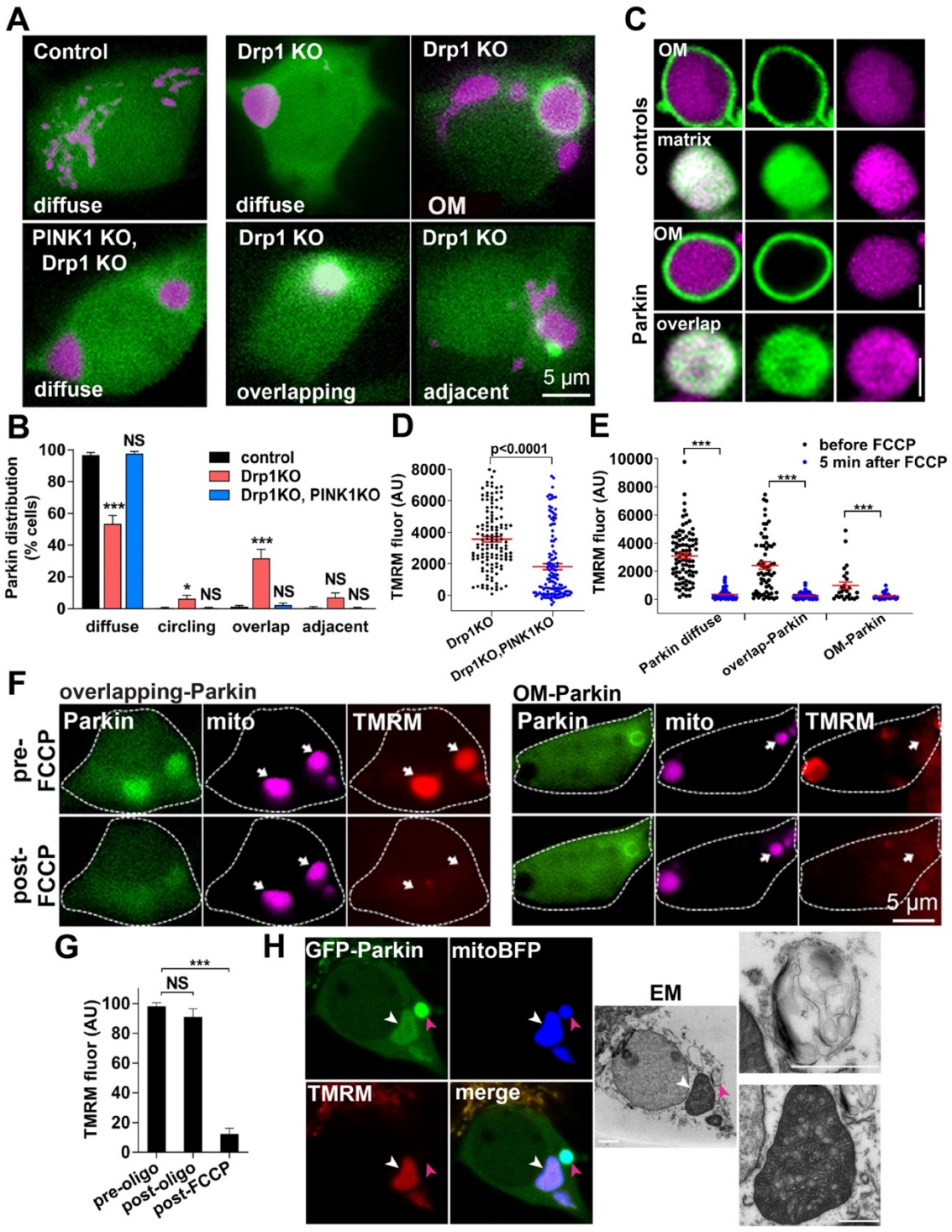

Figure 2.3

Parkin is recruited into polarized Drp1KO mitochondria. (A) Neurons expressing GFP-Parkin (green) and mitoBFP (purple, mitochondrial matrix-targeted BFP). Parkin is diffusely

distributed in control neurons. A subset of Drp1KO neurons contain mitochondria with either adjacent Parkin punctae, overlapping Parkin or Parkin ringing (circling). Drp1KO;PINK1KO blocks all Parkin recruitment. (B) Quantification of Parkin distribution patterns. Data show mean ± SEM; n = 12 coverslips/group, 8–20 neurons/coverslip from three experiments. (C) Confocal microscopy shows single mitochondria in Drp1KO neurons expressing a mitochondrial matrix marker (mitoFarRed, purple) and either a mitochondrial outer membrane marker (OM–GFP) or mitochondrial matrix marker (matrix–GFP) as controls, or GFP-Parkin recruited either in a mitochondrial OM or overlapping pattern. Scale bars are 1 μm. (D) Scatter graph of mitochondrial membrane potential (TMRM) of individual Drp1KO and Drp1KO;PINK1KO mitochondria. n= 128-130 mitochondria/group from 2 experiments. $p<0.0001$ by unpaired t-test. (E,F) Scatter graphs (E) and images (F) of mitochondrial membrane potential (TMRM, red) of mitochondria with different parkin patterns in Drp1KO neurons expressing mitoBFP and GFP-Parkin, before and after FCCP treatment (1.25 μM). n = 26-87 mitochondria/group from three experiments. (G) Mitochondrial membrane potential (TMRM) of mitochondria with overlapping-Parkin in Drp1KO neurons before and after oligomycin (5 μM, 5 min) and FCCP (1.25 μM, 5 min). n=17 cells from 2 experiments. NS, not significant, *$p<0.05$, **$p<0.01$, ***$p\leq0.001$ by one-way ANOVA with Tukey's multiple comparisons test (G) or Games-Howell post hoc test (B,E). (H) Correlative light and electron microscopy (CLEM) showing GFP-Parkin accumulation in polarized (white arrow) and depolarized (pink arrow) mitochondria. Corresponding ultrastructure shows the polarized mitochondrion with internalized Parkin has intact membranes and cristae (lower inset), while the depolarized mitochondria (upper inset) is a vesicular structure containing degraded mitochondrial membranes. Scale bars are 2 μm (main panels) and 1 μm (inset).

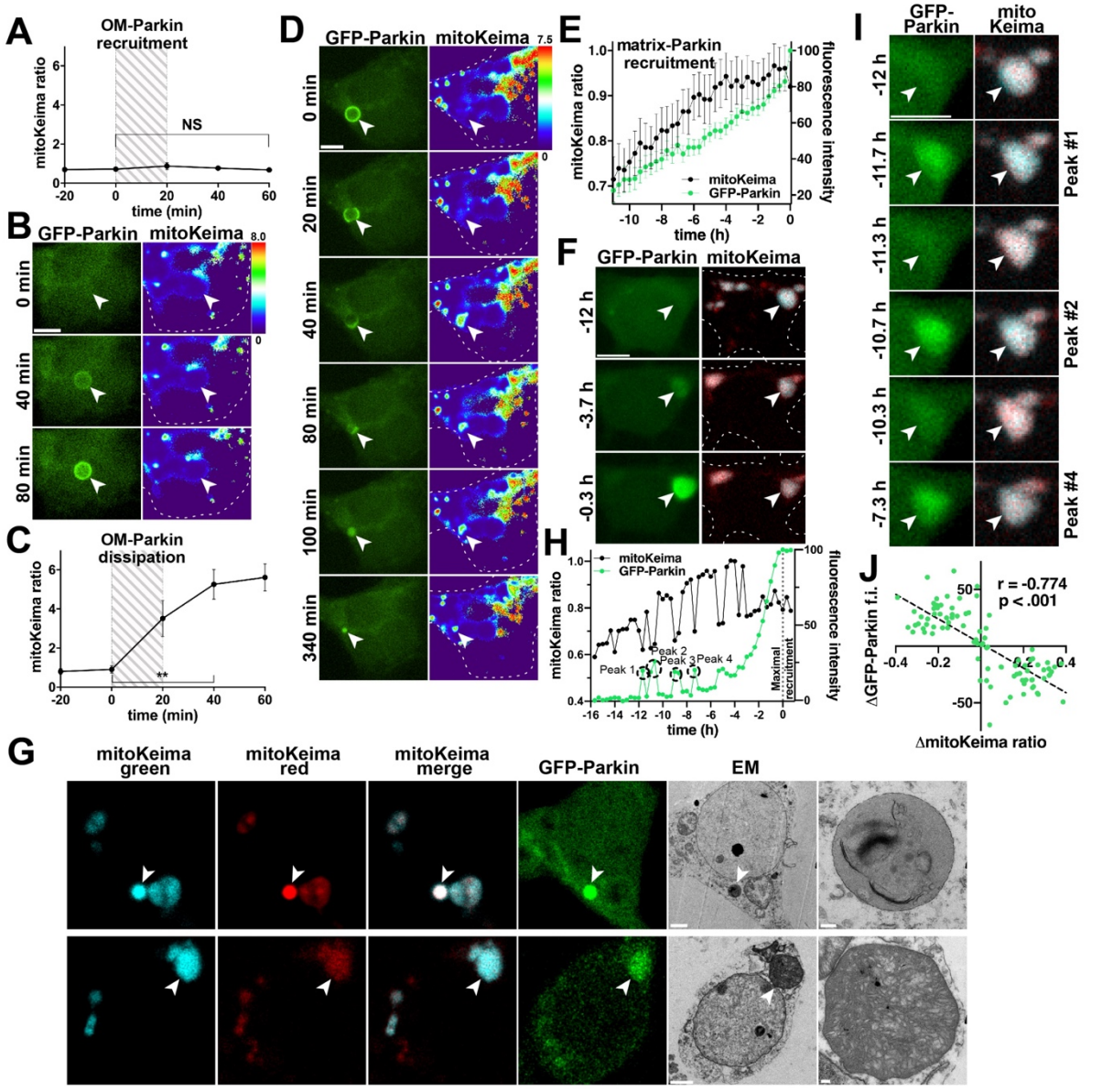

Figure 2.4

Time-lapse imaging reveals distinct Parkin-dependent quality control pathways. Drp1KO neurons co-expressing GFP-Parkin and mitoKeima were imaged every 20 min for up to 21 h. (A) Relative mitochondrial acidity during OM-Parkin recruitment. Hatched area represents period of GFP-Parkin OM accumulation. Data represents means ± SEM. n=10 mitochondria from 9 neurons, 1-4 neurons/dish, 3 experiments. (B) GFP-Parkin accumulates at the OM of a mitochondrion with low acidity. (C) Mitochondrial acidity during OM GFP-Parkin dissipation. Hatched area delineates period when GFP-Parkin begins to dissipate. n=10 mitochondria from 9 neurons, 1-4 neurons/dish, 2 experiments. NS, not significant, **p<0.01 by one-way ANOVA with repeated measures. (D) OM-Parkin dissipates concomitantly with mitochondrial acidification. Parkin then accumulates inside the shrunken mitochondrion. (E) Direct matrix-

Parkin accumulation. GFP-Parkin (green) slowly accumulates in the mitochondrial matrix as acidity (black) increases. GFP-Parkin fluorescence was normalized such that the lower and upper bounds were defined by the nuclear and maximum mitochondrial intensities, respectively. Traces aligned so maximum matrix-Parkin intensity is at 0 h. n = 23 mitochondria from 22 neurons, 1-9 neurons/dish, 7 experiments. (F) GFP-Parkin directly accumulates in mitochondria, without prior OM recruitment. (G) CLEM shows acidified overlapping-Parkin mitochondria are degrading mitochondrial contents within lysosomes (mitolysosomes) (top). Overlapping-Parkin mitochondria with slightly acidic pH (fig. S5F) are intact mitochondria with electron-dense cristae (bottom). Scale bars are 2 μm (cell overviews) and 0.2 μm (insets). (H,I) Corresponding repetitive single spikes of Parkin accumulation and decreased mitochondrial acidity in a Drp1KO mitochondrion during direct matrix-Parkin recruitment. (B,D,F,I) Scale bars, 5 μm. (J) Inverse relationship between changes in GFP-Parkin intensity and mitoKeima ratio during Parkin spikes. The change in GFP-Parkin and mitoKeima were measured between timepoints before, during and after the peak. n = 90 measurements, 40 individual spikes in 6 neurons, 5-9 spikes/neuron, 1 mitochondrion/neuron; Pearson $r = -0.774$, $p<0.001$.

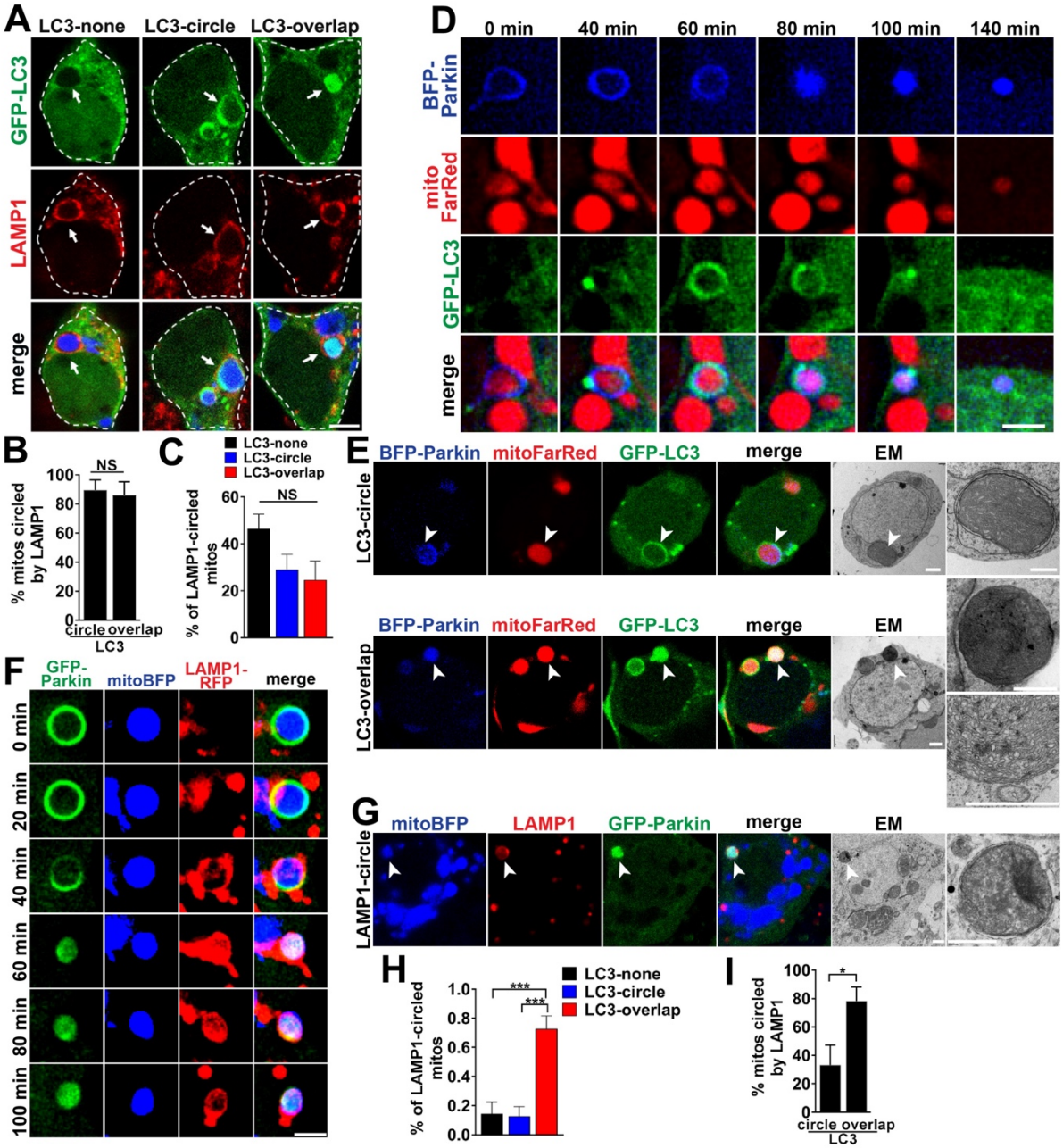

Figure 2.5

PINK1-dependent formation of LC3-positive autophagosomes precedes rapid lysosome fusion. (A) Drp1KO neurons expressing GFP-LC3 (green) and mitoBFP (blue) treated with 100 nM bafilomycin for 4 h and stained for LAMP1 (lysosomes, red). Scale bar, 4 μm. (B) Most mitochondria with circling or overlapping patterns of GFP-LC3 were circled by LAMP1. n=8 coverslips/group, 4-7 neurons/coverslip, 3 experiments. (C) Among LAMP1-circled mitochondria, ≈50% did not have LC3 accumulation (diffuse LC3); others were circled by GFP-LC3 (LC3-circle), or had GFP-LC3 overlapping the mitochondrial matrix (LC3-overlap). n = 8

coverslips/group, n=6-11 cells/coverslip, 3 independent experiments. (D) Drp1KO neurons co-expressing GFP-LC3, mitoFarRed and BFP-Parkin. GFP-LC3 accumulates in a distinct punctum on the mitochondrion with OM-Parkin, before dispersing to encircle the mitochondrion. BFP-Parkin then transitions to the overlapping pattern, and LC3 re-accumulates into a punctum. Scale bar, 2 μm. (E) CLEM shows ultrastructure of Parkin-positive mitochondria with distinct patterns of GFP-LC3. Mitochondria with LC3-circle are surrounded by an isolation membrane (top). LC3-overlap mitochondrion (bottom) is electron-dense but intact, with packed cristae (see insets). Bottom inset is the same structure from a different section. Scale bars, 1 μm. (F) Drp1KO neurons co-expressing GFP-Parkin, LAMP1-RFP and mitoBFP. Images show formation of a LAMP1 ring, indicating lysosomal fusion, concurrent with Parkin shifting from OM to overlapping. Scale bar, 2 μm. (G) Overlapping-Parkin mitochondria circled by LAMP1 are mitolysosomes by ultrastructure. Scale bars, 1 μm. (H) Drp1KO;PINK1KO neurons expressing GFP-LC3 and mitoBFP treated with bafilomycin for 4h and stained for LAMP1. Among LAMP1-circled mitochondria, ≈80% had LC3-overlap, a few were either circled or lacked GFP-LC3 accumulation. n=9 coverslips/group, 5-12 neurons/coverslip, 2 experiments. (I) Most mitochondria with LC3-overlap were circled by LAMP1. n=6 coverslips/group, 5-12 neurons/coverslip, 3 experiments. NS, not significant, *$p<0.05$, ***$p<0.001$ by t-test (B, I) or one-way ANOVA with Tukey's multiple comparisons test (C, H).

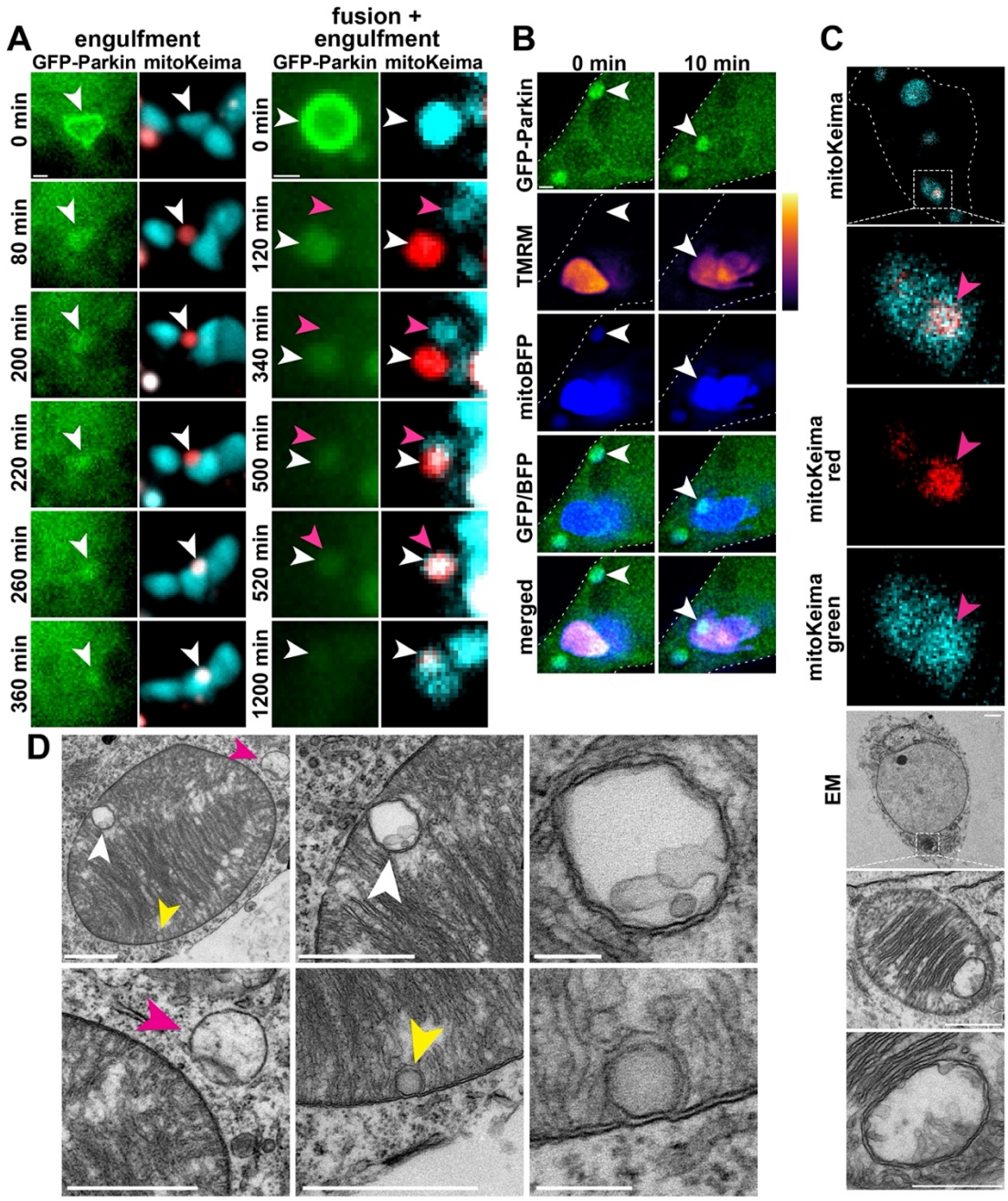

Figure 2.6

Acidified overlapping-Parkin mitochondria are engulfed by mitochondria with normal pH. Mitochondria in Drp1KO hippocampal neurons co-expressing GFP-Parkin and mitoKeima were tracked individually to determine their fates. (A) Time-lapse images show the fates of single mitochondria that were acidified following OM-Parkin disruption (white arrow). Some mitolysosomes are engulfed by non-acidified mitochondria (left). The mitolysosome on the right first fuses with a non-acidified mitochondrion (pink arrow) before being engulfed by another.

Scale bars are 1 µm. (B) Drp1KO neurons expressing GFP-Parkin and mitoBFP were incubated with TMRM and imaged every 10 min for several hours. Representative images show overlapping-Parkin mitochondria being engulfed by polarized mitochondria (white arrow). Overlapping-Parkin co-localizes with mito-BFP before and after engulfment. Scale bar is 1 µm. (C) CLEM images show a healthy mitochondrion with intact cristae that contains a discrete acidified structure (by mitoKeima) that corresponds to a membrane-bound structure enclosing mitochondrial materials. Scale bars are 2 µm (cell overview), 1 µm (mitochondria overview) and 0.5 µm (inset). (D) EM images show a healthy mitochondrion engulfing two structures (white and yellow arrows) similar to what was described in (C). A lysosome (pink arrow) was also observed interacting with the same mitochondrion. Scale bars are 1 µm for images containing arrows and 0.2 µm for insets.

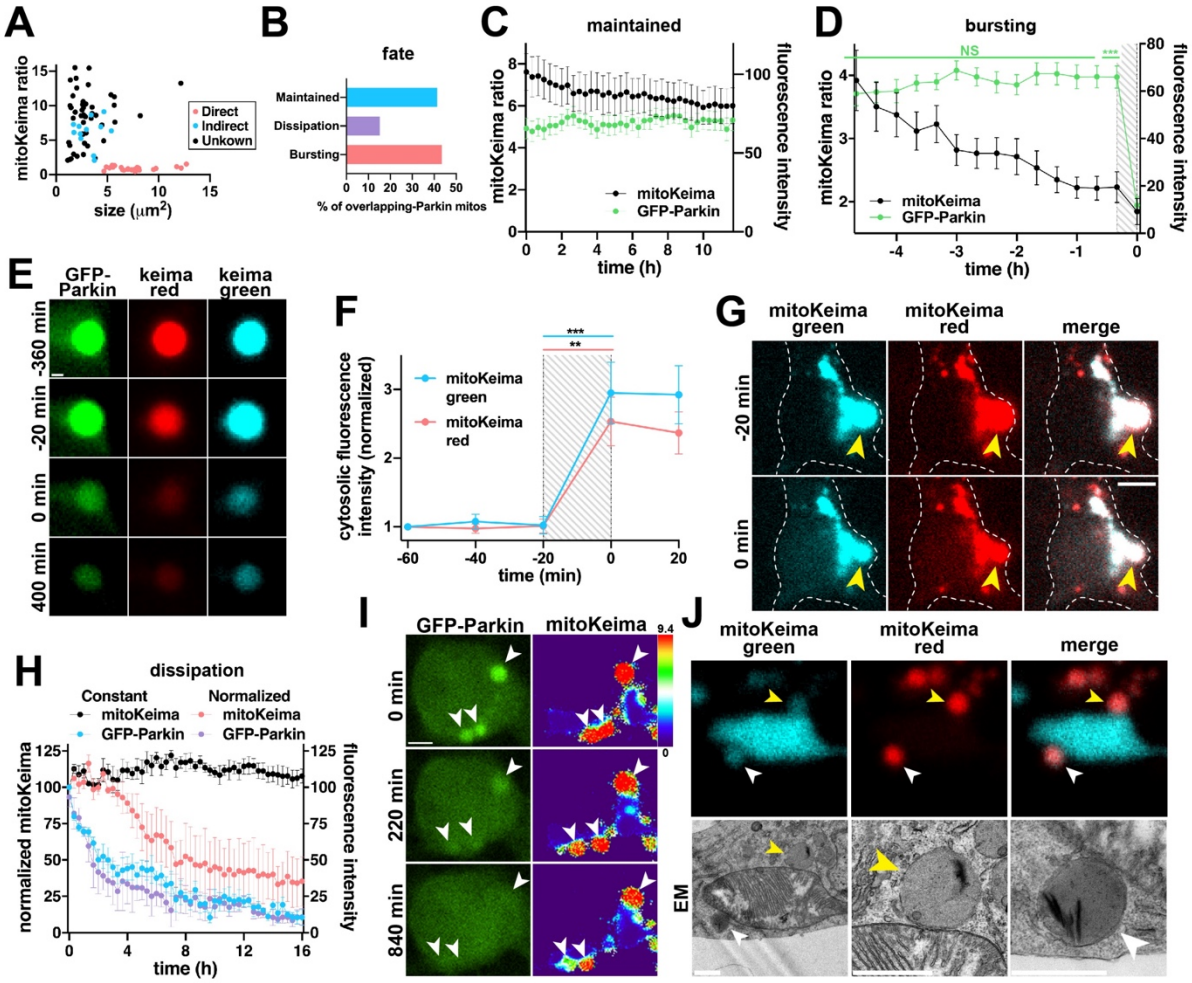

Figure 2.7

Long-lived mitolysosomes burst and release contents. (A) Mitochondria with confirmed indirect OM-Parkin (blue, n=12) are smaller and more acidic than those with direct Parkin recruitment (pink, n=23). Most with overlapping-Parkin from t=0 (unknown origin, black, n=46)

are similar to those from the indirect pathway. (B) Fates of these 46 mitolysosomes. (C) Constant acidity levels in mitolysosomes that maintain GFP-Parkin signal (n=19 mitochondria from 18 neurons, 1-4 neurons/dish, 10 experiments; not significant (NS) for interaction between GFP-Parkin and mitoKeima ratio by two-way ANOVA with repeated measures). (D) GFP-Parkin sharply decreases after bursting. Acidity decreases over hours preceding degradation ($p<0.05$). Traces aligned so bursting occurs at 0 h. n=19 mitochondria from 17 neurons, 1-5 neurons/dish, 7 experiments. (E) Post-burst mitolysosome structure tracked for 400 minutes. Scale bar, 1 µm. (F) Cytosolic mitoKeima increases when mitolysosomes burst. Traces aligned so bursting occurs at 0 min. n=20 mitochondria from 18 neurons, 1-5 neurons/dish, 7 experiments. **$p<0.01$, ***$p<0.001$ by two-way ANOVA with repeated measures and Bonferroni's multiple comparison test. (G) Mitolysosome bursting (yellow arrow) is accompanied by increased cytosolic mitoKeima. Scale bar, 5 µm. (H) In some mitolysosomes, GFP-Parkin dissipates followed by pH normalization (pink, n = 3 mitochondria from 3 neurons, 1 neuron/dish, 3 experiments), while others remain acidic (black, n = 4 mitochondria from 3 neurons, 1-2 neurons/dish, 2 experiments). GFP-Parkin intensity similarly decreases in both (constant acidity: blue, normalized acidity: purple). ***$p < 0.001$ by two-way ANOVA with repeated measures. (I) In three mitochondria with overlapping-Parkin, GFP-Parkin signal fades by 220 min, and is at cytosolic levels by 840 min. By then, the mitolysosome in the lower left corner has normalized acidity. Scale bar, 3 µm. (J) CLEM shows close contacts between a mitochondrion with intact cristae and two acidified mitolysosomes (yellow and white arrows). Scale bars, 1 µm.

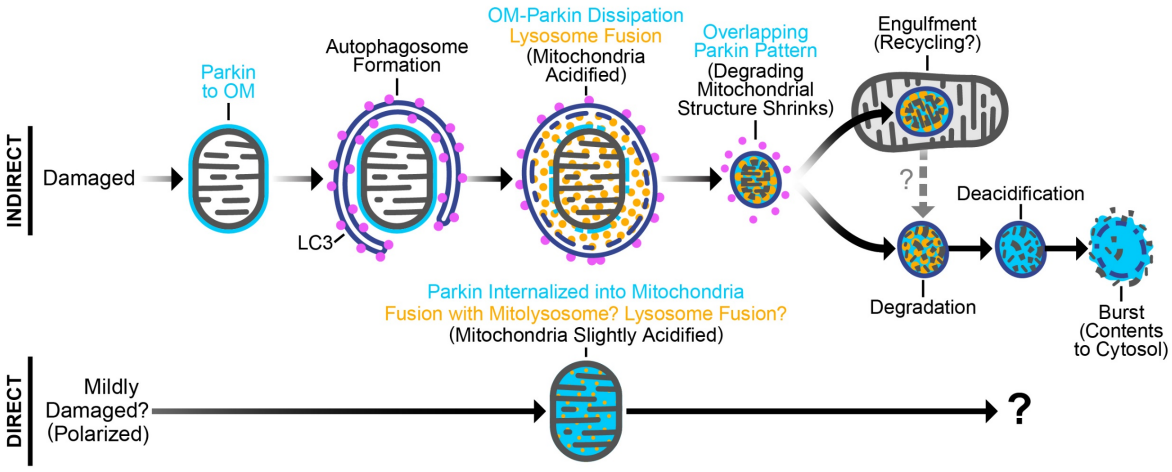

Figure 2.8

Indirect and Direct Pathways of Mitochondrial Parkin Recruitment. Schema shows indirect and direct mechanisms by which Parkin accumulates in mitochondria and the fates of mitochondria in each of these pathways. In the Indirect pathway, Parkin accumulates on the OM of depolarized mitochondria (OM-Parkin). These mitochondria are engulfed by autophagosomes

and then rapidly fuse with lysosomes, which occurs concurrently with Parkin dissipation from the OM. These degrading mitochondrial structures then shrink to form mitolysosomes with an overlapping Parkin pattern (and which are indistinguishable from healthy mitochondria when visualized by either light microscopy with mitochondria-targeted reporters or immunofluorescence against mitochondrial matrix proteins). Mitolysosomes are stable for many hours. A subset are engulfed by mitochondria, and others eventually undergo deacidification prior to bursting and releasing contents into the cytosol. In the Direct pathway, Parkin is gradually recruited directly into mitochondria over many hours, as mitochondria concurrently undergo mild acidification through undefined mechanisms.

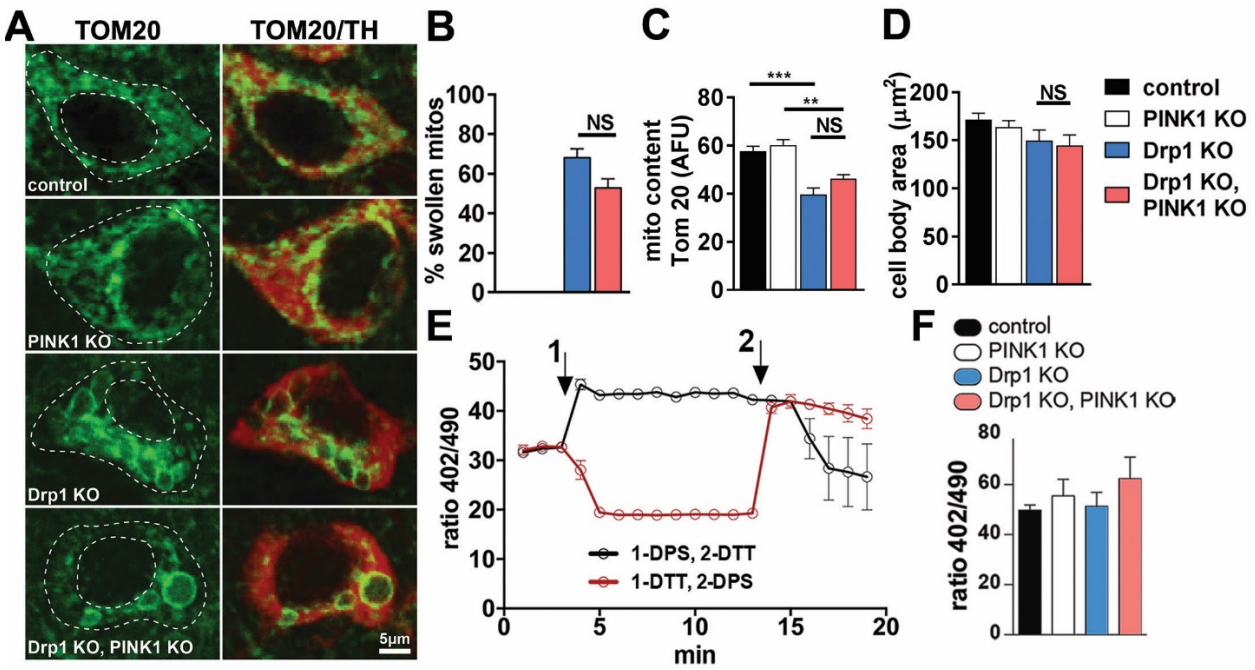

Figure 2.9

S1. Concurrent loss of PINK1 does not impact the effects of Drp1 KO on mitochondrial morphology, content or oxidant stress. (A–D) Mitochondrial morphology and content in midbrain DA neurons from P18 mice lacking Drp1, PINK1 or both. (A,B) Loss of Drp1 causes mitochondria (Tom20 staining, green) to become visibly swollen in most midbrain DA neurons (identified by TH staining, red). However, concurrent loss of PINK1 does not affect the proportion of cells with swollen mitochondria. (C) Drp1KO DA neurons also have decreased mitochondrial content (mean fluorescence of Tom20 staining, normalized to cell area), but concurrent loss of PINK1 does not affect this decrease. (D) Cell size is unchanged. Data show mean±SEM, NS, not significant, **p<0.01, ***p<0.001 by one-way ANOVA with Games-Howell post hoc test (B) or Tukey's multiple comparisons test (C, D), n=4 mice per group, 20 fields/mouse, 45–72 cells quantified per mouse. (E,F) Concurrent loss of PINK1 does not increase mitochondrial oxidant stress. To determine the impact of Drp1KO and PINK1KO on oxidative stress, mouse hippocampal neurons from Drp1lox/lox mice, with or without PINK1, were co-transfected with mitochondria-targeted roGFP (mito-roGFP) and either Cre (to delete

Drp1) or vector control. (E) Validation of mito-roGFP. DPS (2,2'-dipyridyldisulphide) increases oxidation (>402/490), and DTT (dithiothreitol) increases reduction, indicating the sensitivity to detect changes in oxidation. Data show mean ± SEM, n=3–7 cells from 3–7 coverslips, compiled from 2 experiments for DTT-DPS, 1 experiment for DPS-DTT. (F) However, neither Drp1 KO and/or PINK1 KO affected mitochondrial oxidation at the cell body. NS=not significant by one-way ANOVA with Tukey's multiple comparisons test; n=6 coverslips/group, 21–31 cells/group, compiled from two independent experiments.

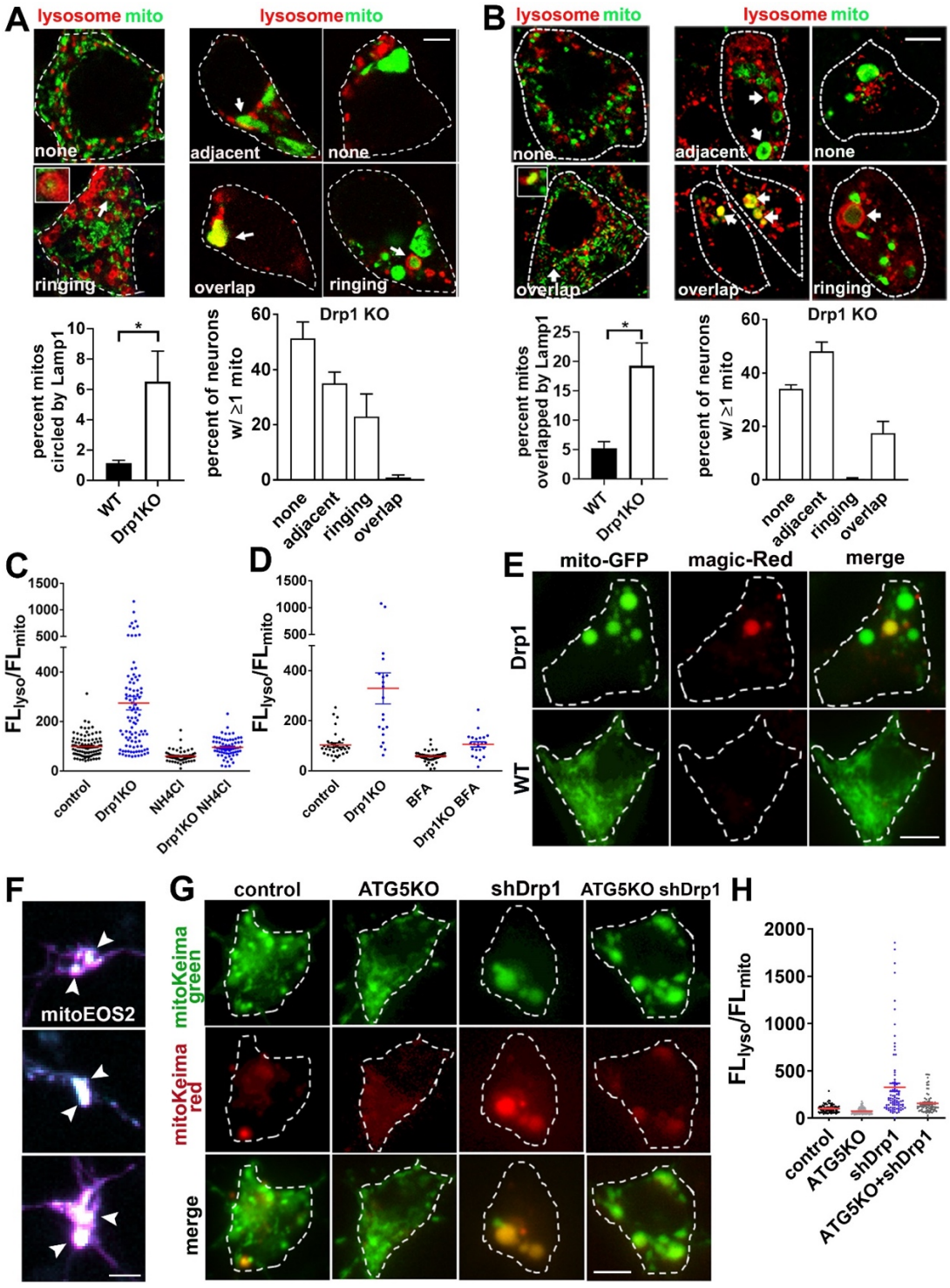

Figure 2.10

S2. Drp1KO mitochondria are degraded by lysosomes. (A) Immunofluorescence of mitochondria (green, PDH) and lysosomes (red, LAMP1) in control (wt) and Drp1KO (right)

hippocampal neurons. A subset of wt (left images) and Drp1KO (right images) neurons contain individual mitochondria that are either adjacent or ringed by LAMP1. However, in wt neurons, the large number of mitochondria made it impossible to distinguish mitochondria that had no contact with LAMP1 (none) from those that were adjacent to LAMP1. Very rarely, LAMP1 overlaps the mitochondrial matrix. In the absence of Drp1, an increased percentage of mitochondria are ringed by LAMP1. Data show mean ± SEM; *$p<0.05$ by unpaired t-test; n= 6-7 coverslips/group, 3-5 cells/coverslip (left graph, percent mitos), and 6-9 coverslips/group, 9-16 neurons/coverslip (right graph, percent of neurons), compilation of two experiments. Scale bar is 4 μm. (B) Midbrain DA neurons from P18 control (left images) and Drp1KO (right images) mice. In contrast to the hippocampal neurons, many cells contain mitochondria (PDH) with overlapping LAMP1 immunofluorescence, while mitochondria ringed by LAMP1 are less common. *$p<0.05$ by unpaired t-test; n=4 brains/group, with 27-28 DA neurons from 3 sections/brain for controls (left graph), and 97-221 DA neurons from 6-7 sections/brain for Drp1KO (right graph), compilation of 2 experiments. Scale bar is 5 μm. (C,D) Scatter graphs corresponding to mitoKeima signal of individual cells shown in Figs. 2B,C, respectively. (E) Neurons were incubated with Magic Red for 1 hour. Images show the accumulation of Magic Red signal in Drp1KO but not control neurons. These images correspond to the data shown in Fig. 2D. Scale bar is 4 μm. (F) Representative cortical neurons co-expressing Drp1 shRNA and mitoEOS2 exhibit enlarged mitochondrial morphology characteristic of Drp1 loss of function (arrows). Scale bar is 3.5 μm. (G) Representative images of wt and ATG5lox/lox neurons co-expressing either empty vector or cre (to delete ATG5) and shDrp1, as well as mitoKeima. Scale bar is 4 μm. (H) Scatter graph of data quantified in Fig. 2I.

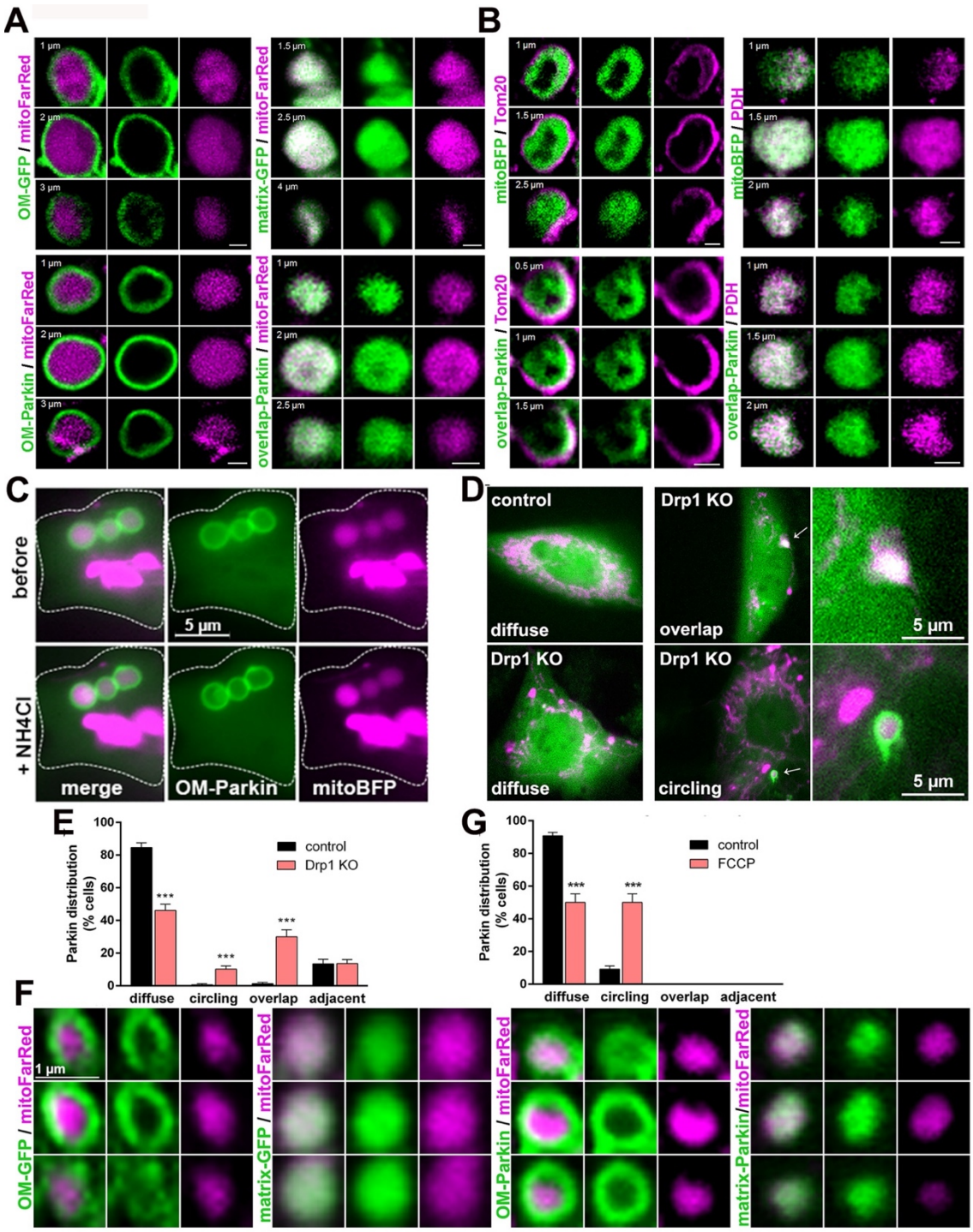

Figure 2.11

S3. Distinct patterns of Parkin localization to mitochondria in Drp1KO neurons and MEFs. (A) Confocal Z-stacks of Drp1KO mitochondria shown in Fig. 3C. Scale bars are 1 µm. (B) Confocal Z-stacks of fixed Drp1KO neurons expressing either mitoBFP (control) or GFP-

Parkin, and processed for immunofluorescence against either Tom20 (mitochondrial outer membrane protein, purple) or PDH (pyruvate dehydrogenase, mitochondrial matrix protein, purple). Different focal depths are indicated at the upper-left corners. Scale bars are 1 μm. (C) Addition of ammonium chloride to alkalinize intracellular compartments had no effect on the OM GFP-Parkin pattern in Drp1KO neurons, suggesting that lack of signal in the matrix reflects the absence of Parkin in this compartment, rather than potential quenching of GFP signal by acidic conditions that might occur following fusion with lysosomes. (D) Images show live Drp1KO and wt MEFs expressing GFP-Parkin (green) and mitoBFP (purple) to label the mitochondrial matrix. Parkin is diffusely distributed in most control and Drp1KO MEFs. However, some Drp1KO MEFs contain individual mitochondria that either colocalize with Parkin (overlapping), are ringed by Parkin (circling) or are adjacent to Parkin punctae (adjacent, images not shown). Examples of individual mitochondria of similar size are indicated with an arrow and were magnified. (E) Quantification of different patterns of Parkin distribution in control and Drp1KO MEFs. Data show mean ± SEM; ***P < 0.001 by t-test; n = 12 coverslips/group, 6–17 cells per coverslip compiled from three independent experiments. (F) Confocal microscopy live images show individual mitochondria from Drp1KO MEFs labeled with a mitochondrial matrix marker (mitoFarRed, purple) and either a mitochondrial outer membrane marker (OM–GFP) or mitochondrial matrix marker (matrix–GFP) as controls, or GFP-Parkin (green) localized to either the outer membrane (OM) or to an overlapping pattern. (G) Quantification of different patterns of Parkin distribution in live wt MEFs treated with 10 μM FCCP or DMSO (control) for 2 hours. Due to the large number of mitochondria in wt MEFs, the diffuse and adjacent categories were combined. ***P < 0.001 by t-test; n = 6 coverslips per group, 20 cells per coverslip, compiled from two independent experiments.

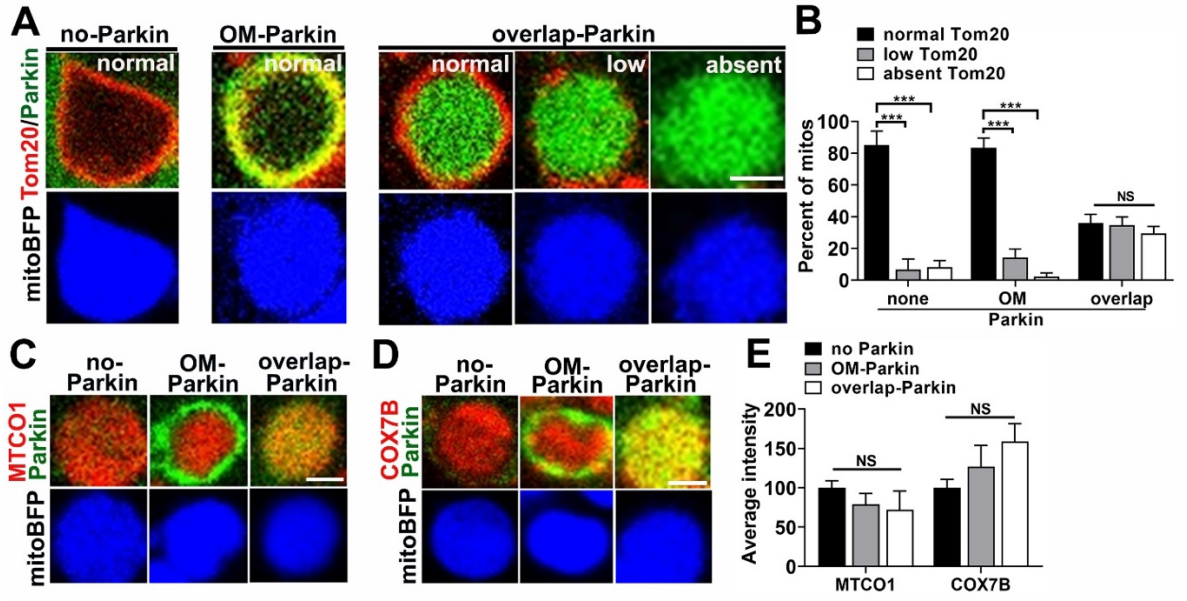

Figure 2.12

S4. Subset of Drp1KO mitochondria with overlapping-Parkin have disrupted OM integrity with normal expression of inner mitochondrial membrane proteins. (A,B) Drp1KO neurons

co-expressing GFP-Parkin and mitoBFP, and processed for immunofluorescence against Tom20 (red) to visualize the outer mitochondria membrane. A subset of mitochondria with overlapping-Parkin have either decreased or absent Tom20 immunofluorescence. Scale bar is 1 μm. n=14 coverslips/group, 5-9 cells/coverslip from 4 experiments. (C-E) Overlapping-Parkin mitochondria have normal pattern and intensity of immunofluorescence against inner mitochondria membrane markers MTCO1 (C) and COX7B (D), scale bars are 0.5 μm. n=6-7 coverslips per group, 3-8 cells/ coverslip, 8-38 mitochondria quantified per phenotype from 3 experiments. NS= not significant, ***P < 0.001 by one-way ANOVA with Tukey's multiple comparisons test.

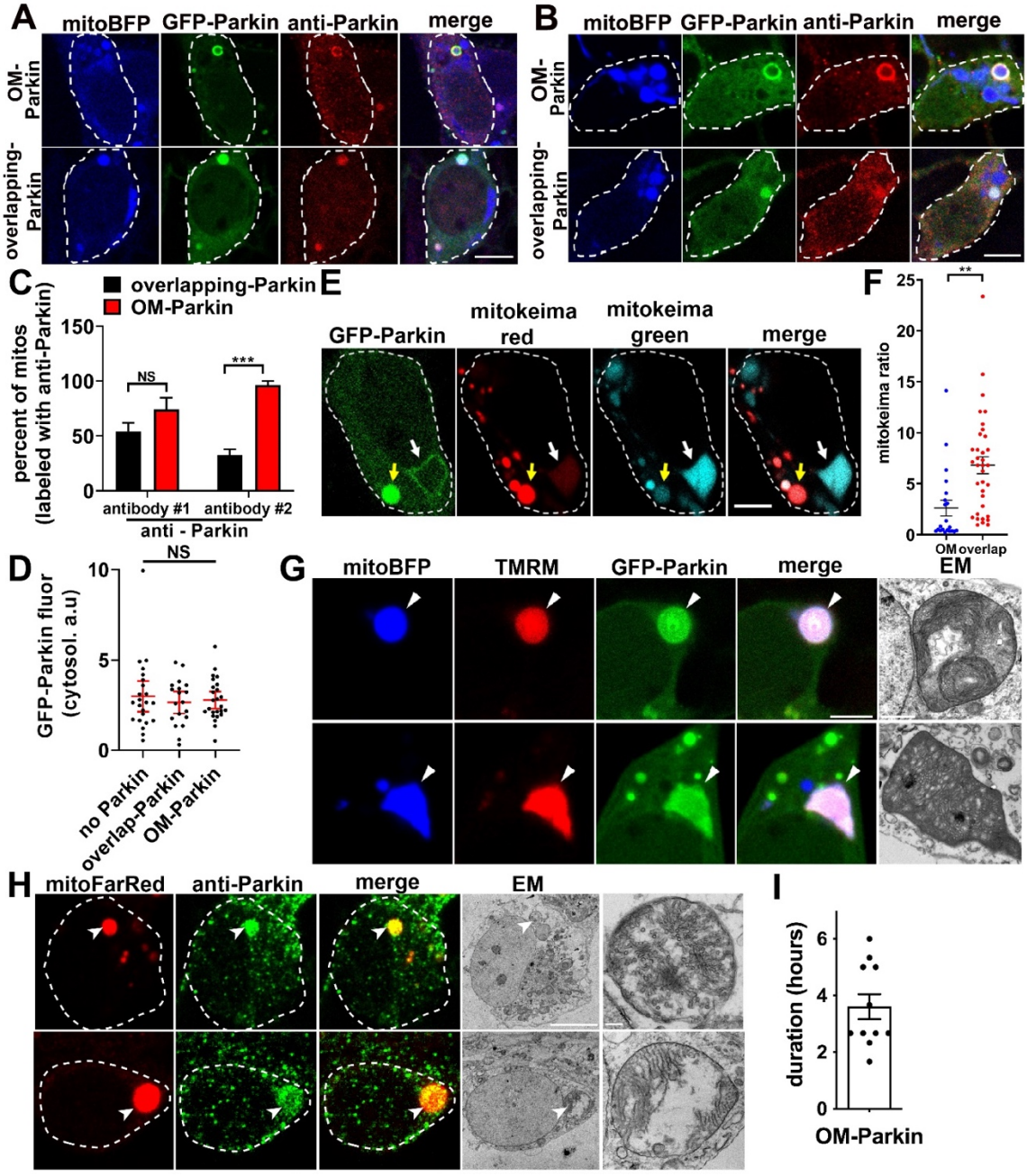

Figure 2.13

S5. Visualization of GFP-Parkin and endogenous Parkin in intact mitochondria. (A-C) Drp1KO neurons expressing mitoBFP and GFP-Parkin and processed for immunofluorescence against Parkin (Red) using one of two anti-Parkin antibodies (antibody1: Abcam, ab#77924, epitope (the second ring domain, aa399-465), (A); antibody2: Proteintech, #14060-1-AP, epitope (aa81-387),(B)). Quantification of the percent of mitochondria in which immunofluorescence against Parkin overlaps with GFP-Parkin fluorescence. Data show mean ± SEM; NS= not

significant, ***P < 0.001 by two-way ANOVA with Tukey's multiple comparisons test. n=4-5 coverslips/group, n=10-26 cells/coverslip from 3 independent experiments. Scale bars are 5 µm. (D) Scatter graph of cytosolic GFP-Parkin intensity for different patterns of Parkin recruitment in Drp1KO neurons, n=19-25 neurons/group from 3 independent experiments. Data show mean ± SEM; NS= not significant by one-way ANOVA with Tukey's multiple comparisons test. (E,F) Drp1KO neurons co-expressing mitoKeima and GFP-Parkin. MitoKeima ratio is higher in mitochondria with overlapping-Parkin (yellow arrows) than those with OM-Parkin (white arrows). n=12 dishes/group, 1-4 cells/dish from 3 independent experiments. **P < 0.01 by unpaired t-test. Scale bar is 5 µm. (G) Correlative light and electron microscopy (CLEM) images show additional examples of mitochondria with GFP-Parkin accumulation in polarized mitochondria, assessed by TMRM fluorescence (see also example in Fig. 3H). The corresponding ultrastructures show that the polarized mitochondria with internalized Parkin (white arrows) have intact membranes and cristae. Scale bars are 4 µm for fluorescent images and 1 µm for EM images. (H) CLEM images show examples of Drp1KO mitochondria with endogenous overlapping-Parkin detected by anti-Parkin antibody (Proteintech, #14060-1-AP). Scale bars are 4 µm (cell overview) and 0.4 µm (inset). (I) Scatter graph shows average duration of the OM-Parkin pattern before dissipation in Drp1KO neurons expressing GFP-Parkin. Data show mean ± SEM. n=11 mitochondria.

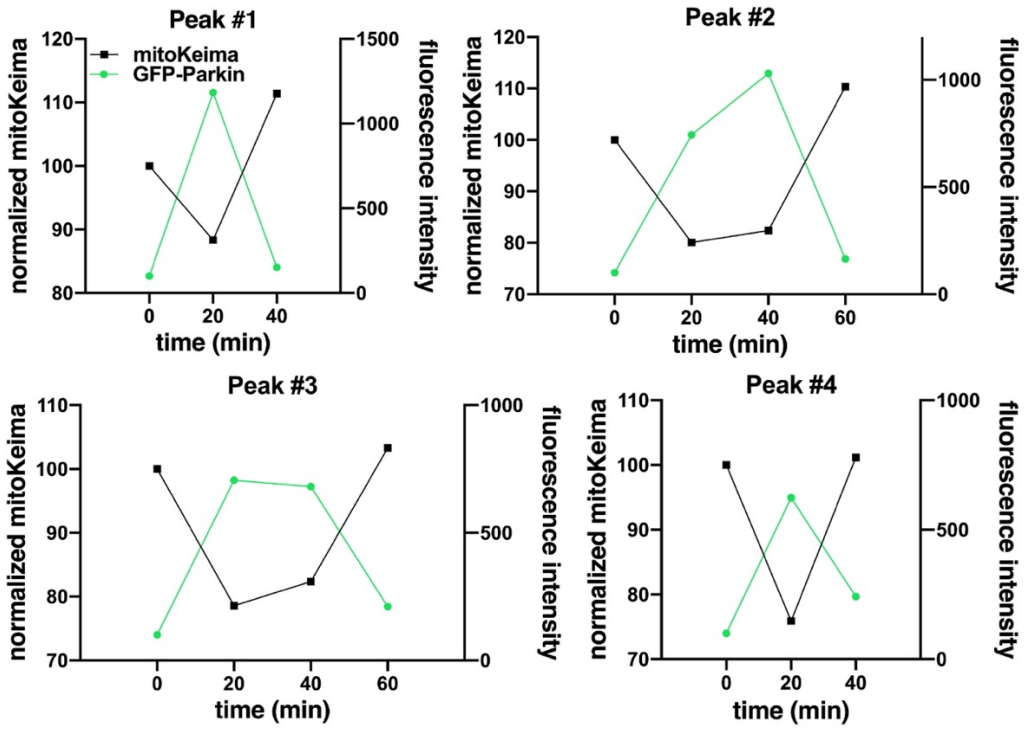

Figure 2.14

S6. Direct Parkin accumulation in mitochondria varies inversely with mitochondrial acidity during Parkin spikes. Quantitation of GFP-Parkin accumulation (green) and concurrent

mitochondria de-acidification in individual mitochondria during direct matrix-Parkin recruitment in Fig. 4H.

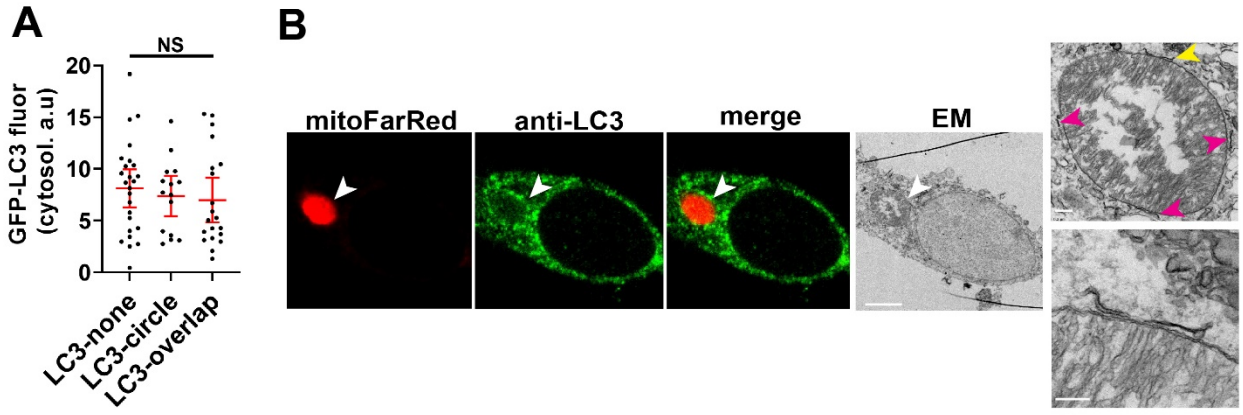

Figure 2.15

S7. Visualization of mitochondrion encircled by endogenous LC3. (A) Scatter graph of cytosolic GFP-LC3 intensity for different patterns of LC3 recruitment in Drp1KO neurons, n=15-25 neurons/group from 3 independent experiments. Data show mean ± SEM; NS= not significant by one-way ANOVA. (B) CLEM images show a Drp1KO neuron treated with 100 nM bafilomycin for 4 h and then processed for immunofluorescence against endogenous LC3. The corresponding ultrastructure shows pieces of isolated membranes surrounding the mitochondria. Scale bars are 4 µm (cell overview), 400 nm (upper inset) and 200 nm (bottom inset) for EM images.

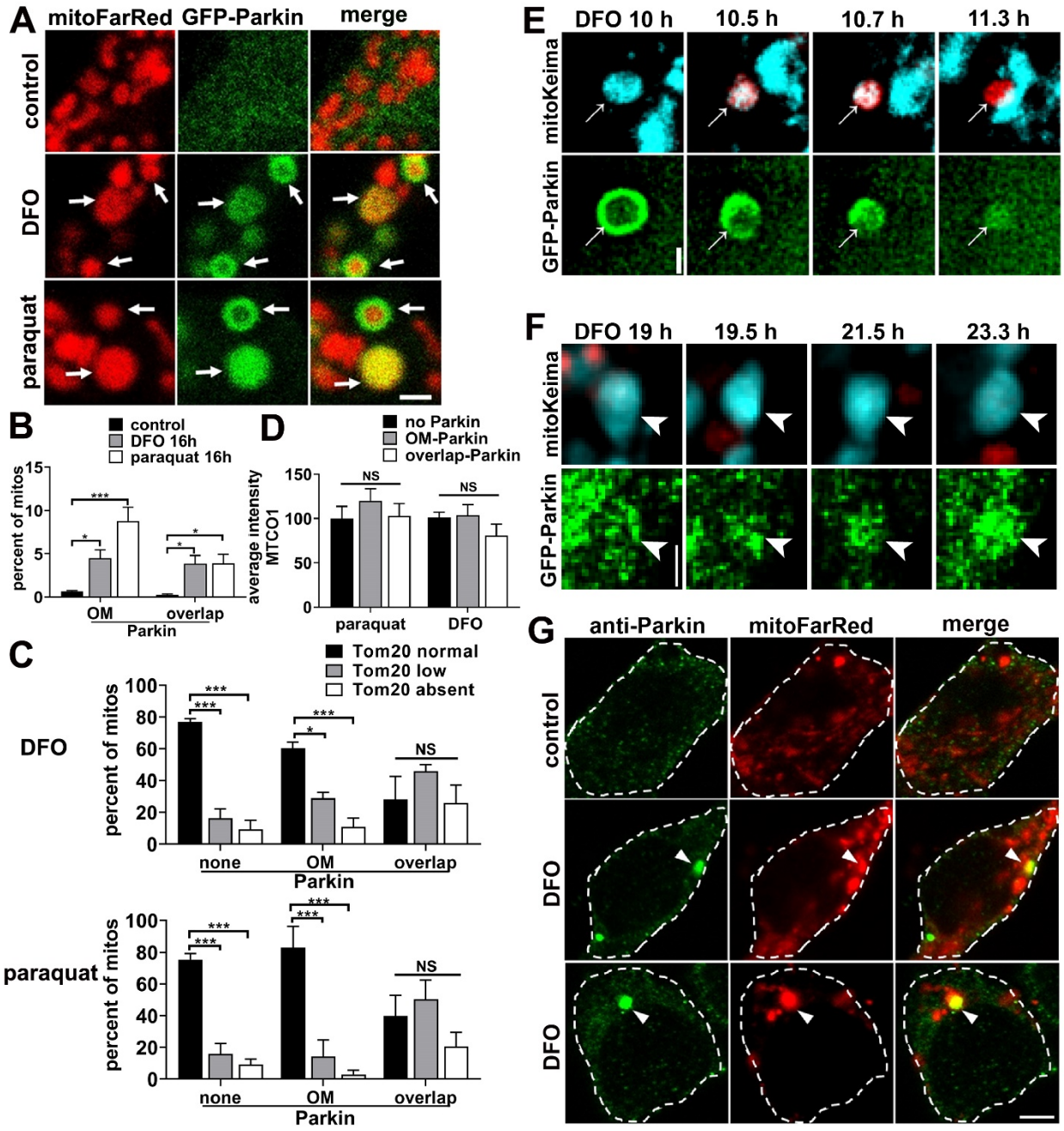

Figure 2.16

S8. Stress induces overlapping Parkin accumulation in wild type neurons (A) Wt neurons co-expressing GFP-Parkin and mitoFarRed were incubated with vehicle control, DFO (500 µM) or Paraquat (10 µM) for 16 hrs. Scale bar is 1 µm. (B) Graph shows the percentage of mitochondria with OM-Parkin and overlapping-Parkin accumulation. n=4 coverslips per group, each with 10-15 cells and 137-980 mitochondria/coverslip, from 2 experiments. (C-D) Wt neurons co-expressing GFP-Parkin and mitoBFP were incubated with DFO or Paraquat for 24

hours, and then processed for immunofluorescence against Tom20 (OM) or MTCO1 (inner mitochondrial membrane). (C) A subset of mitochondria with overlapping-Parkin accumulation have decreased or absent Tom20 staining intensity (n=4 coverslips per group from 2 experiments), while (D) the intensity of the inner mitochondrial membrane protein MTCO1 was unchanged (n=8-52 mitochondria per group from 2 experiments). NS, not significant, *$p<0.05$, ***$p<0.001$ by one-way or two-way ANOVA with Sidak's multiple comparisons test. (E, F) WT neurons co-expressing mitoKeima and GFP-Parkin were imaged every 10 minutes at different stages of DFO incubation. Images show (E) OM-Parkin mitochondria undergoing acidification and overlapping-Parkin transition before making contacts with other mitochondria and (F) direct overlapping-Parkin accumulation in a mitochondrion with normal pH. Scale bars are 1 μm. (G) Representative images show wt neurons expressing mitoFarRed, treated with vehicle control or DFO (500 μM) for 16 h, and immunostained for endogenous Parkin. Scale bar is 4 μm.

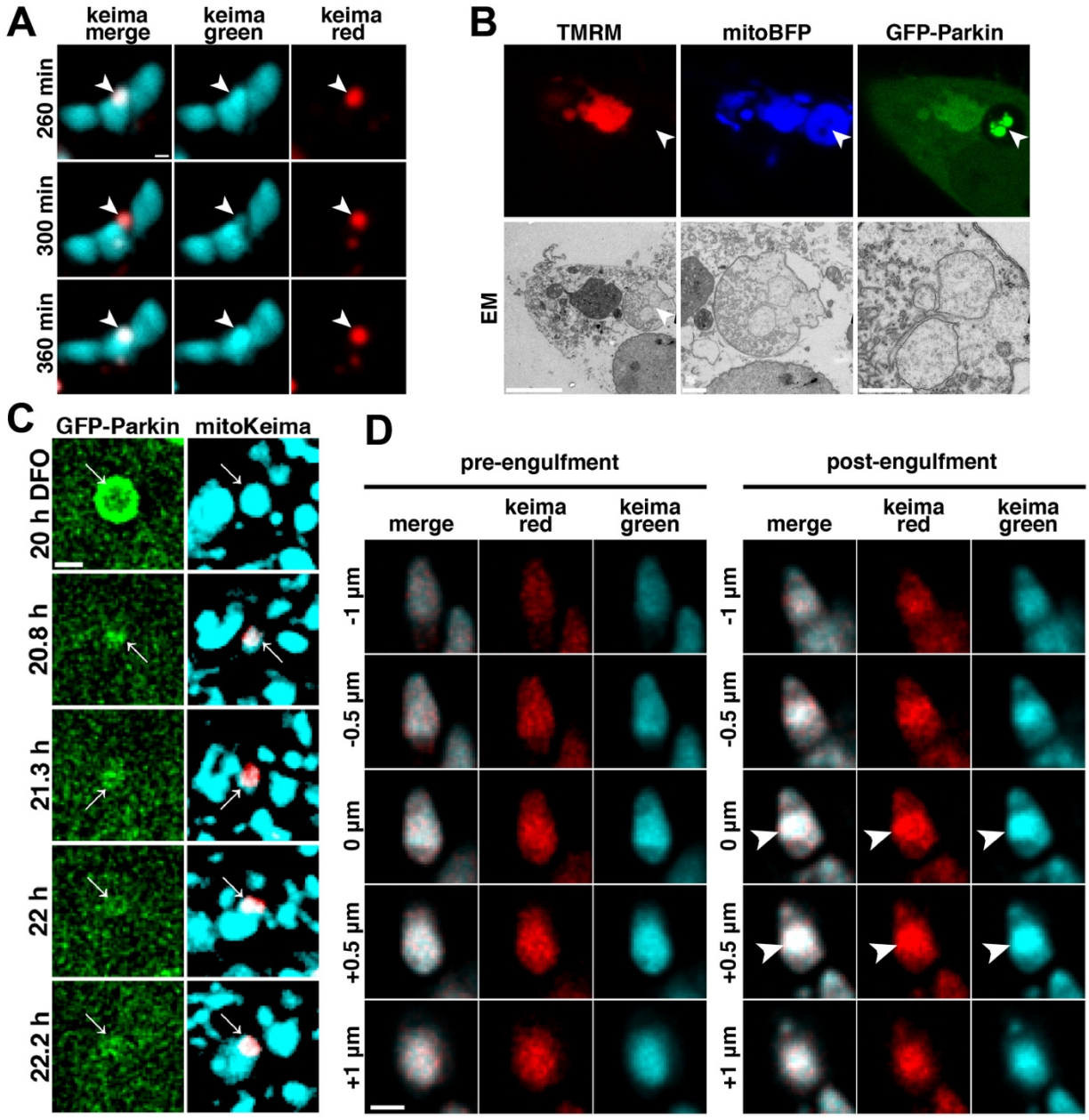

Figure 2.17

S9. Drp1KO and wt mitochondria transiently engulf degrading mitochondrial structures. (A) Additional time lapse images related to Figure 6A show the engulfed mitolysosome (white arrow) at t = 260 min leaving and then re-entering the receiver neutral mitochondria. Scale bar is 1 µm. (B) CLEM images show Parkin-positive membrane-bound structures inside a Drp1KO mitochondrion, suggesting prior engulfment of Parkin-targeted cellular material. Scale bars are 5 µm for cell overview and 1 µm for insets. (C,D) WT neurons co-expressing mitoKeima and GFP-Parkin were imaged every 10 minutes at different stages of DFO incubation. Images in (C) show an OM-Parkin mitochondrion undergoing lysosomal fusion and OM-to-overlapping Parkin

transition before getting engulfed by a normal mitochondrion. Z-stacks in (D) show a neutral mitochondrion before and after (10 min interval) engulfing an acidic structure (arrows). Scale bars are 1 μm.

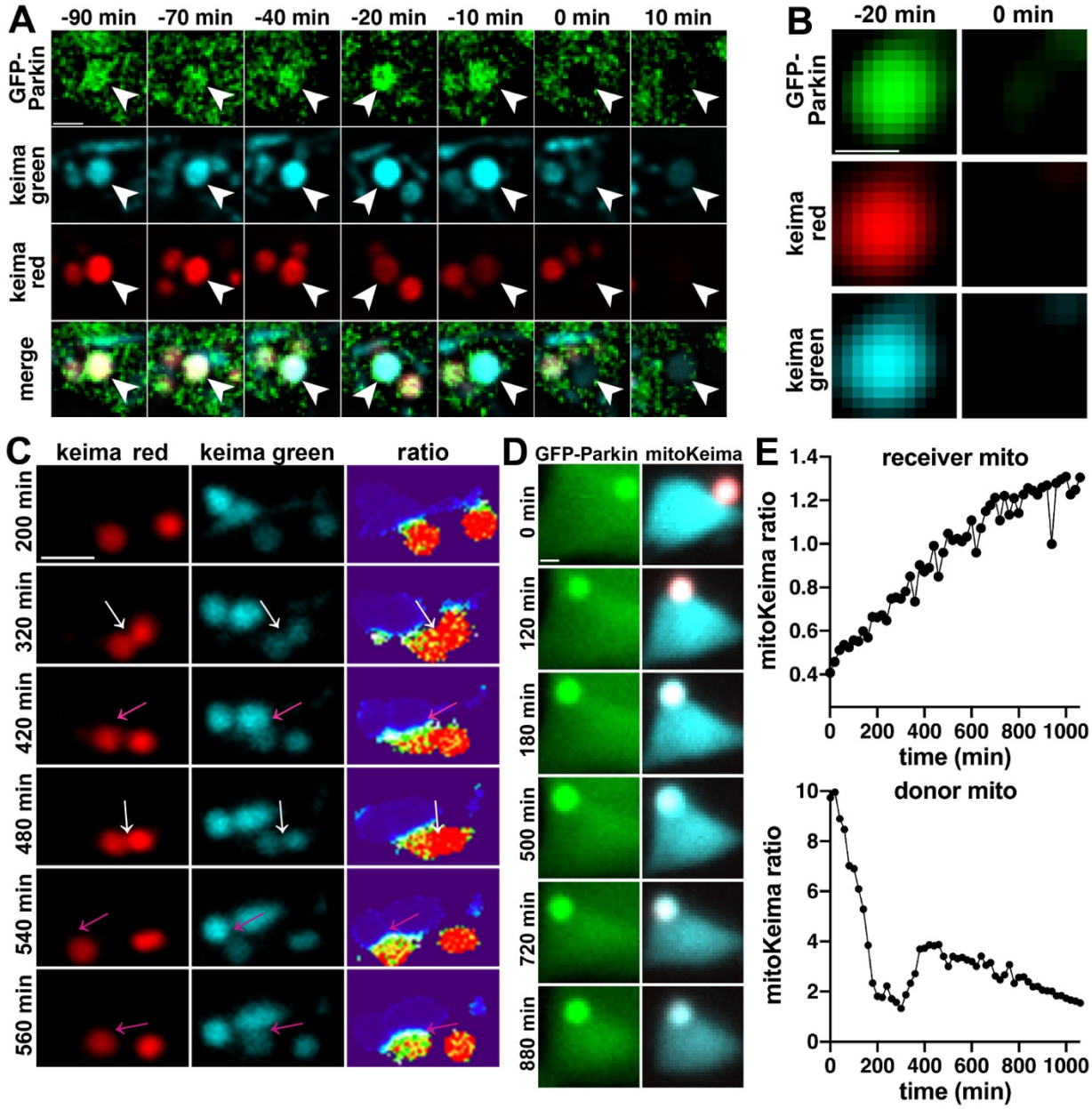

Figure 2.18

S10. Mitolysosomes burst and interact closely with the mitochondrial network. (A) Representative time-lapse images show a Parkin-positive mitolysosome bursting at time t=0 min in a wt neuron co-expressing GFP-Parkin and mitoKeima, and treated with DFO. Prior to bursting, the positive mitolysosome deacidifies. Scale bar is 1 μm. (B) Representative time-lapse

images show the abrupt disappearance of an overlapping-Parkin mitolysosome in a Drp1KO neuron. Scale bar is 1 μm. (C) Inset of Fig. 7I with additional time points. White arrows indicate contacts between acidified mitochondria while pink arrows indicate contacts between acidified and non-acidified mitochondria. Scale bar is 3 μm. (D) Acidified mitochondria can fuse and transfer contents to non-acidic mitochondria, as evidenced by increased acidity and overlapping-Parkin in recipient mitochondria. Scale bar is 1 μm. (E) Quantitation of relative acidity levels for smaller "donor" and larger "receiver" mitochondria during the transfer event exhibited in (D). Receiver mitochondrion becomes more acidic during prolonged contact with donor mitochondrion. Donor mitochondrion concomitantly normalizes pH levels.

2.6 References

1. K. Itoh, K. Nakamura, M. Iijima, H. Sesaki, Mitochondrial dynamics in neurodegeneration. Trends Cell Biol. 23, 64–71 (2013).

2. A. Berthet, E. B. Margolis, J. Zhang, I. Hsieh, J. Zhang, T. S. Hnasko, J. Ahmad, R. H. Edwards, H. Sesaki, E. J. Huang, K. Nakamura, Loss of mitochondrial fission depletes axonal mitochondria in midbrain dopamine neurons. J. Neurosci. 34, 14304–14317 (2014).

3. A. H. Pham, S. Meng, Q. N. Chu, D. C. Chan, Loss of Mfn2 results in progressive, retrograde degeneration of dopaminergic neurons in the nigrostriatal circuit. Hum. Mol. Genet. 21, 4817–4826 (2012).

4. K. Nakamura, V. M. Nemani, F. Azarbal, G. Skibinski, J. M. Levy, K. Egami, L. Munishkina, J. Zhang, B. Gardner, J. Wakabayashi, H. Sesaki, Y. Cheng, S. Finkbeiner, R. L. Nussbaum, E. Masliah, R. H. Edwards, Direct membrane association drives mitochondrial fission by the Parkinson disease-associated protein alpha-synuclein. J. Biol. Chem. 286, 20710–20726 (2011).

5. W. Wang, X. Wang, H. Fujioka, C. Hoppel, A. L. Whone, M. A. Caldwell, P. J. Cullen, J. Liu, X. Zhu, Parkinson's disease-associated mutant VPS35 causes mitochondrial dysfunction by recycling DLP1 complexes. Nat. Med. 22, 54–63 (2016).

6. D. P. Narendra, S. M. Jin, A. Tanaka, D. F. Suen, C. A. Gautier, J. Shen, M. R. Cookson, R. J. Youle, PINK1 is selectively stabilized on impaired mitochondria to activate Parkin. PLOS Biol. 8, e1000298 (2010).

7. A. C. Poole, R. E. Thomas, L. A. Andrews, H. M. McBride, A. J. Whitworth, L. J. Pallanck, The PINK1/Parkin pathway regulates mitochondrial morphology. Proc. Natl. Acad. Sci. U.S.A. 105, 1638–1643 (2008).

8. I. E. Clark, M. W. Dodson, C. Jiang, J. H. Cao, J. R. Huh, J. H. Seol, S. J. Yoo, B. A. Hay, M. Guo, Drosophila pink1 is required for mitochondrial function and interacts genetically with parkin. Nature 441, 1162–1166 (2006).

9. A. Tanaka, M. M. Cleland, S. Xu, D. P. Narendra, D. F. Suen, M. Karbowski, R. J. Youle, Proteasome and p97 mediate mitophagy and degradation of mitofusins induced by Parkin. J. Cell Biol. 191, 1367–1380 (2010).

10. E. Ziviani, R. N. Tao, A. J. Whitworth, Drosophila parkin requires PINK1 for mitochondrial translocation and ubiquitinates mitofusin. Proc. Natl. Acad. Sci. U.S.A. 107, 5018–5023 (2010).

11. G. Twig, A. Elorza, A. J. Molina, H. Mohamed, J. D. Wikstrom, G. Walzer, L. Stiles, S. E. Haigh, S. Katz, G. Las, J. Alroy, M. Wu, B. F. Py, J. Yuan, J. T. Deeney, B. E. Corkey, O. S. Shirihai, Fission and selective fusion govern mitochondrial segregation and elimination by autophagy. EMBO J. 27, 433–446 (2008).

12. Y. Kageyama, M. Hoshijima, K. Seo, D. Bedja, P. Sysa-Shah, S. A. Andrabi, W. Chen, A. Hoke, V. L. Dawson, T. M. Dawson, K. Gabrielson, D. A. Kass, M. Iijima, H. Sesaki, Parkin-independent mitophagy requires Drp1 and maintains the integrity of mammalian heart and brain. EMBO J. 33, 2798–2813 (2014).

13. Y. Ikeda, A. Shirakabe, Y. Maejima, P. Zhai, S. Sciarretta, J. Toli, M. Nomura, K. Mihara, K. Egashira, M. Ohishi, M. Abdellatif, J. Sadoshima, Endogenous Drp1 mediates mitochondrial autophagy and protects the heart against energy stress. Circ. Res. 116, 264–278 (2015).

14. M. Song, K. Mihara, Y. Chen, L. Scorrano, G. W. Dorn II, Mitochondrial fission and fusion factors reciprocally orchestrate mitophagic culling in mouse hearts and cultured fibroblasts. Cell Metab. 21, 273–286 (2015).

15. S. I. Yamashita, X. Jin, K. Furukawa, M. Hamasaki, A. Nezu, H. Otera, T. Saigusa, T. Yoshimori, Y. Sakai, K. Mihara, T. Kanki, Mitochondrial division occurs concurrently with autophagosome formation but independently of Drp1 during mitophagy. J. Cell Biol. 215, 649–665 (2016).

16. J. L. Burman, S. Pickles, C. Wang, S. Sekine, J. N. S. Vargas, Z. Zhang, A. M. Youle, C. L. Nezich, X. Wu, J. A. Hammer, R. J. Youle, Mitochondrial fission facilitates the selective mitophagy of protein aggregates. J. Cell Biol. 216, 3231–3247 (2017).

17. Q. Cai, H. M. Zakaria, A. Simone, Z. H. Sheng, Spatial parkin translocation and degradation of damaged mitochondria via mitophagy in live cortical neurons. Curr. Biol. 22, 545–552 (2012).

18. V. S. Van Laar, B. Arnold, S. J. Cassady, C. T. Chu, E. A. Burton, S. B. Berman, Bioenergetics of neurons inhibit the translocation response of Parkin following rapid mitochondrial depolarization. Hum. Mol. Genet. 20, 927–940 (2011).

19. K. Grenier, G. L. McLelland, E. A. Fon, Parkin- and PINK1-dependent mitophagy in neurons: Will the real pathway please stand up? Front. Neurol. 4, 100 (2013).

20. C. Vives-Bauza, C. Zhou, Y. Huang, M. Cui, R. L. de Vries, J. Kim, J. May, M. A. Tocilescu, W. Liu, H. S. Ko, J. Magrane, D. J. Moore, V. L. Dawson, R. Grailhe, T. M. Dawson, C. Li, K. Tieu, S. Przedborski, PINK1-dependent recruitment of Parkin to mitochondria in mitophagy. Proc. Natl. Acad. Sci. U.S.A. 107, 378–383 (2010).

21. M. Lazarou, D. A. Sliter, L. A. Kane, S. A. Sarraf, C. Wang, J. L. Burman, D. P. Sideris, A. I. Fogel, R. J. Youle, The ubiquitin kinase PINK1 recruits autophagy receptors to induce mitophagy. Nature 524, 309–314 (2015).

22. T. Kitada, A. Pisani, D. R. Porter, H. Yamaguchi, A. Tscherter, G. Martella, P. Bonsi, C. Zhang, E. N. Pothos, J. Shen, Impaired dopamine release and synaptic plasticity in the striatum of PINK1-deficient mice. Proc. Natl. Acad. Sci. U.S.A. 104, 11441–11446 (2007).

23. R. K. Dagda, S. J. Cherra III, S. M. Kulich, A. Tandon, D. Park, C. T. Chu, Loss of PINK1 function promotes mitophagy through effects on oxidative stress and mitochondrial fission. J. Biol. Chem. 284, 13843–13855 (2009).

24. Y. Kageyama, Z. Zhang, R. Roda, M. Fukaya, J. Wakabayashi, N. Wakabayashi, T. W. Kensler, P. H. Reddy, M. Iijima, H. Sesaki, Mitochondrial division ensures the survival of postmitotic neurons by suppressing oxidative damage. J. Cell Biol. 197, 535–551 (2012).

25. H. Katayama, T. Kogure, N. Mizushima, T. Yoshimori, A. Miyawaki, A sensitive and quantitative technique for detecting autophagic events based on lysosomal delivery. Chem. Biol. 18, 1042–1052 (2011).

26. C. Mauvezin, P. Nagy, G. Juhasz, T. P. Neufeld, Autophagosome-lysosome fusion is independent of V-ATPase-mediated acidification. Nat. Commun. 6, 7007 (2015).

27. T. Hara, K. Nakamura, M. Matsui, A. Yamamoto, Y. Nakahara, R. Suzuki-Migishima, M. Yokoyama, K. Mishima, I. Saito, H. Okano, N. Mizushima, Suppression of basal autophagy in neural cells causes neurodegenerative disease in mice. Nature 441, 885–889 (2006).

28. I. Mellman, R. Fuchs, A. Helenius, Acidification of the endocytic and exocytic pathways. Annu. Rev. Biochem. 55, 663–700 (1986).

29. L. A. Pronevich, T. A. Mirzabekov, Z. E. Rozhdestvenskaya, Mitochondrial porin regulates the sensitivity of anion carriers to inhibitors. FEBS Lett. 247, 330–332 (1989).

30. S. R. Yoshii, C. Kishi, N. Ishihara, N. Mizushima, Parkin mediates proteasome-dependent protein degradation and rupture of the outer mitochondrial membrane. J. Biol. Chem. 286, 19630–19640 (2011).

31. S. M. Jin, R. J. Youle, The accumulation of misfolded proteins in the mitochondrial matrix is sensed by PINK1 to induce PARK2/Parkin-mediated mitophagy of polarized mitochondria. Autophagy 9, 1750–1757 (2013).

32. A. E. Vincent, Y. S. Ng, K. White, T. Davey, C. Mannella, G. Falkous, C. Feeney, A. M. Schaefer, R. McFarland, G. S. Gorman, R. W. Taylor, D. M. Turnbull, M. Picard, The spectrum of mitochondrial ultrastructural defects in mitochondrial myopathy. Sci. Rep. 6, 30610 (2016).

33. D. Poburko, J. Santo-Domingo, N. Demaurex, Dynamic regulation of the mitochondrial proton gradient during cytosolic calcium elevations. J. Biol. Chem. 286, 11672–11684 (2011).

34. Y. C. Wong, D. Ysselstein, D. Krainc, Mitochondria-lysosome contacts regulate mitochondrial fission via RAB7 GTP hydrolysis. Nature 554, 382–386 (2018).

35. S. R. Yoshii, N. Mizushima, Monitoring and measuring autophagy. Int. J. Mol. Sci. 18, (2017).

36. S. Kimura, T. Noda, T. Yoshimori, Dissection of the autophagosome maturation process by a novel reporter protein, tandem fluorescent-tagged LC3. Autophagy 3, 452–460 (2007).

37. E. Itakura, N. Mizushima, Characterization of autophagosome formation site by a hierarchical analysis of mammalian Atg proteins. Autophagy 6, 764–776 (2010).

38. G. F. Allen, R. Toth, J. James, I. G. Ganley, Loss of iron triggers PINK1/Parkin-independent mitophagy. EMBO Rep. 14, 1127–1135 (2013).

39. D. E. Johnson, P. Ostrowski, V. Jaumouille, S. Grinstein, The position of lysosomes within the cell determines their luminal pH. J. Cell Biol. 212, 677–692 (2016).

40. G. Favaro, V. Romanello, T. Varanita, M. Andrea Desbats, V. Morbidoni, C. Tezze, M. Albiero, M. Canato, G. Gherardi, D. De Stefani, C. Mammucari, B. Blaauw, S. Boncompagni, F. Protasi, C. Reggiani, L. Scorrano, L. Salviati, M. Sandri, DRP1-mediated mitochondrial shape controls calcium homeostasis and muscle mass. Nat. Commun. 10, 2576 (2019).

41. Y. Yang, Y. Ouyang, L. Yang, M. F. Beal, A. McQuibban, H. Vogel, B. Lu, Pink1 regulates mitochondrial dynamics through interaction with the fission/fusion machinery. Proc. Natl. Acad. Sci. U.S.A. 105, 7070–7075 (2008).

42. S. Gispert, F. Ricciardi, A. Kurz, M. Azizov, H. H. Hoepken, D. Becker, W. Voos, K. Leuner, W. E. Muller, A. P. Kudin, W. S. Kunz, A. Zimmermann, J. Roeper, D. Wenzel, M. Jendrach, M. Garcia-Arencibia, J. Fernandez-Ruiz, L. Huber, H. Rohrer, M. Barrera, A. S.

Reichert, U. Rub, A. Chen, R. L. Nussbaum, G. Auburger, Parkinson phenotype in aged PINK1-deficient mice is accompanied by progressive mitochondrial dysfunction in absence of neurodegeneration. PLOS ONE 4, e5777 (2009).

43. A. K. Lutz, N. Exner, M. E. Fett, J. S. Schlehe, K. Kloos, K. Lammermann, B. Brunner, A. Kurz-Drexler, F. Vogel, A. S. Reichert, L. Bouman, D. Vogt-Weisenhorn, W. Wurst, J. Tatzelt, C. Haass, K. F. Winklhofer, Loss of parkin or PINK1 function increases Drp1-dependent mitochondrial fragmentation. J. Biol. Chem. 284, 22938–22951 (2009).

44. S. Gispert, N. Brehm, J. Weil, K. Seidel, U. Rub, B. Kern, M. Walter, J. Roeper, G. Auburger, Potentiation of neurotoxicity in double-mutant mice with Pink1 ablation and A53T-SNCA overexpression. Hum. Mol. Genet. 24, 1061–1076 (2015).

45. S. Song, S. Jang, J. Park, S. Bang, S. Choi, K. Y. Kwon, X. Zhuang, E. Kim, J. Chung, Characterization of PINK1 (PTEN-induced putative kinase 1) mutations associated with Parkinson disease in mammalian cells and Drosophila. J. Biol. Chem. 288, 5660–5672 (2013).

46. L. Chen, Z. Xie, S. Turkson, X. Zhuang, A53T human α-synuclein overexpression in transgenic mice induces pervasive mitochondria macroautophagy defects preceding dopamine neuron degeneration. J. Neurosci. 35, 890–905 (2015).

47. P. M. Rappold, M. Cui, J. C. Grima, R. Z. Fan, K. L. de Mesy-Bentley, L. Chen, X. Zhuang, W. J. Bowers, K. Tieu, Drp1 inhibition attenuates neurotoxicity and dopamine release deficits in vivo. Nat. Commun. 5, 5244 (2014).

48. E. A. Bordt, P. Clerc, B. A. Roelofs, A. J. Saladino, L. Tretter, V. Adam-Vizi, E. Cherok, A. Khalil, N. Yadava, S. X. Ge, T. C. Francis, N. W. Kennedy, L. K. Picton, T. Kumar, S. Uppuluri,

A. M. Miller, K. Itoh, M. Karbowski, H. Sesaki, R. B. Hill, B. M. Polster, The putative Drp1 inhibitor mdivi-1 is a reversible mitochondrial complex I inhibitor that modulates reactive oxygen species. Dev Cell 40, 583–594.e6 (2017).

49. Y. Kuroda, T. Mitsui, M. Kunishige, M. Shono, M. Akaike, H. Azuma, T. Matsumoto, Parkin enhances mitochondrial biogenesis in proliferating cells. Hum. Mol. Genet. 15, 883–895 (2006).

50. A. B. Harbauer, R. P. Zahedi, A. Sickmann, N. Pfanner, C. Meisinger, The protein import machinery of mitochondria-a regulatory hub in metabolism, stress, and disease. Cell Metab. 19, 357–372 (2014).

51. P. K. Kim, E. H. Hettema, Multiple pathways for protein transport to peroxisomes. J. Mol. Biol. 427, 1176–1190 (2015).

52. Y. Kuroda, W. Sako, S. Goto, T. Sawada, D. Uchida, Y. Izumi, T. Takahashi, N. Kagawa, M. Matsumoto, M. Matsumoto, R. Takahashi, R. Kaji, T. Mitsui, Parkin interacts with Klokin1 for mitochondrial import and maintenance of membrane potential. Hum. Mol. Genet. 21, 991–1003 (2012).

53. V. S. Burchell, D. E. Nelson, A. Sanchez-Martinez, M. Delgado-Camprubi, R. M. Ivatt, J. H. Pogson, S. J. Randle, S. Wray, P. A. Lewis, H. Houlden, A. Y. Abramov, J. Hardy, N. W. Wood, A. J. Whitworth, H. Laman, H. Plun-Favreau, The Parkinson's disease-linked proteins Fbxo7 and Parkin interact to mediate mitophagy. Nat. Neurosci. 16, 1257–1265 (2013).

54. Z. D. Zhou, S. P. Xie, S. Sathiyamoorthy, W. T. Saw, T. Y. Sing, S. H. Ng, H. P. Chua, A. M. Tang, F. Shaffra, Z. Li, H. Wang, P. G. Ho, M. K. Lai, D. C. Angeles, T. M. Lim, E. K. Tan,

F-box protein 7 mutations promote protein aggregation in mitochondria and inhibit mitophagy. Hum. Mol. Genet. 24, 6314–6330 (2015).

55. V. A. Selivanov, J. A. Zeak, J. Roca, M. Cascante, M. Trucco, T. V. Votyakova, The role of external and matrix pH in mitochondrial reactive oxygen species generation. J. Biol. Chem. 283, 29292–29300 (2008).

56. M. Khacho, M. Tarabay, D. Patten, P. Khacho, J. G. MacLaurin, J. Guadagno, R. Bergeron, S. P. Cregan, M. E. Harper, D. S. Park, R. S. Slack, Acidosis overrides oxygen deprivation to maintain mitochondrial function and cell survival. Nat. Commun. 5, 3550 (2014).

57. C. S. Evans, E. L. Holzbaur, Degradation of engulfed mitochondria is rate-limiting in Optineurin-mediated mitophagy in neurons. eLife 9, e50260 (2020).

58. Y. C. Wong, W. Peng, D. Krainc, Lysosomal regulation of inter-mitochondrial contact fate and motility in Charcot-Marie-Tooth type 2. Dev. Cell 50, 339–354.e4 (2019).

59. A. J. Roger, S. A. Munoz-Gomez, R. Kamikawa, The origin and diversification of mitochondria. Curr. Biol. 27, R1177–R1192 (2017).

60. V. K. Mony, S. Benjamin, E. J. O'Rourke, A lysosome-centered view of nutrient homeostasis. Autophagy 12, 619–631 (2016).

61. Q. Zhang, M. Raoof, Y. Chen, Y. Sumi, T. Sursal, W. Junger, K. Brohi, K. Itagaki, C. J. Hauser, Circulating mitochondrial DAMPs cause inflammatory responses to injury. Nature 464, 104–107 (2010).

62. A. P. West, W. Khoury-Hanold, M. Staron, M. C. Tal, C. M. Pineda, S. M. Lang, M. Bestwick, B. A. Duguay, N. Raimundo, D. A. MacDuff, S. M. Kaech, J. R. Smiley, R. E. Means, A. Iwasaki, G. S. Shadel, Mitochondrial DNA stress primes the antiviral innate immune response. Nature 520, 553–557 (2015).

63. A. P. West, G. S. Shadel, Mitochondrial DNA in innate immune responses and inflammatory pathology. Nat. Rev. Immunol. 17, 363–375 (2017).

64. D. A. Sliter, J. Martinez, L. Hao, X. Chen, N. Sun, T. D. Fischer, J. L. Burman, Y. Li, Z. Zhang, D. P. Narendra, H. Cai, M. Borsche, C. Klein, R. J. Youle, Parkin and PINK1 mitigate STING-induced inflammation. Nature 561, 258–262 (2018).

65. A. Rongvaux, R. Jackson, C. C. Harman, T. Li, A. P. West, M. R. de Zoete, Y. Wu, B. Yordy, S. A. Lakhani, C. Y. Kuan, T. Taniguchi, G. S. Shadel, Z. J. Chen, A. Iwasaki, R. A. Flavell, Apoptotic caspases prevent the induction of type I interferons by mitochondrial DNA. Cell 159, 1563–1577 (2014).

66. L. Bonet-Ponce, A. Beilina, C. D. Williamson, E. Lindberg, J. H. Kluss, S. Saez-Atienzar, N. Landeck, R. Kumaran, A. Mamais, C. K. E. Bleck, Y. Li, M. R. Cookson, LRRK2 mediates tubulation and vesicle sorting from lysosomes. Sci. Adv. 6, eabb2454 (2020).

67. L. Fernandez-Mosquera, K. F. Yambire, R. Couto, L. Pereyra, K. Pabis, A. H. Ponsford, C. V. Diogo, M. Stagi, I. Milosevic, N. Raimundo, Mitochondrial respiratory chain deficiency inhibits lysosomal hydrolysis. Autophagy 15, 1572–1591 (2019).

68. Y. Miyamoto, N. Kitamura, Y. Nakamura, M. Futamura, T. Miyamoto, M. Yoshida, M. Ono, S. Ichinose, H. Arakawa, Possible existence of lysosome-like organella within mitochondria and its role in mitochondrial quality control. PLOS ONE 6, e16054 (2011).

69. T. Miyamoto, N. Kitamura, M. Ono, Y. Nakamura, M. Yoshida, H. Kamino, R. Murai, T. Yamada, H. Arakawa, Identification of 14-3-3□ as a Mieap-interacting protein and its role in mitochondrial quality control. Sci. Rep. 2, 379 (2012).

70. A. M. Pickrell, C. H. Huang, S. R. Kennedy, A. Ordureau, D. P. Sideris, J. G. Hoekstra, J. W. Harper, R. J. Youle, Endogenous Parkin preserves dopaminergic substantia nigral neurons following mitochondrial DNA mutagenic stress. Neuron 87, 371–381 (2015).

71. E. S. Vincow, G. Merrihew, R. E. Thomas, N. J. Shulman, R. P. Beyer, M. J. MacCoss, L. J. Pallanck, The PINK1-Parkin pathway promotes both mitophagy and selective respiratory chain turnover in vivo. Proc. Natl. Acad. Sci. U.S.A. 110, 6400–6405 (2013).

72. E. S. Vincow, R. E. Thomas, G. E. Merrihew, N. J. Shulman, T. K. Bammler, J. W. MacDonald, M. J. MacCoss, L. J. Pallanck, Autophagy accounts for approximately one-third of mitochondrial protein turnover and is protein selective. Autophagy 15, 1592–1605 (2019).

73. J. T. Cribbs, S. Strack, Reversible phosphorylation of Drp1 by cyclic AMP-dependent protein kinase and calcineurin regulates mitochondrial fission and cell death. EMBO Rep. 8, 939–944 (2007).

74. H. Imamura, K. P. Huynh Nhat, H. Togawa, K. Saito, R. Iino, Y. Kato-Yamada, T. Nagai, H. Noji, Visualization of ATP levels inside single living cells with fluorescence resonance energy

transfer-based genetically encoded indicators. Proc. Natl. Acad. Sci. U.S.A. 106, 15651–15656 (2009).

75. K. S. Morozova, K. D. Piatkevich, T. J. Gould, J. Zhang, J. Bewersdorf, V. V. Verkhusha, Far-red fluorescent protein excitable with red lasers for flow cytometry and superresolution STED nanoscopy. Biophys. J. 99, L13–L15 (2010).

76. O. M. Subach, I. S. Gundorov, M. Yoshimura, F. V. Subach, J. Zhang, D. Gruenwald, E. A. Souslova, D. M. Chudakov, V. V. Verkhusha, Conversion of red fluorescent protein into a bright blue probe. Chem. Biol. 15, 1116–1124 (2008).

77. S. Kanaji, J. Iwahashi, Y. Kida, M. Sakaguchi, K. Mihara, Characterization of the signal that directs Tom20 to the mitochondrial outer membrane. J. Cell Biol. 151, 277–288 (2000).

78. J. Wakabayashi, Z. Zhang, N. Wakabayashi, Y. Tamura, M. Fukaya, T. W. Kensler, M. Iijima, H. Sesaki, The dynamin-related GTPase Drp1 is required for embryonic and brain development in mice. J. Cell Biol. 186, 805–816 (2009).

79. C. M. Backman, N. Malik, Y. Zhang, L. Shan, A. Grinberg, B. J. Hoffer, H. Westphal, A. C. Tomac, Characterization of a mouse strain expressing Cre recombinase from the 3′ untranslated region of the dopamine transporter locus. Genesis 44, 383–390 (2006).

80. L. Y. Shields, H. Kim, L. Zhu, D. Haddad, A. Berthet, D. Pathak, M. Lam, R. Ponnusamy, L. G. Diaz-Ramirez, T. M. Gill, H. Sesaki, L. Mucke, K. Nakamura, Dynamin-related protein 1 is required for normal mitochondrial bioenergetic and synaptic function in CA1 hippocampal neurons. Cell Death Dis. 6, e1725 (2015).

81. J. H. Shin, H. S. Ko, H. Kang, Y. Lee, Y. I. Lee, O. Pletinkova, J. C. Troconso, V. L. Dawson, T. M. Dawson, PARIS (ZNF746) repression of PGC-1α contributes to neurodegeneration in Parkinson's disease. Cell 144, 689–702 (2011).

82. M. van Lith, S. Tiwari, J. Pediani, G. Milligan, N. J. Bulleid, Real-time monitoring of redox changes in the mammalian endoplasmic reticulum. J. Cell Sci. 124, 2349–2356 (2011).

83. S. J. Barmada, A. Serio, A. Arjun, B. Bilican, A. Daub, D. M. Ando, A. Tsvetkov, M. Pleiss, X. Li, D. Peisach, C. Shaw, S. Chandran, S. Finkbeiner, Autophagy induction enhances TDP43 turnover and survival in neuronal ALS models. Nat. Chem. Biol. 10, 677–685 (2014).

84. M. Arrasate, S. Finkbeiner, Automated microscope system for determining factors that predict neuronal fate. Proc. Natl. Acad. Sci. U.S.A. 102, 3840–3845 (2005).

Chapter 3 Chronic hyperactivation induces preferential axonal degeneration

3.1 Introduction

Neural circuits must retain function in incredibly dynamic and complex biological environments. This task becomes especially onerous in situations where external events such as brain injury or neurodegenerative diseases affect the functional or structural integrity of the circuit. Indeed, the loss of a given node forces the neural circuit to compensate for the change through functional reorganization at cellular and system levels in order to re-establish homeostasis. The extent to which this is achieved will determine the severity of functional loss and therefore, circuit-associated neurological symptoms.

In Parkinson's disease (PD), the loss of substantia nigra (SNc) dopamine (DA) neurons has severe consequences on circuit dynamics of the basal ganglia. Compensation for dopamine loss occurs in a myriad of ways, including regulation of neural activity in surviving SNc neurons and other circuit elements. Rat studies have shown that following partial lesions of the nigrostriatal pathway, surviving SNc DA neurons are hyperactive (1), release additional dopamine (2-5) and have reduced dopamine reuptake (2). This is consistent with evidence from primate models suggesting that the subthalamic nucleus, which sends a glutamatergic projection to the SNc, is hyperactive in PD (6). While all these system-level changes presumably constitute an attempt to reintroduce normal striatal (and nigral?) dopamine, they may also have unintended consequences.

Even at baseline, SNc dopamine neurons carry an immense energetic burden through pacemaking activity, active Ca2+ pumping, poorly myelinated fibers and large axonal arbors (7). In fact, those factors likely account for their intrinsic vulnerability to mitochondrial insults,

including complex I disruption (8-10) and impairments in mitochondrial dynamics (11) and turnover (12). About half of the oxygen consumed by mitochondria in SNc DA neurons is devoted to supporting neuronal firing and transmitter release (13). Thus, combined with disease-related stress, the metabolic impact of even mild hyperactivity may trigger or accelerate the degeneration process in SNc DA neurons. In support of this hypothesis, inhibiting the excitatory input from the STN protects SNc DA neurons from 6-OHDA and MPTP toxicity (14, 15). In addition, a proposed mechanism of action for the beneficial effects of deep brain stimulation (DBS) in PD is the inhibition of the subthalamic nucleus. Recent clinical trial data raises the possibility that DBS may slow disease progression when administered to early-stage patients (16). Finally, chronic nicotine – which is believed to mediate the protective association of smoking in PD (17) – inhibits SNc DA neurons through agonism of nicotinic acetylcholine receptors expressed on presynaptic GABAergic terminals (18).

However, empirical evidence that delineates the contribution of chronic changes in neural activity to the degeneration of SNc DA neurons in PD is lacking. To understand if chronic hyperactivation is a driving force, we developed a mouse model to chronically increase neural activity in midbrain DA neurons using chemogenetics.

3.2 Results

In order to model a chronic increase in neural activity, as may occur in PD, we expressed the excitatory hM3Dq DREADD receptor specifically in dopamine neurons by using Cre-dependent AAV delivery in mice expressing Cre under the dopamine transporter (DAT) promoter. The resulting hM3Dq-expressing $DAT^{IRES}Cre$ mice were then administered Clozapine-n-oxide (CNO, 300 mg/L) via drinking water ad libitum for two or four weeks, while hM3Dq-expressing controls were given vehicle (Figure 1A). This strategy allowed us to simultaneously over-

activate SN and VTA DA neurons, the latter serving as an important control in our experimental paradigm and which we expected to be more resilient to disease-relevant stressors.

To assess how our manipulation affected the dopaminergic system in live animals, mice were single-housed in cages containing wireless running wheels, and locomotion as measured through wheel usage was used as an *in vivo* proxy for assessing changes in neural function over the duration of the experiment. Previous reports indicate that acute CNO treatment in animals expressing hM3Dq specifically in dopamine neurons leads to increased locomotion (19) but the effects of long-term DREADD activation are unknown. While hM3Dq-expressing animals that received vehicle exhibited typical nocturnal behavior, where most activity occurs during the dark cycle, CNO-treated animals experienced significant disruptions in typical activity patterns, which suggests that sleep-wake cycles could be impacted (Figure 1B,C). During the first day of treatment, CNO-treated animals were more active than controls during both light and dark cycles. However, this increase was temporary and at day 7 of treatment, activity during light cycle came back closer to baseline while dark cycle activity was significantly reduced. These findings might not be a surprise given the VTA's role in maintaining wakefulness (20). On a chronic timescale, sleep deprivation may be negatively impacting wheel usage. Additionally, the long-lasting effects we observed on wheel activity suggest that the chemogenetic activation in our model is long-lived.

SNc axons are preferentially vulnerable to chronic Gq-activation

To understand the effect of chronic hyperactivity (2-week) on the integrity and survival of dopamine neurons, we quantified axonal density and estimated cell body number post-hoc. Strikingly, animals treated with CNO, but not vehicle, lost about 40% of their dopaminergic

axons in the caudate putamen, innervated mainly by SNc neurons, as manifest by decreases in both TH immunoreactivity and reporter mCherry fluorescence (Figure 1D-F). The same perturbation had a lesser impact on nucleus accumbens dopaminergic terminals projecting from the VTA. Chronic administration of CNO to animals not injected with AAV-DIO-hM3Dq did not impair the survival of dopaminergic axons, suggesting that the axonal degeneration that we observe requires hM3Dq activation and is not a mere side effect of CNO supplementation (Figure 2A,B). Next, we assessed dopaminergic survival in the midbrain using stereology and found no differences between CNO-treated animals and controls in the SNc (Figure 1G,H). This suggests that consistent with PD progression in humans (21), axonal impairment precedes cell body loss.

We also sought to understand whether prolonging the chronic activation paradigm to 4 weeks would lead to a more profound phenotype, especially at the level of the nucleus accumbens. Animals treated with CNO for 4 weeks exhibited increased axonal loss (~60%) in the caudate putamen compared to their 2-week counterparts (Figure 2C,D). In sharp contrast, nucleus accumbens fibers were almost completely spared. This indicates that VTA DA neurons are much more resilient to prolonged hyperactivation than SN DA neurons.

Chronic activation increases baseline population Ca2+ levels

Next, we investigated the effect of our chemogenetic manipulation on population intracellular calcium levels, which also reflect the extent and duration of the induced increase in neural activity. To this end, we used fiber photometry in order to measure fluorescence of the calcium sensor GCaMP6f in live, freely-moving animals. Animals bred to express Cre and the calcium sensor GCaMP6f specifically in DA neurons were injected bilaterally with the Cre-

dependent hM3Dq AAV (Figure 3A). A few weeks later, the fluorescent signal was used to guide the implantation of an optical probe in the midbrain of animals with confirmed hM3Dq expression in DA neurons (Figure 3B). Animals administered CNO or vehicle were placed in arenas for 10-min long fiber photometry recording sessions every 1-3 days over the 2-week treatment period. By measuring the baseline fluorescence level during every recording session, we measured intracellular calcium levels at a neuronal population level, which we predicted would increase over time with CNO treatment but not vehicle. Indeed, the measurement reveals a significant increase in baseline fluorescence in the CNO-treated group, which reached peak fluorescence levels at day 12 of treatment (Figure 3C). We also wondered if neural activity changes induced by our manipulation were reversible, so we performed two additional recording sessions after putting the animals back on regular water post-treatment. The downward trend we see in baseline fluorescence suggests that the calcium change is at least partially reversible.

Synucleins do not influence the rate of axonal degeneration due to chronic activation

Next, we wanted to gain a better mechanistic understanding of the molecular drivers of degeneration in our model. Given that α-synuclein overexpression (22) and single mutations (23) cause PD and that the normal function of α-synuclein includes regulation of synaptic vesicle release (24), we hypothesized that α-synuclein could be playing a role in mediating terminal loss during chronic hyperactivation. To test this, mice lacking all three synuclein isoforms α, β and γ (i.e. synuclein TKO) and control wildtype mice were injected with non-selective AAV-hM3Dq in the midbrain, and treated with CNO for 2 weeks (Figure 4). Despite the chronic chemogenetic activation being imposed on all neurons that received the AAV during the injection, the effect on axonal survival was recapitulated. However, we detected no difference between synuclein TKO and wildtype mice.

3.3 Conclusions

In summary, our chronic hM3Dq activation model reveals an intrinsic vulnerability of nigral axons to prolonged neuronal hyperactivity. Interestingly, this vulnerability is not present in axons originating from the VTA, a neuronal type more resilient to PD. We also show that chronic administration of the hM3Dq ligand is insufficient to initiate axonal degeneration on its own. We confirm that chronic hM3Dq activation results in a chronic effect on intracellular calcium levels and functional behavioral readouts, suggesting that our model induces long-lasting changes in dopamine neuron activity, as intended.

Taken together, these results suggest that chronic changes in neural activity may contribute to the progression of PD, and could partially account for the selective vulnerability of SNc neurons. However, the molecular mechanisms that drive this axonal degeneration remain obscure and additional work will be required to identify them. Surprisingly, synucleins do not play a major a role in mediating this phenotype. Other potential culprits include increased intracellular calcium levels, known to be cytotoxic to neurons, as well as bioenergetic failure. Taking a multi-omics approach will be critical for identifying genes that mediate the degeneration process.

3.4 Figures

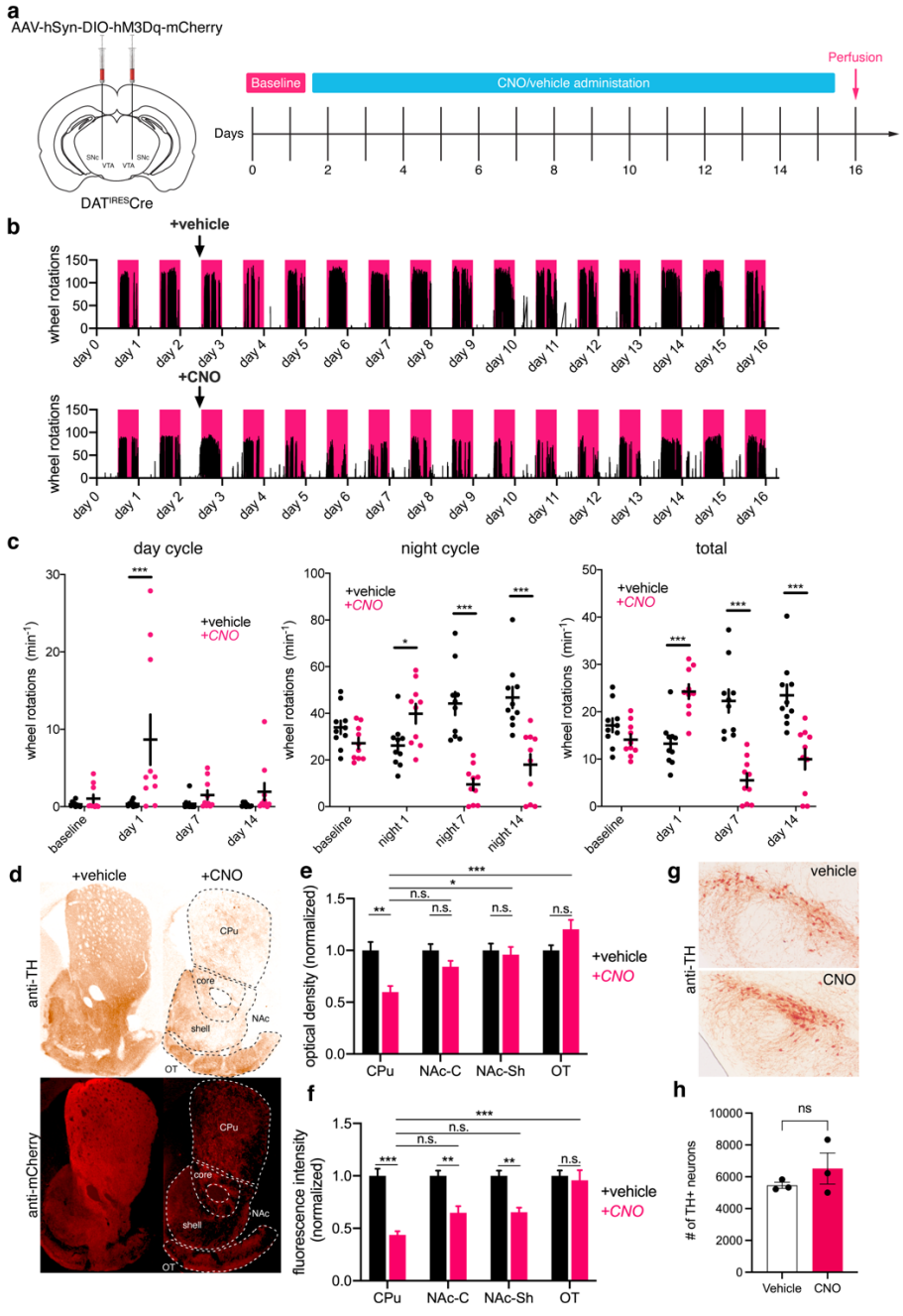

Figure 3.1

Chronic hM3Dq activation is toxic to dopamine neurons in vivo.

(a) Graphical illustration summarizing experimental design. A recombinant AAV encoding a conditional allele of the hM3Dq(DREADD)-mCherry was injected bilaterally into the ventral

midbrain of 4-5 month-old DAT^{IRES}Cre mice. CNO (300 mg/L) or vehicle (2% sucrose in water) was administered *ad libitum* via drinking water for two weeks and the animals perfused the next day. Changes in locomotion were assessed with running wheels. The two days preceding start of treatment were used as a measure for baseline locomotion.

(b) Representative example traces of wheel usage for animals given CNO (bottom) or control vehicle (top). Arrows denote start of treatment.

(c) Mean wheel usage for selected days during the experiment, either segregated by light (left) or dark (center) cycles, or combined (right). n=10 animals/group from 2 independent experiments. *p<0.05, ***p<0.001 by two-way ANOVA and Holm-Sidak post hoc test.

(d) Example images of TH (top) and mCherry (bottom) immunoreactivity in striatal sections of hM3Dq-expressing animals treated with vehicle (left) and CNO (right). DA neuron projection areas in dorsal and ventral striatum are indicated with dotted lines. CPu: caudate putamen, NAc: nucleus accumbens, OT: olfactory tubercule.

(e,f) Quantification for TH immunoreactivity (e) shows loss of reactivity primarily in CPu, with less involvement of the NAc, in particular the shell (-Sh) and OT. Labeling for mCherry (d,below) further demonstrates loss of the projections, not simply immunoreactivity for TH, and quantitation in (f) shows involvement of core (-C) and shell (-Sh) but not OT. Error bars indicate mean ± SEM. *, p<0.05, **, p<0.01, ***, p < 0.001, n = 8-9 animals/group, 3-5 sections/animal, from two independent experiments.

(g) Example images of TH immunoreactive neurons in the SNc of animals treated with vehicle (top) and CNO (bottom).

(h) Stereological estimate of TH immunoreactive SNc neurons shows no impact on cell count. Error bars indicate mean ± SEM. Not significant by t-test, n = 3 animals/group.

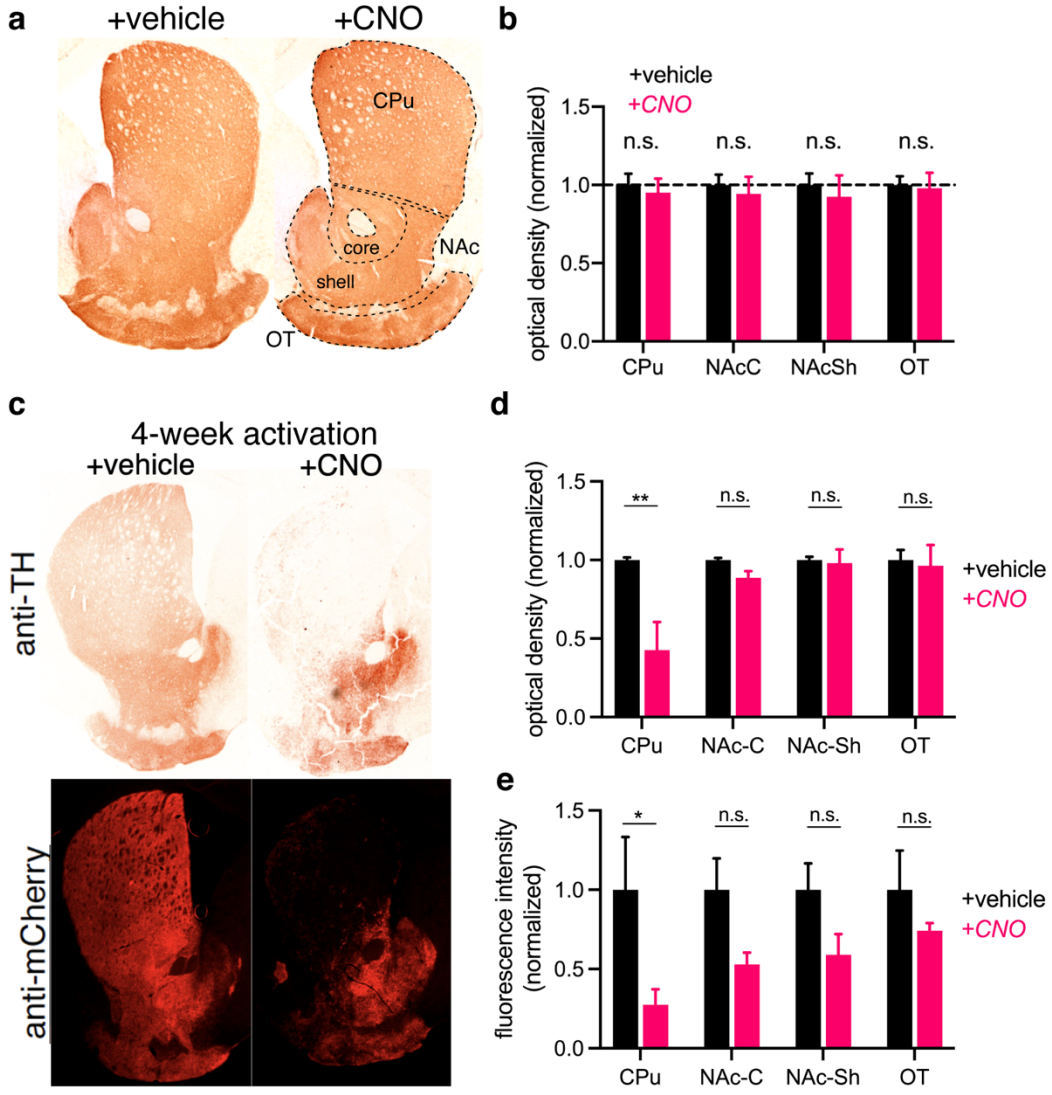

Figure 3.2

Chronic administration of CNO alone is not sufficient to cause degeneration of dopaminergic axons

(a) Example images of TH immunoreactivity in DAT^{IRES}Cre animals treated with vehicle (left) or CNO (right) for 2 weeks via drinking water.

(b) Quantification of TH immunoreactivity in (a) by optical density shows no loss. n=3 animals/group. Not significant (n.s.) by two-way ANOVA and Holm-Sidak post hoc test.

(c-e) hM3Dq-expressing animals treated with vehicle (left) or CNO (right) for 4 weeks. TH immunoreactivity shows a strong loss of reactivity in the CPu for the animals that received CNO (c, above; d), consistent with reporter mCherry fluorescence (c, below; e). Error bars indicate mean ± SEM. *, p≤ 0.05, **, p<0.01, n = 3 animals/group, 4 sections/animal by two-way ANOVA and Holm-Sidak post hoc test.

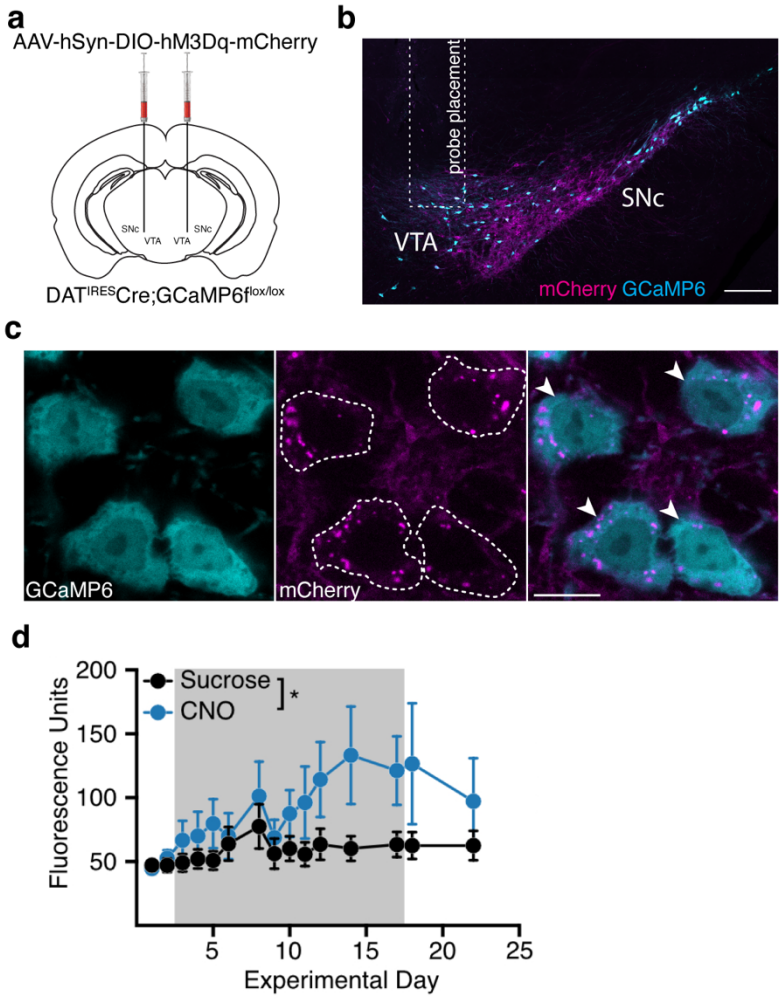

Figure 3.3

Chronic hM3Dq activation reversibly increases baseline calcium levels in dopamine neurons.

(a) Transgenic mice expressing Ca^{2+}-reporter GCaMP6 specifically in dopamine neurons were injected bilaterally with AAV-DIO-hM3Dq-mCherry and implanted with an optical probe for baseline Ca2+ measurements during a 14-day chronic chemogenetic activation.

(b) Representative images of photometry probe placement in mouse midbrain to record from dopamine neurons co-expressing hM3Dq-mCherry (magenta) and GCaMP6 (cyan). Scale bar is 200 µm.

(c) Representative high-magnification images of reporter mCherry (magenta) and GCaMP6 (cyan) co-expression. Scale bar is 10 µm.

(d) Baseline Ca^{2+} fluorescence levels of dopamine neurons in mice treated with CNO or sucrose for 14 days, and following wash. Error bars indicate mean ± SEM. *, $p<0.05$ by two-way ANOVA, n = 7 animals/group from 2 independent experiments.

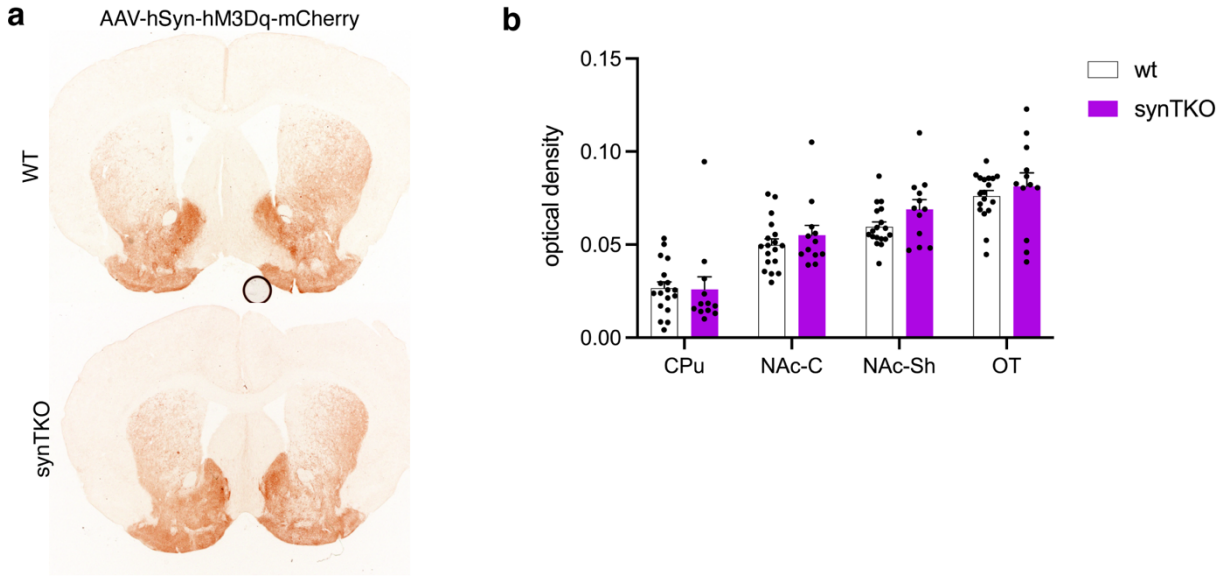

Figure 3.4

Synuclein triple knockout does not impact activation-induced axonal loss.

(a) Representative images of wildtype (above) and synTKO (below) striatal coronal sections immunostained for TH after 2-week activation of non-selective midbrain hM3Dq.

(b) Quantification of TH immunoreactivity in (a). Denervation occurs preferentially at the level of the CPu but there is no difference between genotypes. Error bars indicate mean ± SEM. N.s. = not significant by two-way ANOVA, n = 12-18 hemispheres/group, 4 sections/hemisphere from 2 independent experiments.

3.4 References

1. J. R. Hollerman, A. A. Grace, The effects of dopamine-depleting brain lesions on the electrophysiological activity of rat substantia nigra dopamine neurons. Brain research 533, 203-212 (1990).

2. M. J. Zigmond, A. L. Acheson, M. K. Stachowiak, E. M. Strickerm, Neurochemical compensation after nigrostriatal bundle injury in an animal model of preclinical parkinsonism. Archives of neurology 41, 856-861 (1984).

3. Y. AGID, F. JAVOY, J. GLOWINSKI, Hyperactivity of remaining dopaminergic neurones after partial destruction of the nigro-striatal dopaminergic system in the rat. Nature New Biology 245, 150-151 (1973).

4. F. Hefti, E. Melamed, R. J. Wurtman, Partial lesions of the dopaminergic nigrostriatal system in rat brain: biochemical characterization. Brain research 195, 123-137 (1980).

5. W. Zhang et al., Increased dopamine release from striata of rats after unilateral nigrostriatal bundle damage. Brain research 461, 335-342 (1988).

6. H. Bergman, T. Wichmann, B. Karmon, M. DeLong, The primate subthalamic nucleus. II. Neuronal activity in the MPTP model of parkinsonism. Journal of neurophysiology 72, 507-520 (1994).

7. D. Haddad, K. Nakamura, Understanding the susceptibility of dopamine neurons to mitochondrial stressors in Parkinson's disease. FEBS letters 589, 3702-3713 (2015).

8. R. Betarbet et al., Chronic systemic pesticide exposure reproduces features of Parkinson's disease. Nature neuroscience 3, 1301-1306 (2000).

9. P. González-Rodríguez et al., Disruption of mitochondrial complex I induces progressive parkinsonism. Nature 599, 650-656 (2021).

10. Z. Doric, K. Nakamura, Mice with disrupted mitochondria used to model Parkinson's disease. Nature 599, 558-560 (2021)

11. A. Berthet et al., Loss of mitochondrial fission depletes axonal mitochondria in midbrain dopamine neurons. Journal of Neuroscience 34, 14304-14317 (2014).

12. H. Li et al., Longitudinal tracking of neuronal mitochondria delineates PINK1/Parkin-dependent mechanisms of mitochondrial recycling and degradation. Science advances 7, eabf6580 (2021).

13. C. Pacelli et al., Elevated mitochondrial bioenergetics and axonal arborization size are key contributors to the vulnerability of dopamine neurons. Current Biology 25, 2349-2360 (2015).

14. B. Piallat, A. Benazzouz, A. L. Benabid, Subthalamic nucleus lesion in rats prevents dopaminergic nigral neuron degeneration after striatal 6-OHDA injection: behavioural and immunohistochemical studies. European Journal of Neuroscience 8, 1408-1414 (1996).

15. H. Bergman, T. Wichmann, M. R. DeLong, Reversal of experimental parkinsonism by lesions of the subthalamic nucleus. Science 249, 1436-1438 (1990).

16. M. L. Hacker et al., Deep brain stimulation in early-stage Parkinson disease: Five-year outcomes. Neurology 95, e393-e401 (2020).

17. M. Quik, Smoking, nicotine and Parkinson's disease. Trends in neurosciences 27, 561-568 (2004).

18. C. Xiao et al., Chronic nicotine selectively enhances α4β2* nicotinic acetylcholine receptors in the nigrostriatal dopamine pathway. Journal of Neuroscience 29, 12428-12439 (2009).

19. S. Wang, Y. Tan, J.-E. Zhang, M. Luo, Pharmacogenetic activation of midbrain dopaminergic neurons induces hyperactivity. Neuroscience bulletin 29, 517-524 (2013).

20. A. Eban-Rothschild, G. Rothschild, W. J. Giardino, J. R. Jones, L. de Lecea, VTA dopaminergic neurons regulate ethologically relevant sleep–wake behaviors. Nature neuroscience 19, 1356-1366 (2016).

21. J. H. Kordower et al., Disease duration and the integrity of the nigrostriatal system in Parkinson's disease. Brain 136, 2419-2431 (2013).

22. A. Singleton et al., α-Synuclein locus triplication causes Parkinson's disease. science 302, 841-841 (2003).

23. M. H. Polymeropoulos et al., Mutation in the α-synuclein gene identified in families with Parkinson's disease. science 276, 2045-2047 (1997).

24. J. T. Bendor, T. P. Logan, R. H. Edwards, The function of α-synuclein. Neuron 79, 1044-1066 (2013).

Chapter 4 Concluding remarks

The mechanisms of PINK1- and PRKN-dependent mitophagy have been elucidated in great detail in cell lines, but there have been relatively few such studies in neurons. However, neurons are preferentially vulnerable to disruptions in PINK1 and PRKN in Parkinson disease (PD), and also have fundamentally different responses to mitophagy triggers. In particular, the mitochondrial uncouplers FCCP and CCCP fail to clear mitochondria from neurons, whereas they remove essentially all mitochondria in many cell lines. Interestingly, neurons continue to turn over mitochondria even when PINK1 and PRKN are absent, and PINK1 KO and PRKN KO neurons have normal complements of mitochondria.

Does this mean that neurons do not require PINK1 and PRKN for mitochondrial turnover, and that disruptions in mitochondrial quality control do not contribute to the pathophysiology of PINK1- and PRKN-dependent PD? While this possibility remains, the robust convergence of PINK1 and PRKN on mitochondria across model organisms suggests a key role in disease pathogenesis.

In fact, while not required for basal mitophagy, PINK1 and PRKN can become indispensable for mitochondrial turnover in stressed neurons. To investigate this process, we used neurons lacking the mitochondrial fission protein DNM1L/Drp1, a stress condition that markedly increases the toxicity of losing PINK1 to midbrain dopamine neurons. Importantly, dnm1l KO mitochondria have a characteristic swollen shape and are far more segregated and less mobile than those in wild-type cell lines, which allowed us to track their individual fates and functions for up to 21 h. Moreover, we combined this approach with correlative light electron microscopy/CLEM, which allowed us to resolve the ultrastructure of mitochondria labeled with fluorescent markers. Using this approach, we visualized the initial phases of PINK1- and PRKN-

based mitophagy in neurons and delineated their kinetics. As observed in studies of PRKN-based mitophagy in cell lines, these early steps included first the recruitment of PRKN by depolarized mitochondria, followed by their engulfment by phagophores and their eventual fusion with lysosomes to form mitolysosomes.

By tracking individual mitochondria, we also gained unprecedented insight into their fate after targeting to lysosomes. We found that the formation of highly acidic mitolysosomes depends largely on PINK1 and PRKN. Moreover, rather than being inert structures that are rapidly degraded, mitolysosomes that emerge from PINK1-PRKN targeting are dynamic, and often long-lived structures that interact closely with neighboring mitochondria. Remarkably, some mitolysosomes are even engulfed by other, apparently healthy mitochondria. Ultimately, both dnm1l KO and wild-type mitolysosomes formed via PINK1-PRKN targeting burst, and release their contents, including functional proteins, into the cytosol. Interestingly, the mitolysosomes deacidify before bursting, which we hypothesize represents the protective inactivation of lysosomal elements that could otherwise be detrimental to the cell.

The dynamic nature of the neurons' mitolysosomes argues against the common assumption that mitolysosomes are solitary structures whose sole function is to break down mitochondrial components into cellular building blocks. Instead, mitochondria may have evolved an ability to intercept and pillage mitolysosomes. We hypothesize that the close interactions between mitolysosomes and healthy mitochondria allow the recycling and exchange of still salvageable components of the degrading mitochondria stuck inside a lysosome: engulfment supplies recycled materials to the healthy mitochondria, while bursting releases other mitochondrial components to the cytosol. If true, this could lead to important energy and resource savings by avoiding the rebuilding of new mitochondrial parts from scratch. While this particular function

may be dispensable in times of plenty, it could be of critical importance in conditions of scarcity associated with stressful environments, especially for cells such as neurons with high metabolic demands.

We speculate that bursting and engulfment may also have signaling functions. Bursting, in particular, which we hypothesize occurs primarily in stressed cells, may bridge PINK1-PRKN mitophagy and the immune system. By releasing mitochondrial components not typically present in the cytosol, bursting may alert the immune system to threats that are putting pressure on the cell. Alternatively, bursting could serve as a negative feedback regulator of mitophagy that prevents the deletion of too many mitochondria.

In addition to the highly acidified mitolysosomes, we observed mildly acidified mitochondria that contained PRKN in their matrix. How could PRKN, a cytosolic protein lacking a mitochondrial targeting sequence, gain access to a sheltered mitochondrial compartment, and what is its function there? The presence of PRKN inside these mitochondria appears to have physiological relevance, because it depends on PINK1, a detector of mitochondrial damage. We speculate that these mitochondria might have engulfed mitolysosomes, which would explain both their acidification and their harboring PRKN. Alternatively, they may have some defect that somehow led PRKN to get in. Regardless, further experiments are required to determine whether PRKN inside these mitochondria mediates the local degradation of dysfunctional structures, for instance through ubiquitination, or contributes to mitochondrial repair through other mechanisms.

To summarize, we have identified new mechanisms of PINK1- and PRKN-based mitochondrial quality control – engulfment, bursting, and PRKN internalization – that may also

contribute to the vulnerability of neurons to loss of PRKN and PINK1 under conditions of stress. However, our work raises new questions, including whether these processes are unique to PINK1-PRKN mitophagy, and whether abrogating them worsens neuronal survival. If true, they could underlie the "value-add" of PINK1 and PRKN mitophagy. Beyond providing new insights into how PINK1 and PRKN dysfunction may contribute to PD pathogenesis, these processes may be important areas of focus for basic biology studies investigating mitochondrial and cellular homeostasis.

Publishing Agreement

It is the policy of the University to encourage open access and broad distribution of all theses, dissertations, and manuscripts. The Graduate Division will facilitate the distribution of UCSF theses, dissertations, and manuscripts to the UCSF Library for open access and distribution. UCSF will make such theses, dissertations, and manuscripts accessible to the public and will take reasonable steps to preserve these works in perpetuity.

I hereby grant the non-exclusive, perpetual right to The Regents of the University of California to reproduce, publicly display, distribute, preserve, and publish copies of my thesis, dissertation, or manuscript in any form or media, now existing or later derived, including access online for teaching, research, and public service purposes.

DocuSigned by:
Zak Doric
AE87F8544B21449...
Author Signature

3/15/2022
Date